q-deformations and its applications in nonlinear maps

A Thesis submitted to the University of Hyderabad for the award of the degree of Doctor of Philosophy in Physics

By

SUDHARSANA V. IYENGAR
(10PHPH02)

School of Physics
UNIVERSITY OF HYDERABAD

JUNE 2016

q-deformations and its applications in nonlinear maps

A Thesis submitted to the University of Hyderabad for the award of the degree of Doctor of Philosophy in Physics

By

SUDHARSANA V. IYENGAR
(10PHPH02)

School of Physics
UNIVERSITY OF HYDERABAD

JUNE 2016

Dedication

This thesis is dedicated to my Family.

Acknowledgments

As Neil Armstrong pointed out, a small step of man is giant leap for the mankind. Similarly is my journey in this wild where every small step of mine is achieved by every person behind me who made me take the step.

I would like to thank all my teachers of my school who have been supporting and encouraging me. Mainly I would like to thank Mr Gopi Menon who was my physics tutor, who made physics easy for me.

In my bachelor years my lecturers always encouraged me to be curious and learn new things. I thank Dr Rajalakshmi, Dr Ranganayaki, Dr Senthamarai, Dr Lakshmi and Mrs Lalitha for being a backbone during my bachelors days. In the University of Madras, I was gifted to be tutored by Prof. M. S. Sriram, Prof. S. S. Vasan, Prof. K. Raghunathan. Prof. Ranabir Chakraborthy, Prof. A. S. Vytheeswaran, Prof. P. R Subramaniyam, Prof. V. Ravichander, Prof. K. Ravichandar, Prof. Shivaji, Prof. A. Stephan, and Prof. C Venkateshwaran. I thank them all for showing the path of my life.

I thank my supervisor Prof. Janaki Balakrishnan who has helped me both personally and professionally. She supported me during my marriage my sibling's marriage, my mother's ill-health which all delayed my work. I thank her for her understanding. Thanks to you ma'am.

I also thank Prof. B. Ashok, who used to give ideas for my work.

I thank Prof C. Bansal, Prof. S. Chaturvedi, Prof. R. Singh, Prof. S. P. Tewari, the various deans of the Physics department from 2010 to 2016 for providing me with all facilities required during the course of work. I thank my Doctoral review committee members Prof. A. Kapoor and Prof. S. Chaturvedi for valuable comments and being a constant source of support.

I thank Mr T. Abraham, for constant support and help towards the administrative work and other official paper work.

I thank CSIR for funding my research.

I thank Mrs. Mary Stella A, Prof. N. Ramani, Mrs. Hamsa Kalyani, Mr. Ramakrishna for helps that they have offered me during the course of work.

I finally thank my family members, My father, mother, sister, brother who have been supporting me all my life. I thank my husband and mother in law for the courage and support they have extended.

And finally a big thanks to all my friends who have been withstanding me and supporting me.

CERTIFICATE

This is to certify that the research work compiled and presented in the thesis titled ‚Äúq-deformations and its applications in nonlinear maps", has been carried out by Sudharsana V Iyengar at the School of Physics, University of Hyderabad, Hyderabad under the Supervision of Prof. Janaki Balakrishnan and the same has not been submitted for any degree/diploma or any other academic award by any other University.

.....	.....
PROF JANAKI BALAKRISHNAN	DEAN
(SUPERVISOR)	SCHOOL OF PHYSICS
DATE:	UNIVERSITY OF HYDERABAD

AUTHOR'S DECLARATION

I , Sudharsana V. Iyengar, hereby declare that this thesis entitled “q-deformations and its applications in nonlinear maps" submitted by me under the guidance and supervision of Prof. Janaki Balakrishnan is a bonafide research work which is also free from plagiarism. I also declare that it has not been submitted previously, in part or in full to this University or any other University or Institution for the award of any degree or diploma. I hereby agree that my thesis can be deposited in Shodhganga/INFLIBNET. A report of plagiarism statistics from the University Librarian is enclosed.

SIGNED: ..... DATE: .....

SIGNED: ..... DATE: .....
(Supervisor)

TABLE OF CONTENTS

List of Tables

Table **Page**

List of Figures

Figure **Page**

CHAPTER 1

PREFACE

Nature has always been somewhat of a mystery, never easily revealing her true properties and powers. From the little that is unveiled, mankind tries to understand her to the best of our ability. The more we try to unlock her secrets, the more challenges and mysteries do we stumble upon. There is a saying in Tamil which may be translated as: "What is learnt is as small in amount as a handful of sand, what is not learnt is of the size of the earth"; this saying truly reflects the current state of knowledge after the several millenia since Homo sapiens first walked on the surface of this planet. With the limited tools at our disposal, no matter how deeply we may probe and analyze, there will always be still more to discover and ever new questions will arise. Yet, as we go through the pages of history, we find that in the early 1900s physicists thought that the physical universe was completely known and no unsolved problems were left [1]. Maxwell had unified the theories of electricity and magnetism, and gravity was the only force which was left ununified. Then Roentgen discovered X rays and for which he was awarded the Nobel prize. Henri Becquerel set out to prove experimentally with uranium salts (uranium oxide) that the X radiation was just phosphorescence. Wrapping the salt in photographic plates, he exposed some to light while others were kept in the dark. The sample which was in the dark still emitted radiation, and this led to Becquerel's accidental discovery of spontaneous radioactivity. This incident changed the notion that all the forces of physics were known. 120 years thence, we are still uncovering new facts every day. The discovery that X rays were not phophorescence but involved new forces, gave birth to quantum mechanics, atomic physics, nanotechnology, string theory, quantum entanglement, quantum computation, etc.

Surprisingly, many of the scientific puzzles resolved so far have used linearized equations to a first approximation, simplifying the system's motion to simple harmonic motion. However discrepancies have been reported in almost all arenas of research, and it has become clear that

nonlinearities play a very important part in nearly all observed phenomena.

Newtonian mechanics which has answers all our mechanical problems, fails as the velocity of the system approaches the speed of light. In a region where gravitational force field is strong, Euclidean geometry fails as one needs to consider the curvature of spacetime. Bringing in curvature into the equations, the Newtonian equations are no longer valid and one needs to use general relativity, which is highly non linear in both space and time.
In 1963 E. N. Lorenz modelled atmospheric air circulation using nonlinear equations [2]. He discovered in the course of his simulations that changing the initial conditions by very little led to very different results.

This sensitivity to the initial conditions is the main feature of chaos. Complex systems that we see in nature are all nonlinear and thus exhibit this sensitivity to the initial conditions in the chaotic regime.

In ecology, we see a lot of plant and animal interaction. Most of these interactions between species are not simple. Consider, for example, a system consisting of a predator and its prey. One might think that the more the prey, the greater would be the predator population and growth, and this would be true in linear systems. However, what we see in Nature is exactly opposite. An increase in the *carrying capacity* (or maximum (prey) population the system can support) actually result in a decrease in predator population. This is known as the "paradox of enrichment" [3].
Another example of a non-trivial ecological system is that of lake algae. Due to industrialization and use of fertilizers, eutrophication occurs in lakes, increasing algal bloom. It might be expected that zooplankton that fed the algae would multiply, thereby also increasing the small fish population. This, in turn, should increase the numbers of aquatic birds that feed off these fish. In reality, this scenario of a multi-species, rich biosystem never materializes. Eutrophication causes excess bloom of algae, forming a turbid layer on top of the lake. With excessive resources, the zooplankton population rises and falls, the oscillations being so large that the species may also be driven to extinction causing the rest of the food chain to collapse, with only the algae prospering. This is one more example of a complex system whose features can be modelled using nonlinear terms, and for which one needs to go beyond the simplifications made in conventional linear physics and mathematics.
As would only be expected, once interactions between the various components of a system are included, the resulting dynamics become complicated. Most of the simulations and models that seek to capture the behaviour of a real-life ecological system, do not, till today, factor in the effect of the environment. The moment environmental factors are brought in, the system starts to behave differently.

In this thesis, we report our studies of some nonlinear systems.
In order to capture the observed behaviour of real-life systems, such as the ecological system we have studied, where the influence of a previous population lives on in the next generation and there is thus “memory" built into the system, we find the requirement of q-deformed numbers and the

(relatively) new statistics of Tsallis.

We start with an introductory exposition in Chapter 2, giving a brief history on $q-$deformation and discussing its success-stories in application to observed physical phenomena. We also discuss the various phenomena that seem to obey the statistics due to Tsallis. The reasons for the failure of the conventional classical physics approaches in such scenarios are also explained in this chapter.

In Chapter 3, we motivate the application of $q-$deformation to discrete systems. We discuss our results for four 2-dimensional q-deformed maps. These exhibit phenomena such as Neimark-Sacker bifurcation, period-twinning, formation of paired cascades, occurrence of exterior and interior crises, etc.

In Chapter 4, as a prelude to reporting our original models and results of an ecological system, namely that of the larch budmoth, we first discuss the observations and experimental results extant in the literature. This moth and its larvae infest the larch trees in various high-altitude regions of the world, including those in the Engadine valley in the Alps. We give a brief introduction to mathematical ecology, and discuss several of the standard models in ecology. We also summarize the previous attempts made in modelling the larch budmoth system (comprising of larch trees, the budmoth and parasitoids that infest the budmoth), which is known to exhibit periodic cycles in population densities. The larch budmoth exhibits a population rise and fall. The data of 1200 years records 123 outbreaks, with a striking periodicity of 8-9 years. We look at the earlier models in the literature and their deficiencies, and the motivation for our new model.

In Chapter 5 we present our $q-$deformed tritrophic model. We discuss the various parameters that are present, and perform a linear stability analysis for the system.

We then discuss, in Chapter 6, a four-dimensional model for this ecological system where a new level of complexity is included, and its mathematical analysis is presented.

Finally, we summarize the results of both the models in Chapter 7.

CHAPTER 2

q-DEFORMATIONS AND SOME APPLICATIONS DISCUSSED IN THE LITERATURE

Understanding a system and breaking it down into equations requires extensive understanding of the interactions it undergoes. Interactions themselves may vary from being very simple to complex. Most of the analysis done till today are based on various assumptions that simplify the problem. As an example, consider a pendulum of length L and bob of mass M (made of iron) swinging from a nail. The first assumption that is made is that the system is in vacuum and there are no frictional forces. The second assumption which is imposed on the system is that the oscillations are small. Under these circumstances the equation for the pendulum is completely solvable and the solution is just that of the simple harmonic oscillator — a sinusoidal function of the pendulum's displacement from its mean position. In reality, there is friction at the pivot which decelerates the bob and halts it. Secondly the oscillations need not be small. Under these circumstances, the pendulum equation no longer simplifies to the simple harmonic oscillator equation, but is complicated, and solving it requires advanced tools. Further if one positions magnets below the bob, the system becomes completely unpredictable.

Although most systems are complex, several simplifying assumptions are usually made to find solutions to the equations. In several situations such simplifications do not reproduce the actual behaviour observed. An example is the use of Boltzmann-Gibbs distribution of equilibrium statistical mechanics for describing non-ergodic systems and systems with memory. Statistical mechanics is a very powerful tool for describing the thermodynamics of a system based on the statistical studies of its microscopic properties.

The Boltzmann-Gibbs (BG) formulation of statistical physics relies on the fact that the system has attained equilibrium. Once a system has reached equilibrium, all states are taken to be equally probable, having no memory of past configurations, giving rise to ergodicity. The key-word of BG statistics is the assignment of equal a priori probabilities to all microstates. This formalism fails

however for systems which are not in equilibrium or have memory or do not have equal a priori probabilities for their microstates. For descriing such non ergodic systems, Constantino Tsallis introduced non extensive statistical mechanics[4].

Entropy is a fundamental concept of any thermodynamic formalism. The extensive use of entropy as a thermodynamic concept of Boltzmann and Gibbs in the 19^{th} century laid the foundation for classical statistical mechanics. Boltzmann postulated that the entropy of a system is given by

$$S_{BG}(\{p_i\}) = -k \sum_{i=1}^{w} p_i \ln p_i \tag{2.1}$$

where k is the Boltzmann constant, w is the total number of available microstates and p_i is the probability distribution associated with the ith microstate.
Entropy is an extensive quantity, i.e., one whose value is directly proportional to the amount of material present in the system. Such a quantity can be described as the sum of the quantities for the separate subsystems that make the entire system.
The classical BG-statistics has been very successful in describing many physical systems to a very high degree of accuracy. In these systems the entropy scales as $\{p_i\}$ which is a direct consequence of the extensivity property of entropy. However, there are many physical situations in which the entropy does not scale as $\{p_i\}$ but rather as $\{p_i^q\}$ where q is some real parameter. For such anomalous systems, the BG-statistics fails to give an accurate physical description of the system. To describe such physical systems, Tsallis postulated a new form of entropy S_q in 1988[4] as

$$S_q = k \left[\frac{\sum_{i=0}^{w} p_i^q - 1}{1-q} \right] \tag{2.2}$$

where q is a real parameter and in the limit $q \to 1$, the new generalized entropy, S_q reduces to the classical BG-entropy S_{BG} given in Eqn.(2.1) which is extensive in nature. From equal a priori probability, i.e.,

$$p_i = \frac{1}{w} \tag{2.3}$$

we have,

$$S_{BG} = k \ln w \tag{2.4}$$

MATHEMATICAL PROPERTIES:

Consider a differential equation

$$\frac{dy}{dx} = y \tag{2.5}$$

Its solution is given by

$$\ln y = x \quad or \quad y = e^x \tag{2.6}$$

However if

$$\frac{dy}{dx} = y^q \ , \tag{2.7}$$

its solution would be

$$y = [1 + x(1-q)]^{1/(1-q)} \tag{2.8}$$

or

$$x = \frac{y^{1-q} - 1}{1-q} \tag{2.9}$$

Equations (2.8) and (2.9) can be considered as the deformed exponential and logarithm respectively and referred to as $\exp_q(x)$ and $\ln_q(y)$. It can be verified that these reduce to the usual exponential and natural logarithm functions respectively when $q \to 1$. In a similar way, the derivative of a function f(x) defined by,

$$\frac{dy}{dx} = \lim_{\Delta x \to 0} \frac{f(x + \Delta x) - f(x)}{(x + \Delta x - x)} \tag{2.10}$$

is generalised to

$$D_q(x) = \frac{f(qx) - f(x)}{qx - x} \tag{2.11}$$

Eq(2.11) is called the Jackson derivative [5] and in the limit $q \to 1$ the Jackson derivative reduces to the ordinary derivative:

$$D_{q \to 1} \equiv \frac{d}{dx} \tag{2.12}$$

Using the normal derivative the Eqn.(2.1) can be rewritten as,

$$S = -k \left[\frac{\partial}{\partial \alpha} (\sum_{i=1}^{w} p_i^{\alpha}) \right]_{\alpha=1} = -k \sum_{i=1}^{w} p_i \ln p_i \tag{2.13}$$

Using the generalised derivative, it can be seen that Eqn.(2.2) can be rewritten as [4],

$$S_q = -k \left[D_q (\sum_{i=0}^{w} p_i^q) \right]_{q=1} \equiv -k \frac{1 - \sum_{i=1}^{w} p_i^q}{q-1} \tag{2.14}$$

Assuming equiprobability, we get,

$$S_q = -k \frac{w^{1-q} - 1}{1-q} \tag{2.15}$$

Now using Eq(2.9) in Eq(2.15), we can write,

$$S_q = k \ln_q w \tag{2.16}$$

In the Boltzmann-Gibbs statistics the entropy is equal to constant times logarithm of the total number of states. In the non-extensive statistical mechanics too a similar relationship is maintained. However, the $q-$deformed logarithm enters the equations. The original BG statistics is recovered when $q \to 1$. The presence of the $q-$deformed logarithm causes the loss of extensivity. The following example illustrates this. Consider two sub-systems A and B. Since the entropy S_{BG} is an extensive quantity, it obeys the additive law:

$$S^{(A+B)} = S^{(A)} + S^{(B)} \tag{2.17}$$

which is a manifestation of the fact that $\ln(x_A x_B) = \ln x_A + \ln x_B$.

Similarly for the q-logarithm, from eqn.(2.9) we get:

$$\ln_q (x_A x_B) = \ln_q x_A + \ln_q x_B + (1-q)\ln_q x_A \ln_q x_B. \tag{2.18}$$

From equations (2.18) and (2.9) it immediately follows that,

$$S_q^{(A+B)} = S_q^{(A)} + S_q^{(B)} + (1-q)S_q^{(A)}S_q^{(B)} \tag{2.19}$$

When $q \to 1$, eqn.(2.19) reduces to eqn.(2.17). Thus eqn.(2.19) implies that the new form of entropy given by eqn.(2.2) is not an extensive quantity. In other words, the real parameter q deforms the entropy, making it non-extensive. The parameter q can take values $q > 1, q < 1$. For:
$q > 1 \Rightarrow$ the system is sub-extensive
$q = 1 \Rightarrow$ the system is extensive
$q < 1 \Rightarrow$ the system is super-extensive.
Thus the parameter q gives the degree of non-extensivity of the system.

Maximisation of entropy - choices of internal energy constraints

According to the laws of thermodynamics, any configuration of particles which maximises the entropy is the most probable one. Entropy is maximised using the Lagrange multipliers technique in the presence of appropriate constraints. For the micro-canonical ensemble wherein the system is in isolation, there is only one constraint, namely,

$$\sum_{i=1}^{w} p_i = 1 \tag{2.20}$$

Maximizing entropy using this constraint, we get the equi-probability condition given by eqn.(2.3). For the canonical ensemble, apart from the constraint in eqn.(2.20), we have an internal energy constraint also. Three choices of internal energy constraints[6]: $U_q^{(1)}, U_q^{(2)}, U_q^{(3)}$ can be considered as discussed below. As the theory of non-extensive statistical mechanics began to develop, the choice of the simple internal energy constraint which resembled that of the canonical ensemble was used first:

$$U_q^{(1)} = \sum_{i=1}^{w} p_i \epsilon_i \tag{2.21}$$

Using this constraint, maximization of entropy S_q yields,

$$p_i^{(1)} = \frac{[1-\beta^*\epsilon_i(q-1)]^{\frac{1}{q-1}}}{Z^{(1)}} \tag{2.22}$$

where

$$Z_q^{(1)} = \sum_{i=1}^{w} [1-\beta^*\epsilon_i(q-1)]^{\frac{1}{q-1}} \ , \tag{2.23}$$

$$\beta^* = \frac{\beta}{\alpha(q-1)} \ . \tag{2.24}$$

Here α and β are the Lagrange multipliers associated with the constraints. However, this choice of internal energy constraint was not satisfactory because in systems showing Leèvi super-diffusion, symmetry in the system makes $\int_0^\infty x_i p_i dx = 0$. Thus an obvious choice to use as constraint is the second moment, which for this system is divergent [7]. To avoid running into infinities the second constraint $U_q^{(2)}$ was introduced [7]:

$$U_q^{(2)} = \sum_{i=1}^{w} p_i^q \epsilon_i \tag{2.25}$$

With this choice of second constraint, maximization of the entropy leads to

$$p_i^{(2)} = \frac{[1-\beta\epsilon_i(1-q)]^{\frac{1}{1-q}}}{Z_q^{(2)}} \tag{2.26}$$

with the partition function given by:

$$Z_q^{(2)} = \sum_{i=1}^{w} [1-\beta\epsilon_i(1-q)]^{\frac{1}{1-q}} \tag{2.27}$$

These can be written using eqn.(2.8) as

$$p_i^{(2)} = \frac{e_q^{-\beta\epsilon_i}}{Z_q^{(2)}} \tag{2.28}$$

$$and \quad Z_q^{(2)} = \sum_{i=1}^{w} e_q^{-\beta\epsilon_i} \tag{2.29}$$

The Lagrange multiplier β associated with the internal energy constraint can be shown to be identically equal to $\frac{1}{kT}$ [7]. Using $T \equiv \frac{1}{k\beta}$, it can be shown that [7]

$$\frac{1}{T} = \frac{\partial S_q}{\partial U_q^{(2)}}. \tag{2.30}$$

$$F_q^{(2)} = U_q^{(2)} - TS_q = \frac{-1}{\beta}\ln_q Z_q^{(2)} \tag{2.31}$$

$$U_q^{(2)} = -\frac{\partial}{\partial\beta}\ln_q Z_q^{(2)} \tag{2.32}$$

$$\text{and} \quad C_q^{(2)} \equiv T\frac{\partial S_q}{\partial T} = \frac{\partial U_q^{(2)}}{\partial T} = -T\frac{\partial^2 F_q^{(2)}}{\partial T^2} \tag{2.33}$$

where $F_q^{(2)}$ is the generalized free energy and $C_q^{(2)}$ is the generalized specific heat.
Thus we see that the thermodynamic Legendre structure is maintained for any q. However, this suffers from a serious drawback that it is not invariant under uniform translations of the energy spectrum $\{\epsilon_i\}$ [6], i.e., the probability distribution depends upon the choice of origin of energy[8]. Secondly in this constraint $\Sigma_{i=1}^{w} p_i^q \neq 1$, but equals some constant c [8]. When this constraint is used to maximise the entropy, the constant retrieved is different from the original constant. The third problem in using this constraint is that when the assumption $p_{i,j}^{A+B} = p_i^A p_j^B$ and $E_{i,j}^{A+B} = E_i^A + E_j^B$ are made, the result expected is: $U_q^{A+B} = U_q^A + U_q^B$. However this is violated [7]. In practice this has not posed a great problem as in most of the physical problems the ground state is chosen as

the origin or zero point for the energies. To overcome the problems posed by the second constraint, the third constraint is introduced as follows[6, 8]. The third constraint is the final form which is accepted in the theory of non extensive statistical mechanics:

$$U_q^{(3)} = \frac{\sum_{i=1}^{w} p_i^q \epsilon_i}{\sum_{i=1}^{w} p_i^q} \tag{2.34}$$

i.e., the weighted eigenvalues of the Hamiltonian are taken by a weight factor of $P_i = \frac{p_i^q}{\left(\sum_{j=1}^{w} p_j^q\right)}$. P_i is called the escort probability distribution of the system citeescort. Distributions which are very general and unknown, and whose distribution function is deduced are called as the escort distributions [9]. Here,

$$\sum_{j=1}^{w} p_j^q = c \ , \quad c \neq 1 \tag{2.35}$$

so that $\Sigma_i^w P_i = 1$. With this constraint, the extremization of S_q yields,

$$p_i^{(3)} = \frac{[1 - \frac{\beta}{c}(\epsilon_i - U_q^{(3)})(1-q)]^{\frac{1}{1-q}}}{\overline{Z_q^{(3)}}} \tag{2.36}$$

with the generalized partition function being given by:

$$\overline{Z_q^{(3)}} = \sum_{i=1}^{w} \left[1 - \frac{\beta}{c}(\epsilon_i - U_q^{(3)})(1-q)\right]^{\frac{1}{1-q}} \tag{2.37}$$

Similar to the second constraint, the probability distribution due to the third constraint can be written using the generalized (q-deformed) functions in eqn.(2.8) as:

$$p_i^{(3)} = \frac{\exp_q\left[-\frac{\beta}{c}(\epsilon_i - U_q^{(3)})\right]}{\overline{Z_q^{(3)}}} \tag{2.38}$$

where

$$\overline{Z_q^{(3)}} = \sum_{i=1}^{w} \exp_q\left[-\frac{\beta}{c}(\epsilon_i - U_q^{(3)})\right] \tag{2.39}$$

Using $T \equiv \frac{1}{k\beta}$, it can be shown that [7]

$$\frac{1}{T} = \frac{\partial S_q}{\partial U_q^{(3)}} \tag{2.40}$$

The other thermodynamic quantities are found similarly with this third constraint:

$$F_q^{(3)} = U_q^{(3)} - TS_q = \frac{-1}{\beta} \ln_q Z_q^{(3)} \tag{2.41}$$

$$S_q = k_T \ln_q \overline{Z_q^{(3)}} \tag{2.42}$$

$$and \quad c = \sum_{i=1}^{w} (p_i^{(3)})^q = [\overline{Z_q^{(3)}}]^{1-q} \tag{2.43}$$

Using eqn.(2.43) we can write $p_i^{(3)}$ in eqn.(2.38) as,

$$p_i^{(3)} = \frac{\exp_q\left[-\frac{\beta}{[\overline{Z_q^{(3)}}]^{1-q}}(\epsilon_i - U_q^{(3)})\right]}{\overline{Z_q^{(3)}}} \tag{2.44}$$

Here the generalized partition function $\overline{Z_q^{(3)}}$ is defined in terms of the energy eigenvalues $\{\epsilon_i\}$ with reference to the energy U_q. This as well as all the thermodynamic quantities may be instead rewritten with zero as the energy reference by a redefinition of the partition function as $Z_q^{(3)}$:

$$Z_q^{(3)} = \overline{Z_q^{(3)}} - \frac{\beta U_q^{(3)}}{c} \tag{2.45}$$

Using eqn.(2.41) and the relations:

$$\beta\frac{\partial U_q^{(3)}}{\partial\beta} = \frac{\partial}{\partial\beta}\ln_q \overline{Z_q^{(3)}} \tag{2.46}$$

$$U_q^{(3)} = \frac{\partial}{\partial\beta}(\beta F_q^{(3)}) \quad , \tag{2.47}$$

equations (2.41) and (2.47) can be rewritten as

$$F_q^{(3)} = \frac{-1}{\beta}\ln_q Z_q^{(3)} \tag{2.48}$$

$$and \quad U_q^{(3)} = -\frac{\partial}{\partial\beta}\ln_q Z_q^{(3)} \tag{2.49}$$

so that the specific heat can be written as

$$C_q^{(3)} \equiv T\frac{\partial S_q}{\partial T} = \frac{\partial U_q^{(3)}}{\partial T} = -T\frac{\partial^2 F_q^{(3)}}{\partial T^2} \tag{2.50}$$

With the third choice of constraint, we see that the addition of some constant arbitrary energy ϵ_0 to all sets of energy $\{\epsilon_i\}$ leads to $U_q^{(3)}$ getting incremented to $U_q^{(3)} + \epsilon_0$. The difference between $\epsilon_i - U_q^{(3)}$ remains invariant for any value of ϵ_0. Since only differences enter the expression of $\{p_i^{(3)}\}$, this also remains invariant under uniform translation of the energy spectrum [8].
Now consider Eq(2.36). By taking out a common factor of $[1+(1-q)U_q^{(3)}\frac{\beta}{c}]^{\frac{1}{1-q}}$, from both the numerator and the denominator, and canceling it out we can rewrite it as

$$p_i^{(3)}(\beta') = \frac{[1-\beta'\epsilon_i(1-q)]^{\frac{1}{1-q}}}{[Z_q^{(3)}]'} \equiv \frac{e_q^{-\beta'\epsilon_i}}{[Z_q^{(3)}]'} \tag{2.51}$$

$$where \ \beta' = \frac{\beta}{[\sum_{i=1}^{w}(p_i^{(3)})^q + (1-q)\beta U_q^{(3)}]} \tag{2.52}$$

$$and \ \ [Z_q^{(3)}]' = \sum_{i=1}^{w} e_q^{-\beta'\epsilon_i} \tag{2.53}$$

Hence by defining $T' = \frac{1}{k\beta'}$ it can be shown that [8]:

$$p_i^{(3)}(\beta) = p_i^{(2)}(\beta') \tag{2.54}$$

And from comparing Eq(2.53) with Eq(2.29) we get

$$[Z_q^{(3)}(\beta)]' = [Z_q^{(2)}(\beta')] \tag{2.55}$$

Thus we see that the probability distribution at equilibrium, associated with the third choice of constraint is precisely identical to that associated with the second choice of constraint but with a renormalised temperature given by Eq(2.52). It is for the reason that the second constraint works very well for systems that do not have explicit temperature dependence and it works well for a system that is considered at some fixed arbitrary finite temperature. Although the third constraint is able to explain physical systems, solving it becomes difficult, as it is an implicit equation. So the system is solved using the second constraint and scaling is done to the third constraint. The third constraint overcomes all the difficulties that the first and the second constraints brought in.

2.1 $q-$deformed numbers

Jackson defined the $q-$deformed exponential as[5],

$$e_q^x = \Sigma_{n=0}^{\infty} \frac{x^n}{[n]_q!} \tag{2.56}$$

$$[n]_q! = [n-1][n-2][n-3]...[1] \tag{2.57}$$

$$[n]_q = \frac{1-q^n}{1-q} \tag{2.58}$$

$[n]_q$ tends to n, when $q \to 1$. $[n]_q$ in the eq(2.58) is known as the Heine deformation of numbers, which was introduced by Heine [10]. $q-$deformed exponential can also be written as

$$e_q^x = 1 + \Sigma_{n=1}^{\infty} \frac{Q_{n-1} x^n}{n!} \tag{2.59}$$

Here Q_n is defined as

$$Q_n = 1 \times q \times (2q-1) \times (3q-2) \times .... \times (nq-(n-1)) \tag{2.60}$$

defining $1-q = \epsilon$, and rewriting the $q-$exponential as

$$e_q^x = \tau_\epsilon(x) = (1+\epsilon x)^{\frac{1}{\epsilon}} \tag{2.61}$$

Using the definition from Eq(2.59) τ_ϵ can be rewritten as

$$\tau_\epsilon(x) = \Sigma_{n=0}^{\infty} \frac{T_n x^n}{n!} \tag{2.62}$$

where T_n is given by

$$\begin{aligned} T_n &= 1 \qquad\qquad n = 0 \\ &= 1 \times (1-\epsilon) \times (1-2\epsilon) \times ... \times (1+(1-n)\epsilon) \qquad n > 0 \end{aligned} \tag{2.63}$$

Comparing equations (2.62) and (2.56), a new deformation scheme can be found which is given by,

$$[n]_\epsilon = \frac{n}{1+(1-\epsilon)n} \tag{2.64}$$

when $\epsilon = 0$, $[n]_{\epsilon=0} = n$. Thus the series $\tau_\epsilon(x)$ can be defined as

$$\tau_\epsilon(x) = \Sigma_0^\infty \frac{x^n}{[n]_\epsilon!} \tag{2.65}$$

The equations (2.65) and (2.56) are similar. This new deformation of numbers will be used for further analysis. This deformation is related to Tsallis' deformation used in the definition of entropy. Throughout this thesis $q-$deformation will refer to this form and not the Heine's form[10] given in equation (2.58).

2.2 Application of $q-$ deformations

$q-$ deformed Tsallis' statistics have been applied in many fields [11, 12]. Some of the examples cited below show how classical statistical physics fails, while $q-$deformed Tsallis' statistics is able to explain discrepancies.

2.2.0.1 Velocity distribution of ions in the stellar interior

The stars are made of ions that have mutually condensed due to their collective gravitational potential. Due to high pressure, the temperatures in a star are very high. This high temperature is responsible for the ionisation of the atoms in the stellar interior and other nuclear reactions. The velocity of the particles inside a stellar interior follows a Gaussian. Most of the particles are assumed to have an energy of kT, where T is the stellar temperature. Very few ions have extremely high energies. Two like-charged ions get repelled by the Coulomb force as they approach each other. This is true for most particles with average energies.

Nuclear reactions that power the solar interior are the result of quantum tunneling of particles through the Coulomb barrier. The cross section for such reactions increases as the energy of particles increases. Energies corresponding to kT where T is the temperature of stellar body, in general are too low to penetrate the barrier and thus it is only the high energy particles that penetrate the barrier and participate in the nuclear reactions.

The velocity of ions in the solar interior is assumed to have a Maxwellian distribution. Even a slight correction to this can change the number of particles [13]with high energies, which in turn would alter the reaction rates. The number fluxes of various particles emanating from stellar interiors can be calculated. Neutrinos are by-products of reactions (nuclear fusions) that power the solar interior. One of the main discrepancies between calculated values and experimentally measured values is in the number of neutrinos received at various stations placed on earth. The flux of neutrinos received on earth is half of what theory predicts. One explanation to resolve the discrepancy observed between the theoretical prediction and the experimental observation is that some neutrinos went undetected as they changed their flavour [14]. However, by using a different

statistics, the discrepancy could be explained[13] by incorporating a different form for the velocity distribution – the deformed Gaussian [13] which modifies the reaction rates. The idea has been illustrated in [13] by considering a system having two types of particles n_1 and n_2 for simplicity. Denoting the reaction rate by r and the relative velocity of these particles by v, the number of reactions per unit volume per unit time is given by $< v\sigma >$ where $\sigma(v)$ denotes the cross section of the reaction:

$$r = \frac{n_1 n_2 < v\sigma >}{1+\delta_{12}} \tag{2.66}$$

where δ_{12} in the equation (2.66), is the Kronecker delta function

$$\delta_{ij} = 1 \qquad i = j \tag{2.67}$$

$$= 0 \qquad i \neq j \tag{2.68}$$

Averages in eqn.(2.66) are defined as

$$< v\sigma >= \int_0^\infty f(v)\sigma v dv \tag{2.69}$$

$f(v)$ represents the particle distribution which has a dependence on the temperature of the order of kT. The reaction rates are related to the tunneling probability given by

$$p = \exp(-2\pi\eta(E)) \tag{2.70}$$

where

$$\eta(E) = z_1 z_2 \alpha \sqrt{\frac{\mu c^2}{2E}} \tag{2.71}$$

Here, z_i stands for the atomic number of the particles, α is the fine structure constant, μ is the reduced mass, c is the velocity of light and E is the energy. Redefining $E_g = 2\mu c^2 (z_1 z_2 \alpha\pi)^2$ and substituting in equations (2.71) and (2.70) we have,

$$p = \exp\left(-\sqrt{\frac{E_g}{E}}\right) \tag{2.72}$$

The cross section of the reaction is defined as

$$\sigma(E) = \frac{S(E)}{D} p \tag{2.73}$$

S is an astronomical factor which is introduced to make the energy dependence weaker so that the effects of the Coloumb force are not neglected [13]. It is seen that the cross section of the reaction increases as E increases.

The velocity distribution in general is assumed to be non-degenerate, non-relativistic and one in thermal equilibrium. The following assumptions lead to Maxwellian nature of the velocity distribution of ions in stellar plasma:

1. The collision time is smaller than the time between collisions.

2. Interactions are localized.

3. Velocity of any two particles are not correlated.

4. Energy is locally conserved (there is no energy transfer to fields, etc.,)

Due to the third assumption the total energy is just the sum of the potential and kinetic energies. However, if assumptions 1 and 2 are violated, there is a non-zero correlation between velocities which gives rise to non-local interactions which depend on the momentum and energy of the particle. This gives rise to a distribution which leads to non-extensive statistical mechanics. The probability is altered as

$$p(E) \propto \exp(-\beta E)\exp(-\delta(\beta E)^2) \tag{2.74}$$

where $\delta = \frac{1-q}{2}$. The value of q is close to one, which confirms the almost Maxwellian behaviour in the solar interior. This correction gives a very good match between the predicted and the observed number of the neutrinos. The equation (2.74) was originally developed by Clayton from phenomenological studies[15]. Quarati and co-workers used $q-$deformed statistics to find the analytical relation between δ and q[13, 16].

2.2.0.2 Atmospheric turbulence

When a system is in a non-equilibrium state, there are large-scale fluctuations of parameters both temporally and spatially. However, in such systems we do have local equilibrium, wherein there is a system parameter which is governing a distribution locally, while the system parameter itself is governed by another distribution. In such a scenario, we have superstatistics. Experimentally, this was verified by finding out the wind velocities at two points in an airport in Italy [17]. The points were separated by a distance of 900 meters. Both the spatial as the temporal variation of the wind velocities were recorded at the points. Analysis of the data showed the presence of two temporal scales τ and T. The wind velocity was found to be governed by an energy dissipation factor, which fluctuates slowly on longer time scales T while it varied as τ at shorter length scales. For a particle passing through the entire spatial distance, the probability distribution for its energy is given by

$$p = \exp(-\beta\frac{mv^2}{2})f(\beta)d\beta \tag{2.75}$$

where β is related to the energy dissipation factor. Experimentally this factor is found to follow a Gamma distribution[17]. The distribution of velocities governed by this Γ distribution follows a $q-$deformed Gaussian and the value of q is found to equal $\frac{<\beta^2>}{<\beta>^2}$ [17].

2.2.0.3 Self gravitating systems

A galaxy contains millions of stars, which revolve around the galactic centre in a gravitational potential created by all the stars in it. The potential ϕ created by all stars is a function of the spatial variable. When there are no collisions, the description of the state is given by a distribution function

which evolves in 6-dimensional phase space [18]. The time evolution of the distribution function F is given by the Vlasov equation:

$$\frac{\partial F}{\partial t} + v\nabla_x F + \nabla_x \phi . \nabla_v F = 0 \tag{2.76}$$

Since astronomical phenomena happen in a time scale which is very large compared to human life-span, once can effectively assume the galaxy to be in equilibrium. In equilibrium, the system does not have the memory of the past and has the maximum entropy. To find the distribution, one needs to maximize the entropy. The general procedure adopted to maximize the entropy is to use the technique of Lagrange multipliers which involves using constraints. The constraints are usually the conserved quantities of the system. The obvious choice here is the total energy of the system, which is the sum of kinetic and potential energy as given in equation (2.77) [18].

$$E = m/2 \int v^2 F(x,v) d^3x d^3v - \frac{Rm^2}{2} \int \frac{F(x,v)F(x',v')}{|x-x'|} d^3x d^3x' d^3v d^3v' \tag{2.77}$$

Maximization of $S_{BG} = F \ln F$ leads to an isothermal distribution. However, it violates the fact that the constraint (total energy) which we used to maximize entropy becomes infinity along with the mass of the entire system. In real systems neither is mass infinity nor is the energy infinity. Instead of using the normal Boltzmann-Gibbs entropy if one uses Tsallis' $q-$entropy, these problems do not arise. The long range interaction with the gravitational systems makes the system non-ergodic which is why the use of S_{BG} becomes inappropriate. It was shown in [18] that the polytropic index n is related to q through the following expression :

$$\frac{1}{1-q} = n - \frac{1}{2} \tag{2.78}$$

and that the case $q = 1$, $n = \infty$ corresponds to the iso-thermal sphere [18]. Further it was shown in [18] that for $n < 5$ and $q < \frac{7}{9}$ finite mass and energy is restored. The cut-off arises naturally, and this physically corresponds to the fact that there is an escape velocity associated with every radial coordinate r[18]. The new formalism for entropy introduced by Tsallis, helps in understanding the stellar polytropes. The gravitational force has long range interaction and this could be a possible reason for failure of S_{BG} in giving accurate results. It must be noted that S_q was not enunciated for astronomical problems. S_q was only introduced to generalize the entropy, as the original entropy due to Boltzmann and Gibbs were based on certain assumptions. However the use of this generalized entropy as resulted in many interesting results in the field of stellar polytropes[18].

2.2.0.4 Relaxation and aging in long range interaction

Consider a system containing N particles each with unit mass, and each of which interacts with all other particles. Each particle rotates about itself and each is described by an angle θ_i and its conjugate momentum p_i. The system is defined by the Hamiltonian [19]

$$H = \Sigma_{i=1}^{N} \frac{p_i^2}{2} = \frac{1}{2N} \Sigma_{i,j=1}^{N} 1 - (\cos(\theta_i - \theta_j)) \tag{2.79}$$

Associated with this system is an order parameter which is defined as $\vec{M} = \frac{1}{N}\sum_i \vec{m}_i$ where $\vec{m}_i = (cos\theta_i; sin\theta_i)$. This system shows a phase transition where there is a non zero value of $\vec{M}$ at lower values of a control parameter T. The equations describing the system are given by,

$$\begin{aligned} \dot{\theta}_i &= p_i \\ \dot{p}_i &= M_y \cos\theta_i - M_x \sin\theta_i \qquad i = 1...N \end{aligned} \tag{2.80}$$

The fixed points occur for $p_i = 0$ and $\frac{M_x}{M_y} = cot\theta_i$. For the linearized system, the ith block diagonal of the $2N \times 2N$ Jacobian matrix of this system is given by $\begin{bmatrix} 0 & 1 \\ -M_y \sin(\theta_i) - M_x - \cos\theta_i & 0 \end{bmatrix}$
Depending upon the values of θ_i and M_i, the eigenvalues can take different values. Thus we see that the initial conditions play a very vital role in this system. Certain initial conditions get trapped in quasi-stationary states and remain trapped there for a long time. To analyze the system the 2-time auto-correlation function was used [19] which is dependent upon the history of the system. On attaining genuine equilibrium the memory effects disappear – the auto-correlation functions $C(t,t')$ do not depend upon the system's history, but rather depend only upon time differences: $C(t,t') \equiv C(t-t')$. In [19], the system was initially prepared with random momentum and zero positions for all N particles. (N was chosen to be 1000). The system was allowed to evolve and the 2-time auto-correlation functions were calculated from the simulation for all realizations. It was noted that for various values of t equal to waiting time t_w, the system remains trapped in the quasi-stationary states. The longer the waiting time, longer is the 2-time auto-correlation function and slower their decay [20]. This phenomenon is called aging, as these states take a longer time to reach equilibrium[20]. The time taken by the system to time to reach equilibrium depends upon the system size. For an infinitely large system, equilibrium is never a possibility. The 2-time auto-correlation functions follow a $q-$exponential. The angles of the mean field Hamiltonian also follow the q-deformed Gaussian[20]. This dynamics is similar to spin glass dynamics which shows aging phenomenon [19].

2.2.0.5 Diffusion in Hydra Vulgaris

Hydra vulgaris is an organism that lives in water and moves using its tentacles. It has a cylindrical body. Its inner cells, the endodermal cells have an adhesive property. An experiment was performed to measure the vertical component of the velocity v_y of the endodermal cells in an aggregate of (outer) ectodermal cells [21]. The results confirm that the probability distribution for the velocities follows a q distribution, given by

$$p(|V_y|) = \frac{p(0)}{[1+(q-1)(\frac{V_y}{V_0})^2]^{\frac{q}{q-1}}} \tag{2.81}$$

Here normal diffusion is not possible due to strong adhesion between the endodermal cells leading to long range interactions between the cells [21].

2.2.0.6 Earthquakes

Seismic data which have spatial and temporal components are complex in nature as the events are global in nature. All the tectonic plates are connected to each other due to which there is a long-range interaction[22]. Analysis from two seismic zones (Japan and California) revealed that the calm time, which is the time between two earthquakes followed a $q-$deformed exponential[23].

2.2.0.7 Foraging Movements and Food search in Amoeba

The foraging movements of the albatross, the bumble bee and deer were collected and it was found that their search patterns did not follow a Gaussian distribution [24, 25, 26]. Amoebae live in the soil and engulf bacteria for food[27]. Initially, it was assumed that the movement of an amoeba in search of food is Gaussian. Similarly experiments confirm that the amoeba follows a common gradient that attracts it towards its food. The interaction between the amoeba's receptors and the external chemical signals it receives makes the system non ergodic, thus following a non-Gaussian distribution for its movement.

2.2.0.8 Identification of tumours and micro-calcification in medical images. Tsallis' statistics in image processing

MRI (Magnetic Resonance Imaging) is used extensively to distinguish between various tissues all over the body. This technique is particularly useful to study the brain, where other invasive methods could potentially be harmful. A diagnosis of brain tissues helps to identify certain conditions in the early stage of tumours, which enhances the probability of saving the individual when detected early[28, 29]. In greyscale, different tissues in the brain have different shades of gray. Each shade is represented by a particular pixel in which the luminosity itself can vary from 20 to 90 units. The values in this range corresponds to a particular value of entropy. Image processing separates the regions of cerebro-spinal fluid from the gray matter and the white matter. The value of q dictates the degree of correlations between the various pixels which are taken from the image of the same object. The pixels which show scale invarince spatially and are correlated in terms of grey scales denote the long range interactions[29]. It has been shown in [29], that the use of $q-$deformed entropy, is able to clear demarcate the various regions of the brain, thereby making identifications easier.

Mammograms are images of breast tissue which show the extent of micro-calcification. The presence of micro-calcification acts as an early signal to detect cancer. Thus, identifying the micro-calcification in the tissue at an earlier stage can save a life. In a dense breast tissue micro-calcification is hard to identify — fat appears dark while glands, ligament and stroma appear white. Tumours and micro-calcification are also white in colour, which makes it difficult to identify them. However the micro-calcification and the tumour that grows are fractal in nature[30]. Since mammograms have long range interaction, long time memory and capture fractal growth, use of Tsallis' statistics helps in processing the image and showing the diseased part clearly[30]. This

image processing also uses fuzzy logic to assign a q index for various grades of the mammogram. The more advanced the disease, the greater is the non-extensiveness of the entropy in the mammogram.

2.2.0.9 Momentum distribution of cold atoms in an optical lattice

Optical lattices are created by lasers which trap atoms in a specific place. "Cold" atoms are called so as their kinetic energies are very small. The laser beams interfere with each other, creating constructive and destructive patterns spatially onto which the atoms sit [31]. Depending on the strength of the beam the potential created by it may be weak or strong. The stronger potentials separate the atoms from each other, while weak potentials allow the atoms to interact. The moment the laser beams are removed, the atoms start diffusing and their momentum distribution is captured. It is found that the momentum distribution of shallow potentials follow a $q-$Gaussian while those from stronger potentials follow a Gaussian. These results prove experimentally that long range interactions alter the momentum distributions. This had in fact been theoretically predicted by solving the Fokker-Planck equations which yielded solutions that resembled the Tsallis distribution [32].

2.2.1 Conclusions

The basic assumptions of standard statistical physics do not suffice to understand observations in the various systems discussed above and require the use of Tsallis' formulation of non-extensive statistical mechanics to explain the observations. These have been concisely summarized in Table (2.1).

Thus we clearly see that q-deformations come in handy, when classical assumptions fail. For ecological systems, most of the modelling is done after excluding the external world. By isolating interacting species from other species while constructing models, the system acquires the form of a microcanonical ensemble. However this is an over-simplification since actually the system interacts with the environment. Now the environmental parameters themselves are not constant as they depend upon the seasons, the diurnal length, etc. Some parameters change locally, while some change globally. In Subsection 2.2.0.2 (Atmospheric turbulence) fluctuations in a global variable affected the distributions locally. Similarly in 2.79 (Relaxation and aging in long range interactions), co-existence of attractors were seen. Co-existence of attractors immediately signifies the sensitivity to the choice of initial conditions, which automatically breaks the ergodicity of the system under consideration. Subsection 2.2.0.7 (Foraging in animals) discussed how chemosensory receptors responded to chemical signals, and made the amoeba diffusion non-Gaussian. Similarly in the ecological system we discuss in Chapter (4-7), the larch budmoth selectively responds to fresh foliage rather than to the damaged foliage. This again makes the system non ergodic. Moreover the system has memory of past events and has several varying parameters.

S.No	System	The problem Statement	Reason for failure of classical physics
1	Finding reaction rates for various particles in the solar interior	Discrepancy in the amount of neutrinos predicted and observed	Exclusion of long range interactions
2	Atmospheric Turbulance (systems which are not in equilibrium)	System in local equilibrium have two time scales thus their distribution is not Gaussian.	Fluctuation in the system parameter
3	Self gravitating system	Finding the distribution of stars in gravitational potential leads to isothermal distribution with infinite energy and mass	Exclusion of long range interactions
4	Relaxation and aging in certain lattices	System shows sensitivity to initial condition and thus may never reach equilibrium.	Existence of quasi stationery states & memory of past states
5	Diffusion of cells in Hydra vulgaris	Adhesive endodermal cells do not diffuse normally	Exclusion of long range interaction
6	Studies on earthquake data	The spatial and temporal pattern of earthquakes follow $q-$exponential	Complex interaction in space and time
7	Foraging movement of albatross, bumble-bee and deer; Food searching by amoeba	A fit of the movement data of various animals turned out to follow a power law distribution	Searches are not random but based on information extracted by organism & memory of the past
8	Cold atoms distribution in an optical lattice	The momentum distribution of cold atoms is not Gaussian	Exclusion of long range interactions
9	Image Processing in MRI and mammograms	The healthy tissues and the diseased ones demarcated better using Tsallis' statistics	Long range interaction and fractal nature of growth of tumor.

TABLE 2.1. Applications of $q-$ deformation to various fields and the reason for failure of classical statistical mechanics.

CHAPTER 3

APPLICATION OF Q-DEFORMATION TO SOME 2-DIMENSIONAL NONLINEAR MAPS

Q-deformations have been applied to many areas of physics — in flows and in maps. The simplest map where q-deformation is studied in the literature is the logistic map [33, 34]. It was shown there that the deformation parameter q controlled the onset of chaos. For certain values of q the system is periodic, while for certain values it is completely chaotic. Attractors co-exist which imply a possible hysteresis in the system. In [34], an application of such a q deformed map is discussed where starting from a losing side one can go to the winning side in fewer iterations, as the q-deformation changes the concavity of the map. In [35] q-deformations were applied on a Gaussian map. The map under q-deformation showed co-existence of attractors and displayed bubbling effect which has interesting implications which will be discussed later. In [36] q-deformation was applied to a 2 dimensional map (Henon map) and the parameter space was explored for chaotic and periodic domains. As q varied, the regions that were periodic become chaotic.
In this chapter we use the deformation technique and study four well-known maps.

3.0.2 Duffing Map

The Duffing equation models a damped oscillator in which the elasticity of the spring is nonlinear with a cubic term. The equations for the forced Duffing oscillator are given by

$$\frac{d}{dt}\begin{pmatrix} x \\ y \\ \psi \end{pmatrix} = \begin{pmatrix} y \\ -\delta y - \beta x - \alpha x^3 + \gamma \cos\psi \\ \omega \end{pmatrix} \tag{3.1}$$

Here ψ is the frequency with which the system is forced. By choosing a constant ψ plane one can study the Poincare section of the system. To generate the Poincare plane, the following method is adopted. The simulation is run for a long time, the transients are discarded, and the values of

the three variables that govern this system are recorded. To construct a Poincare section, a plane must be defined. The choice of the plane is not holy, as any choice can be made. For simplicity, we choose the $\psi = 0$ plane. From the data generated, x and y are plotted whenever ψ=0. The system is periodic if all the points generated fall at a single point on the plane. If the points smear on the plane the system is chaotic. Depending on the distribution of points one can determine the nature of the system. The Poincare map for the Duffing Oscillator is given by,

$$X_{n+1} = Y_n \tag{3.2}$$

$$Y_{n+1} = -bX_n + aY_n - Y_n^3 \tag{3.3}$$

Fig.3.1 shows the Poincare section of the Duffing oscillator.

Figure 3.1: Poincare section of the Duffing Map

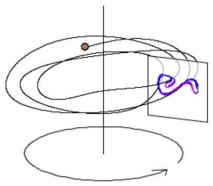

3.0.2.1 Linear Stability analysis

The linear stability matrix, which is constructed from the first derivatives of the map, allows us to study the local behavior of the system around the fixed point. The q-deformed Duffing map is given by:

$$X_{n+1} = \frac{Y_n}{1+(1-q)(1-Y_n)} \tag{3.4}$$

$$Y_{n+1} = -b\frac{X_n}{1+(1-q)(1-X_n)} + a\left(\frac{Y_n}{1+(1-q)(1-Y_n)}\right) - \left(\frac{Y_n}{1+(1-q)(1-Y_n)}\right)^3 \tag{3.5}$$

It is immediately evident that the value of q decides the nature of stability of the concerned fixed points. Determination of fixed points other than $(0,0)$ for the deformed system is non-trivial and may be numerically obtained. For the undeformed map, the fixed points are $(0,0)$, $(\sqrt{(a-b-1)}, \sqrt{(a-b-1)})$ and $(-\sqrt{(a-b-1)}, -\sqrt{(a-b-1)})$. The linear stability matrices J_1 and J_2 respectively for the undeformed and the deformed maps at the fixed point $(0,0)$ are:

$$J_1 = \begin{pmatrix} 0 & 1 \\ -b & a \end{pmatrix} \quad : \quad J_2 = \begin{pmatrix} 0 & \frac{-1}{q-2} \\ \frac{b}{q-2} & \frac{-a}{q-2} \end{pmatrix}$$

J_1 has eigenvalues $\frac{a\pm\sqrt{a^2-4b}}{2}$, while for the deformed system the eigenvalues are $-\frac{-a\pm\sqrt{a^2-4b}}{2(q-2)}$. The attractor for the deformed and undeformed systems are plotted for the choice $a = 2.77$ and $b = 0.1$ as the parameter q is varied from -2 to 2 (Fig.(3.2(a))). For this choice of a and b, the origin is unstable for the undeformed system [37] while the deformed system also shows an unstable origin until $q = 2$

after which origin becomes stable [38]. In Figure(3.2(a)) we have plotted the entire 2 dimensional bifurcation diagram for the q-deformed Duffing map as $q5$ is varied, the various colours indicating different q values. The classic "S" shaped attractor which the Duffing map is always associated with, occurs at q=1. Below and after the value of $q = 1$, the system's attractor is restricted to negative and positive values respectively which is shown in Fig.(3.2(a)). Satellites appear in both the positive and negative wings corresponding to $q > 1$ and $q < 1$ respectively. The close-up snapshots depicted in Fig.(3.2(b) and 3.2(c)) reveal the structure of the satellites. Satellites occur whenever there is an interior crisis. Interior crises refer to changes in the shape of the attractor[39]. This happens when the stable manifold of a saddle falls on an attractor making the entire attractor stable, and leading to a sudden expansion in its size. The satellites appear only for certain values of initial conditions, implying that there is coexistence of attractors. Although the bifurcation diagram looks symmetric, it is really not so as closer inspection reveals that there are differences in the structure of the satellites that lie alongside the main attractor. The satellites occurring for $0.9593 < q < 0.9599$ is a part of a cascade[40] which begins abruptly which as shown in figure(3.2(c)). However the satellites which occur for $1.13 < q < 1.14$ show an entire period doubling cascade, each starting from a single branch (Fig.(3.2(b)). The figure(3.2(d)) shows the co-existance of attractor in the Duffing map. The values of the initial condtions are $x = 0.01$, while y is changed. $y = 0.1$ for the gray shade attractor, while it is equal to 0.2 for the attractor shown in color[37].

3.0.2.2 Applications

In high energy physics experiments require particles travel at relativistic speeds. To attain such speeds, the particles are accelerated using high electric fields while magnetic fields bend and turn the trajectories of the particles to keep them inside the accelerator. The longer the particle stays in the accelerator, the greater is the speed it achieves. The intention is to have the particle visit the same point in that accelerator despite going many round trips. Since the particles go around the accelerator many times, even a slightest deviation from the design trajectory crashes the particles on the walls of the accelerator leading to loss of particles [41]. In a circular accelerator, maintaining the particle in the designed trajectory and having it visit the same point despite going round many trips is a very big task. Particle physicists define a quantity called the tune[41] of the machine which is a measure of the phase advance acquired by the particle after completing a round trip in the accelerator. All particles in an accelerator have the same tune [41]. Each particle is tagged by its tune and its momentum, the latter being referred to as its "amplitude". Tune is a constant in the case of a linear accelerator, while it is a function of the amplitude for nonlinear including circular accelerators. A Poincarë section or a plane defined on the particle trajectory records the particle motion whenever the particle passes the plane.

To contain the particles in the design trajectory, powerful magnets are used. The magnetic field itself is controlled by the temperature felt by the magnets and the electric supply that is fed to the magnets. Any fluctuations in these parameters can change the actual magnetic field which in turn

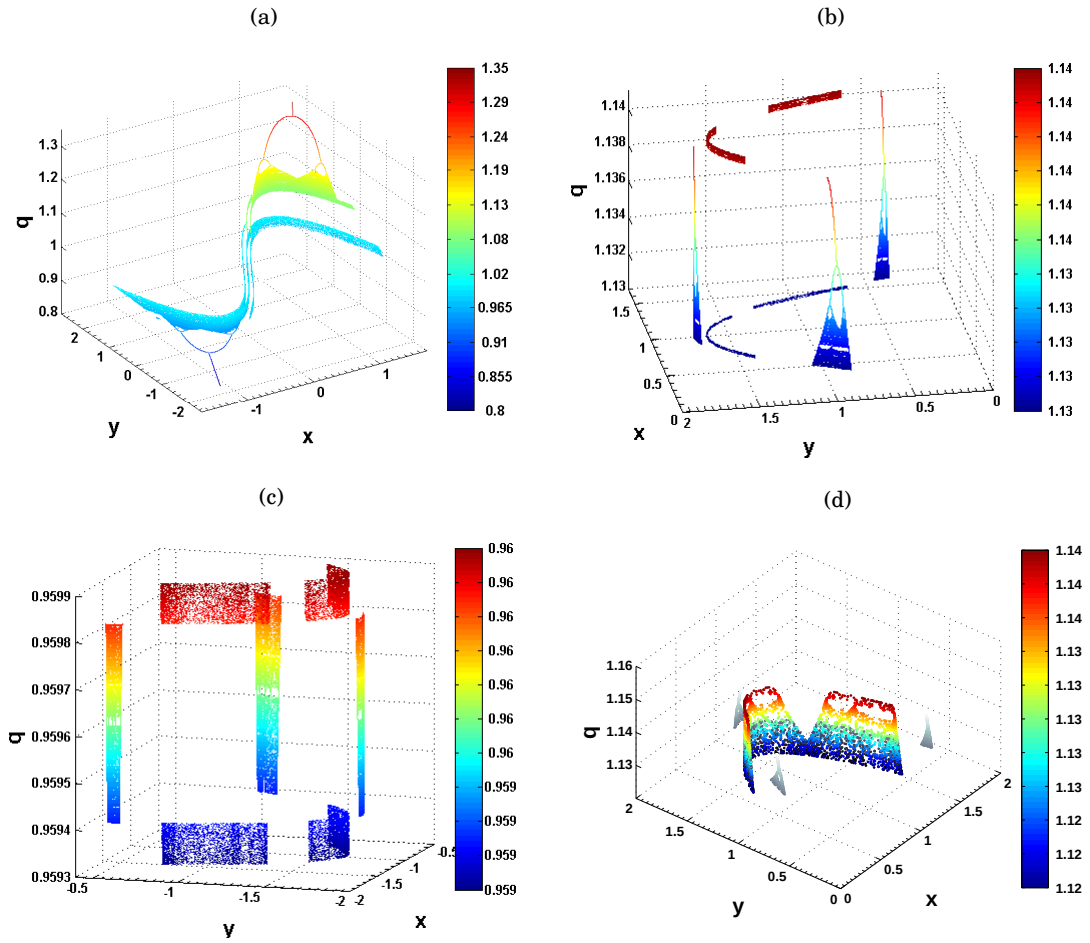

FIGURE 3.2. The values of the parameters are $a = 2.77$ and $b = 0.1$. The initial conditions chosen are $x = 0.01$ and $y = 0.1$. For a different choice of initial condition $x = 0.01$ and $y = 0.2$ the satellites are not present.(a)The 2-D bifurcation diagram of Duffing map for various values of q ranging from $0.8 to 1.3$. (b)The 2-D bifurcation diagram of Duffing map revealing the satellite for values of q between 1.13 and 1.14. (c) The 2-D bifurcation diagram of Duffing map revealing the satellite for values of q between 0.9593and 0.9599. (d) The map showing co-existence of attractor. The choice of the initial conditions are $x = 0.01$ and $y = 0.1$ (colored attractor). and $x = 0.01$ and $y = 0.2$ (attractor in grey shade).

would affect the particle trajectory. With ground vibrations and other factors included this becomes a problem in 6 dimensions.

The Duffing equation was first employed in accelerator physics to address the important problem of preserving the beam size which is influenced by tiny fluctuations in the power supply of the guiding magnets in the superconducting supercollider. Protons circulating in the ring collider are influenced by an additional force for their transverse motion arising from the magnetic field ripples in the electric power supply which feed the dipole magnets in the accelerator. In the absence of fluctuations in the power supply and other nonlinearities the transverse motion of a proton inside the accelerator is given by

$$\frac{d^2x}{ds^2} + K(s)x = 0 \tag{3.6}$$

where x is the particle's deviation from the design trajectory, $K(s)$ represents the strength of the quadrupole magnets located at position s inside the accelerator[42]. With suitable coordinate transformation the equation (3.6) can be reduced to that of a simple harmonic oscillator, which results in a constant tune and constant beam emittance which is related to the average spread of the particle's position and momentum.

Fluctuations in the electric field and magnetic field nonlinearities make the tune a function of the amplitude (momentum), and the emittance non-constant. There is a quadratic relationship between the tune and the particle's momentum, which can be taken into consideration most easily by adding a cubic term in eqn.(3.6) giving the Duffing equation for the equation of motion [42] :

$$\frac{d^2\chi}{d\phi^2} + \omega^2\chi + \epsilon\alpha\chi^3 = 0 \tag{3.7}$$

where $\epsilon\alpha$ is related to the magnetic field strength. χ and ϕ are related to the old coordinates x and s respectively [42]. The right hand side which is zero becomes a periodic function of time when the magnetic field ripples are taken into consideration.

Since the number of components (number of magnets) in an accelerator is large, it was proposed by Forest and Hirata [43] that a one turn map can be used instead of differential equations, capturing all the relevant dynamics [44]. Instead of the Duffing equation one can use the Duffing map to study the particle trajectory in the accelerator [44].

The variables x and y of the Duffing map represent the position and the momentum of the particle.

Since we desire that the proton should not stray away from the desired trajectory, it immediately implies that the attractor size should be smaller. In the q-deformed Duffing map when q was varied from -10 to 10, the following features were noted.

1. For $-10 < q < -0.63$, $(0,0)$ is the only fixed point.

2. For $-0.63 < q < 0.88$ we have a single non zero fixed point.

3. For $0.88 < q < 1.31$, the attractor size increases with the system being most chaotic at $q = 1$.

4. For $1.31 < q < 3.47$ we have a single non zero fixed point.

5. For $3.47 < q < 4.81$, the attractor size increases.

6. for $3.47 < q < 10$, $(0,0)$ is the only fixed point.

For $q < -0.63$ and for $q > 3.47$, there is only one fixed point which is $(0,0)$. However the aim of an accelerator is to accelerate the particles which implies a non zero value for velocity, so that a choice of q in these regimes is to be avoided. For $-0.63 < q < 0.88$ and $1.31 < q < 3.47$, there is only one non-zero fixed point and the velocity remains constant. For $0.88 < q < 1.31$, and $3.47 < q < 4.81$, the attractor size is larger, but not as large as for the case $q = 1$. So this region of q could allow acceleration to occur while minimizing the spread in the particle's position and momentum.

If the system's behaviour were to change due to changes in the surroundings, one could use q-deformations as a means to model the system. The limit $q \to 1$ essentially restores the system to the isolated, ergodic case with no effects of changing environment or system conditions. In the context of the particle accelerator, apparently tiny changes in the magnetic field due to fluctuations or the effects on the particles due to interactions of the emitted radiation with the surroundings may all culminate in influencing the dynamics of a pasrticle. This may manifest itself in the form of a memory effect where the previous location of the particle is crucial in its behaviour.

3.0.3 Ikeda Map

Ikeda map [45] was formulated by K. Ikeda to model light going through a nonlinear optical resonator. The laser light beams interact through an absorber in the ring cavity and the complex interactions leads to chaotic behavior of the transmitted light. Adding $q-$deformations makes it spell a variety of behaviors.

The modified Ikeda map which is considered here is obtained by ignoring saturable absorption in the original Ikeda map. Saturated absorption occurs when most of the electrons in an atom are in a high energy state and the ground state is devoid of any electrons. Under these circumstances the in-phase and the out-phase components of the electric field in the resonator are denoted by x_n and y_n, where n is the number of turns the laser beam has traversed inside the ring resonator. The variable t_n is the phase shift picked up after a round trip. The equations for Ikeda map are given by

$$x_{n+1} = A + u(x_n \cos t_n - y_n \sin t_n) \tag{3.8}$$

$$y_{n+1} = u(x_n \sin t_n + y_n \cos t_n) \tag{3.9}$$

$$t_n = B - \frac{C}{1 + x_n^2 + y_n^2} \tag{3.10}$$

A denotes the intensity of the incoming laser beam immediately after the first mirror and u denotes the reflection coefficient of the mirrors. A higher the value of u implies lesser intensity-loss and thereby greater amplification. B is the value of the phase shift of the empty cavity and C determines the speed with which the phase shift changes with intensity of light in the absorber. The extent of departure of the difference $(B-C)$ from an integer mulltiple of 2π determines the degree of detuning

in the cavity. The higher the detuning, the greater is its departure from the resonant frequency. In a normal Ikeda map, as A increases, $x_n^2 + y_n^2$ increases, t_n varies from a minimum value of $B - C$ to B. When C is large t_n begins to oscillate. Some of the main assumptions that were used to derive the Ikeda map are

1. The electric field, polarization and the number of photons are varying slowly, i.e., these are constant with respect to the optical period and wavelength.

2. There are no free charges in the absorber material used in the cavity.

3. There is no spatial modulation of the laser perpendicular to the direction of propagation, which enforces that we are dealing with plane waves.

It was shown by Hammel *et al* [46] that $\det J = u^2 < 1$ where J is the Jacobian matrix for the Ikeda map leading them to conclude that local bifurcations such as the period doubling bifurcation and saddle node bifurcation only can occur since this is an area contracting map while Hopf bifurcations are immediately excluded[47]. The $q-$deformed Ikeda map is:

$$x_{n+1} = A + u\left(\frac{x_n}{1+(1-q)(1-x_n)}\cos t_n - \frac{y_n}{1+(1-q)(1-y_n)}\sin t_n\right) \tag{3.11}$$

$$y_{n+1} = u\left(\frac{x_n}{1+(1-q)(1-x_n)}\sin t_n + \frac{y_n}{1+(1-q)(1-y_n)}\cos t_n\right) \tag{3.12}$$

$$t_n = B - \left(\frac{C}{1+\left(\frac{x_n}{1+(1-q)(1-x_n)}\right)^2 + \left(\frac{y_n}{1+(1-q)(1-y_n)}\right)^2}\right) \tag{3.13}$$

It is noted from the bifurcation diagram that the in-phase and the out-phase electric field are bound to smaller values for $q < 1$, while these become large and unbounded for $q > 1$. The bifurcation diagram shown in figure (3.3(a)) shows interior crises, which is sudden increase in the size of the attractor. At $q = 1$, the original attractor is restored (Figure (3.3(b))). One sees co-existence of attractors in this system. At higher values of q there is interior crisis, however the points are almost confined to two lines appearing to intersect each other as shown in Figure (3.3(c)). There are periodic and chaotic domain that alternate, which is visible from the figures(3.3(d) and 3.3(e)). The figures (3.3(d) and 3.3(e)) are the 1 D bifurcation diagrams, which show the behavior of variable x and y as the parameter q is varied (with all other parameters fixed). Figures(3.3(f) and 3.4(a)) show the alternating domains of periodicity and chaos, as the parameter q is varied. Figures(3.3(f) and 3.4(a)) show the details of Figures (3.3(d)) and (3.3(e)).

3.0.4 Tinkerbell Map

The name Tinkerbell is given to this map, due to the shape of the attractor which resembles Tinker Bell's movement over Cinderella's castle, in Disney pictures. The equations that govern the

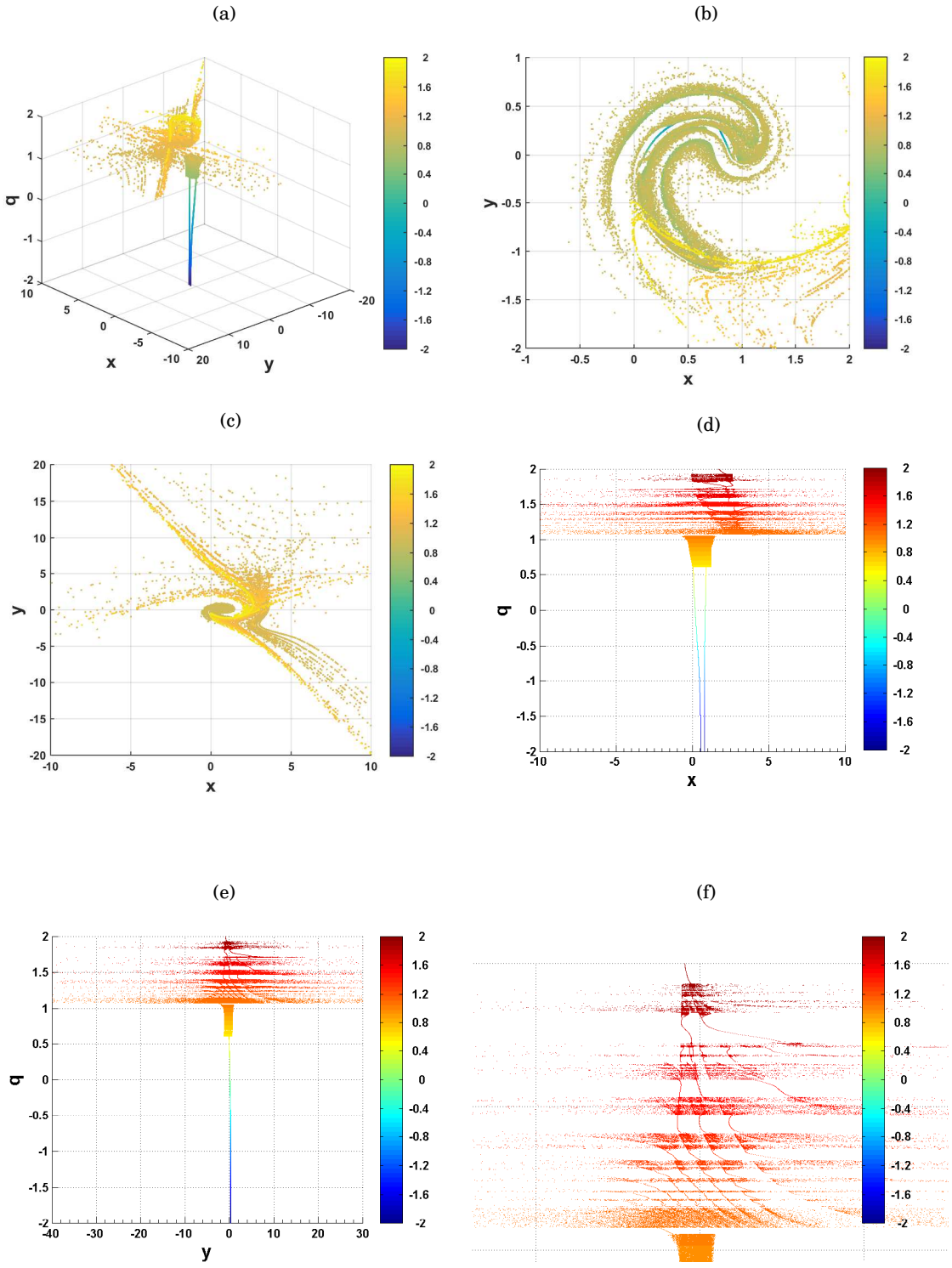

FIGURE 3.3. 2-D bifurcation diagram of Ikeda map for different q values (in colourscale). Parameters: $B = 0.4$, $A = 1$, $C = 6$ and $u = 0.9$. (a)for q ranging from -2 to 2. (b)for q ranging from -2 to 2, showing the classic attractor at $q = 1$ (grey shade). (c) for $q > 1$ (till $q = 2$). (d) x vs q. (e) y vs q. (f) inset of bifurcation diagram shown in Fig.(3.3(d)) (x vs q).

(a)

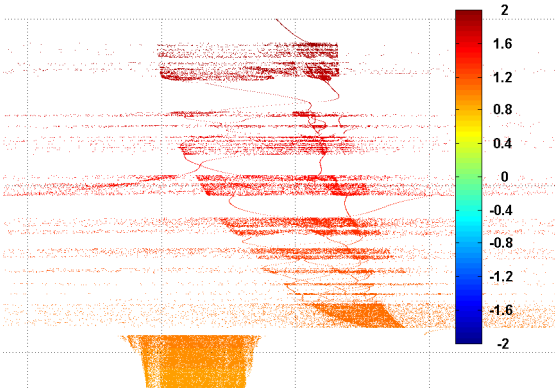

FIGURE 3.4. (a) Inset of the bifurcation diagram of the Ikeda map shown in Fig.(3.3(e))(y *vs* q). Parameters: $B = 0.4$, $A = 1$, $C = 6$ and $u = 0.9$.

Tinkerbell map are

$$x_{n+1} = x_n^2 - y_n^2 + ax_n + by_n \tag{3.14}$$

$$y_{n+1} = 2x_n y_n + cx_n + dy_n \tag{3.15}$$

The deformed map is given by[48],

$$x_{n+1} = \left(\frac{x_n}{1+(1-q)(1-x_n)}\right)^2 - \left(\frac{y_n}{1+(1-q)(1-y_n)}\right)^2 + a\left(\frac{x_n}{1+(1-q)(1-x_n)}\right) \tag{3.16}$$

$$+b\left(\frac{y_n}{1+(1-q)(1-y_n)}\right) \tag{3.17}$$

$$y_{n+1} = 2\left(\frac{x_n}{1+(1-q)(1-x_n)}\right)\left(\frac{y_n}{1+(1-q)(1-y_n)}\right) + c\left(\frac{x_n}{1+(1-q)(1-x_n)}\right) \tag{3.18}$$

$$+d\left(\frac{y_n}{1+(1-q)(1-y_n)}\right) \tag{3.19}$$

The map is chaotic for values of $a = 0.9, b = 0 - 0.6013, c = 2$ and $d = 0.50$ and $a = 0.3, b = 0.6$, $c = 2$ and $d = 0.27$. The following figures show the Tinkerbell map as the parameter q is varied.

3.0.4.1 Linear Stability Analysis

Linear stability analysis helps in investigating the local behavior of the system around the fixed point. The Jacobian matrix of the original Tinkerbell map is given by $\begin{pmatrix} 2x_n + a & b - 2y_n \\ 2y_n + c & 2x_n + d \end{pmatrix}$

The eigenvalues are found from the characteristic equation:

$$\lambda^2 + A(x_n, y_n)\lambda + B(x_n, y_n) = 0 \tag{3.20}$$

where

$$A(x_n, y_n) = -(4x_n + a + d) \tag{3.21}$$

$$B(x_n, y_n) = (2x_n + a)(2x_n + d) + (2y_n + c)(2y_n - d) \tag{3.22}$$

Depending on the values of the parameters, the Tinkerbell map can have one to four fixed points[49]. Any fixed point $Z(x, y)$ is stable if it follows the following conditions [49]:

$$(a-d)^2 > 4(2y + c)(2y - b) \tag{3.23}$$

with

$$\begin{aligned} max(-2, -1 - B(x_n, y_n)) &< 4x + a + d \\ &< min(2, -1 - B(x_n, y_n)) \end{aligned} \tag{3.24}$$

(or)

$$(a-d)^2 < 4(2y + c)(2y - b) \tag{3.25}$$

with

$$-2 < -1 - B(x_n, y_n) < -1 \quad , \quad x \neq 0 \text{ or } \ y \neq 0 \ . \tag{3.26}$$

At the fixed point $(0,0)$, the Jacobian becomes $\begin{pmatrix} a & b \\ c & d \end{pmatrix}$.

In what follows (unless specified otherwise), all the figures and numerical work have been done by us using the following set of values for which the Tinkerbell map exhibits chaotic behaviour: $a = 0.9$, $b = -0.6013$, $c = 2.0$ and $d = .5$. The initial conditions chosen are $x_0 = -0.72$ and $y_0 = -0.64$.

The Jacobian for the q-deformed Tinkerbell map is: $\begin{pmatrix} E & F \\ G & H \end{pmatrix}$

where the various entries are

$$\begin{aligned} E &= -\frac{(q-2)(9qx + 11x - 9q + 18)}{10(2 - q - x + qx)^3} \\ F &= \frac{(q-2)(6013qy + 13987y - 6013q + 12026)}{10000(2 - q - y + qy)^3} \\ G &= -\frac{2(q-2)(qy - q + 2)}{(2 - q - x + qx)^2(2 - q - y + qy)} \\ H &= -\frac{(q-2)(qx + 3x - q + 2)}{2(2 - q - x + qx)(2 - q - y + qy)^2} \end{aligned} \tag{3.27}$$

We see that the stability of the system is altered depending on the value of q. The characteristic equation for the q-deformed Tinkerbell map is given below

$$\lambda^2 + A(x_n, y_n)\lambda + B(x_n, y_n) = 0 \tag{3.28}$$

$$A(x_n, y_n) = -(E + H) \tag{3.29}$$

$$B(x_n, y_n) = EH - GF \tag{3.30}$$

$(0,0)$ is one of the fixed points of the system. The Jacobian at this point is given by,

$\begin{pmatrix} -\frac{0.9}{2-q} & -\frac{0.6013}{2-q} \\ -\frac{2}{2-q} & -\frac{0.5}{2-q} \end{pmatrix}$

which is similar to the original map, except that it is scaled by a factor of $\frac{1}{2-q}$. Without solving for the eigenvalues of the Jacobian, one can determine the stability of the fixed point by using the Routh-Hurwitz criterion[50, 51]. Routh-Hurwitz coefficients are extracted from the characteristic equation which we obtain from the Jacobian matrix. The Routh array for the undeformed Tinkerbell map at the fixed point $(0,0)$ is given by

$$\begin{pmatrix} 1 & \frac{8263}{5000} \\ \frac{-7}{5} & 0 \\ \frac{8263}{5000} & 0 \end{pmatrix}$$

For the deformed Tinkerbell Map at the fixed point $(0,0)$, we find that the Routh array is:

$$\begin{pmatrix} 1 & \frac{8263}{5000(q-2)^2} \\ \frac{7}{5(q-2)} & 0 \\ \frac{57841((5q)/7-10/7)}{25000(q-2)^3} & 0 \end{pmatrix}$$

From the two Routh arrays presented above it is clear that for the $q-$deformed system and for $q > 2$, the origin is a stable fixed point as signs of all the entries of the Routh coefficients are the same. On the other hand, for the undeformed system and for $q-$deformed system with $q < 2$, the origin is unstable.

Analysis of the 2-Dimensional bifurcation diagram reveals new behavior of the q-deformed Tinkerbell map. The Tinkerbell map is simulated for the following values of the parameters and initial conditions: $a = 0.9$, $b = -0.6013$, $c = 2.0$, $d = .5$, $x_0 = -0.72$ and $y_0 = -0.64$. q is varied from 0 to 4. The entire attractor is shown in Fig.(3.5(a)). For values of $0 < q \leq 1$, the system is more or less bounded as shown in Fig.(3.5(f)). In Fig.(3.5(f)), q is varied from 0.7 to 1. From $q = -2$ till $q = 0.7$, there is only one fixed point, which is not shown in the figure. The q-deformed Tinkerbell map undergoes a Neimark-Sacker bifurcation when $q = 0.7$. The limit cycles grow in size and as $q = 1$, the original system is restored which is chaotic as seen in Fig.(3.5(a)). As q increases the size of the limit cycle grows. From the two dimensional bifurcation diagram, formation of paired cascades is seen. Paired cascades are created when the montonicity of the system is lost [40]. A paired cascade is made of equal numbers of period-doublings and period-halvings that result in closed structures like bubbles. Depending upon the values of other parameters, the degree of period halving and period doubling would vary. Sometimes there may be just one period-doubling followed by period-halving resulting in a closed structure, while sometimes one may have a more complicated structure also. Figures (3.5(b),3.6(a)), show a paired cascade. The figure(3.6(b)), shows the blow up of figure(3.6(a)), which shows the closed bubble structure more clearly. From the $x-y$ view it is clear that disconnected point of the attractor at $q = 0.945$ slowly grows in size via period-doubling and becomes connected with increasing q. Beyond $q = 1$, interior crises occur that expand the size of the attractor. For certain values of q, the attractor is split and looks disconnected (Fig.(3.5(c))). For values of $3.2 \leq q \leq 3.3$, the system shows 3 limit cycles and one fixed point. Out of the 3 limit cycles, 2 of them belong to the same basin of attraction, and any initial condition that is attracted to this basin, hops between the limit cycles (A and B) as depicted in Figures (3.5(d) and 3.5(e)). The other limit cycle (C) co-exists solitarily along with the fixed point (D). We find that as q is increased from 3.2 to 3.3, the two limit cycles grow in size and are created via Neimark-Sacker bifucation, while

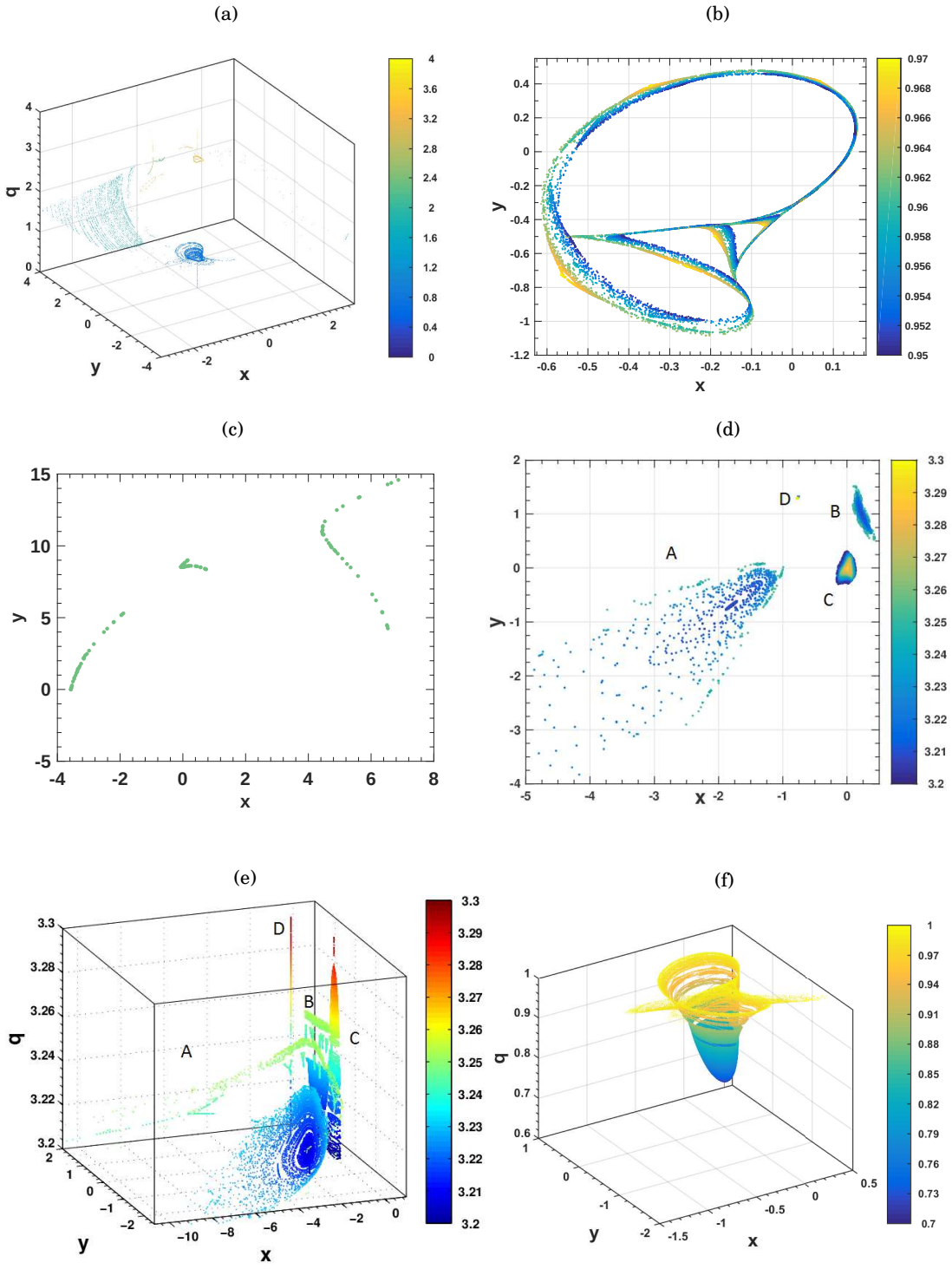

FIGURE 3.5. (a)The 2-D bifurcation diagram of Tinkerbell map for values of q from 0 to 4 with $a = 0.9$, $b = -0.6013$, $c = 2.0$, $d = .5$, $x_0 = -0.72$ and $y_0 = -0.64$. (b)X-Y view of a paired cascade (q varying from 0.945 to 0.97.). (c) Disconnected attractor at $q = 1.57$ (d) $x - y$ view of the Tinkerbell attractor for larger values of q ($3.2 \leq q \leq 3.3$). The limit cycles are labeled A B C. D is the fixed point. (e) Tinkerbell-map attractor for q ($3.2 < q < 3.3$), showing three limit cycles and fixed point.The limit cycles are labeled A B C. D is the fixed points. (f) The 2-D bifurcation diagram of Tinkerbell map showing the attractor from $q = 0.7$ to $q = 1$. Neimark-Sacker bifurcation occurs at $q = 0.7$.

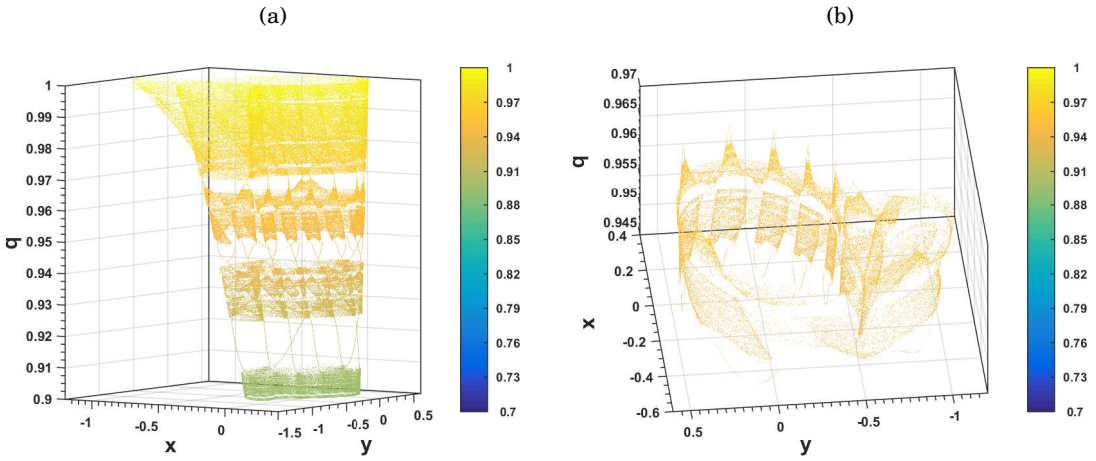

FIGURE 3.6. (a)Paired cascade for $a = 0.9$, $b = -0.6013$, $c = 2.0$, $d = .5$, $x_0 = -0.72$ and $y_0 = -0.64$. q varying from 0.9 to 1. (b) The blow up of the figure(3.6(a)), which shows the paired cascade (q varying from 0.945 to 0.97).

the solitary limit cycle undergoes a reverse Neimark-Sacker bifurcation, wherein the limit cycle loses its stability and a fixed point is created. For $q > 3.3$, there is only one fixed point at $(0,0)$. The figure(3.6(b)), shows the blow up of figure(3.6(a)), which shows the closed bubble structure more clearly.

3.0.4.2 Applications

A system which has co-existence of attractors can exhibit hysteresis due to the existence of multi-stable states. In a Tinkerbell system, due to the existence of different basins of attractions that depends on parameter q, one can use q as a control parameter and vary it to get different behavior. Given an initial condition, depending on the value of q one can let the system evolve into different behavior. Such a switching mechanism can be used in encryption and decryption of messages. By altering the value of q, one can select a different attractor for encrypting different parts of the message. Tinkerbell map has been used in encrypting and decrypting images [52]. For encrypting an image one needs to perform a series of steps. The message can be decrypted in a robust manner by checking all the possible keys and using all computing power. Thus to make the message free from any attack, one has to make the key space extremely large. The two initial conditions and the parameter q are the real values that control the encryption technique. Assigning 64 bits [52] to a real number there are totally 3 variables, which results in 3×64, i.e., 2^{198} keys. To make the system more secure, one can vary the parameters a,b,c and d. By using different deformations for different coordinates, i.e., by keeping deformation parameter q_x for deforming the x coordinates and a different value for q_y for deforming the y coordinates, we add 2 more parameters to the system. Thus we have a total of 8 parameters, thereby making the key space very large, i.e., 2^{512}. Thus, using the q-deformed map helps in the secure transmission of information. This may be made more

robust by coupling with a tent map or any other piecewise continuous map which decodes the values of q, thereby making the parameter space richer.

3.0.5 Circle Map

A circle map by definition maps a bounded interval onto itself. The most general form of the circle map is given by[53]

$$\theta_{n+1} = f(\theta_n) \tag{3.31}$$

For a purely sinusoidal map, the equations take the form

$$\theta_{n+1} = \theta_n + \Omega - \frac{K\sin(2\pi\theta_n)}{2\pi} \quad (mod 1) \ . \tag{3.32}$$

Ω here is the addition in phase after every time step. To study the general behavior, we monitor the parameter termed the winding number W which is the total additional phase that the oscillator has accumulated after n steps. If this quantity is a rational number, then the oscillator is periodic, else it is quasi-periodic. Ω is the driving frequency of the oscillator. K is the coupling strength which decides the effect of non linearity on the oscillator. For $K = 0$ the circle map reduces to a shift map with no fixed points unless $\Omega = 0$. For $0 < K < 1$, the function is monotonic and the map is invertible; beyond $K > 1$ the map is not invertible. More precisely θ_{n+1} now cannot be mapped to one particular value of θ_n. Thus the system is more sensitive to initial conditions. In general, any multi-dimensional time series may have more frequencies due to which the motion of the trajectories may be on an n-torus, where n is the number of frequencies in the system. To study these multi-dimensional systems, one can resort to studying the Poincarè section. A plane is inserted in the n-torus, which would record the point whenever the trajectory intersects the plane. This reduces the dimension of the system and the angle variables can be used to study the system. The intersection of the plane at the $i+1^{th}$ iteration is related to i^{th} iteration, which gives rise to the circle map. In general the functional form for the undeformed map is

$$\theta_{n+1} = \theta_n + \Omega - Kf(\theta) \tag{3.33}$$

The map represents a simplified form of the phase-locked loop in electronics. Systems that are governed with two frequencies tend to mode-lock. This mode locking is done by adjusting the frequencies so that they are in step. This results in minimizing the dissipation. When there is a mismatch between the two frequencies, quasi-periodic behavior emerges. This makes the system wander all through the phase space without visiting the same point again, though it may visit its neighborhood.

Let r be the number of iterations in which the circle map makes p revolutions. The winding number W is defined as the ratio of p and r: $W = \frac{p}{r}$. For rational values of W, the system exhibits periodic motion, while irrational values lead to quasi-periodic motion. If many mode-locked states overlap, chaos sets in. When the winding number is calculated for all possible values of Ω and K, we get an idea of how the parameter space is divided between various types of motion, namely the

chaotic, quasi-periodic and the periodic. The regions in the space of parameters where the map has locally constant, rational winding numbers are called the Arnold tongues. The tongues correspond to the region where periodic behavior is observed.

When $q-$deformations are brought in, the parameter space is also deformed. The deformation distorts the shape of the tongue and shifts it from its original position. The classic Arnold tongue is restored when $q = 1$. The $q-$deformed circle map is given by

$$\theta_{n+1} = \left(\frac{\theta_n}{1+(1-q)(1-\theta_n)}\right) + \Omega - \frac{Ksin(2\pi\left(\frac{\theta_n}{1+(1-q)(1-\theta_n)}\right))}{2\pi} \quad mod(1) \tag{3.34}$$

As q is varied from -2 to 2, there is a shift of the tongue in the parameter space as shown in the figure(3.7(a)) below.

For the q-deformed map, the bifurcation diagram does not significantly alter, except that now there is period twinning (Fig.(3.8(b), 3.9(a) and 3.9(b))). Similarly the plot of the parameter space (Fig. (3.7(a), 3.7(b) and 3.8(a))) also does not show a strong distortion. However it is noted that at q=2, when the bifurcation diagram showed periodic behavior, the parametric space is also dominated by periodic motion. Although there is not much change in the bifurcation diagram, we find that that there is twinning of period doubling cascades before and after q=1, seen in Fig.(3.8(b)). For very high values of q the system is very periodic. From $q = -2$, the twins begin to come closer. For certain regimes there are satellites (a small period-doubling cascade in a periodic window) which are also twins. As q approaches 1, the twins merge and become one. For values of $q > 1$, the twins are again born and they separate from each other. For large values of q, the cascades become less and less chaotic, and they join to form periodic windows which dominate the entire frame.

3.0.5.1 Applications

Circle maps are generally used in physical systems where there is cyclicity due to periodic forcing. As an example heart beats are initiated by pace-makers. The pace-maker is the forcer while the heart is the responder. The frequency of forcing is Ω and K is the strength of the pace-maker's effect on the heart[54, 55]. In experiments performed on chick embryonic heart cells[56], it was found that the heart beat was synchronized with the forcing stimulus. The circle map in general can be used to model any oscillator which alters its behavior based on an external stimulus. Any multidimensional time series, which is dominated by many frequencies can be reduced to a circle map, by defining a Poincareè section. Since there is a multitude of systems which have a similar behavior, describing all of them here is out of scope of this thesis. The mathematical description given above gives a general description which can be easily adapted to any system.

(a)

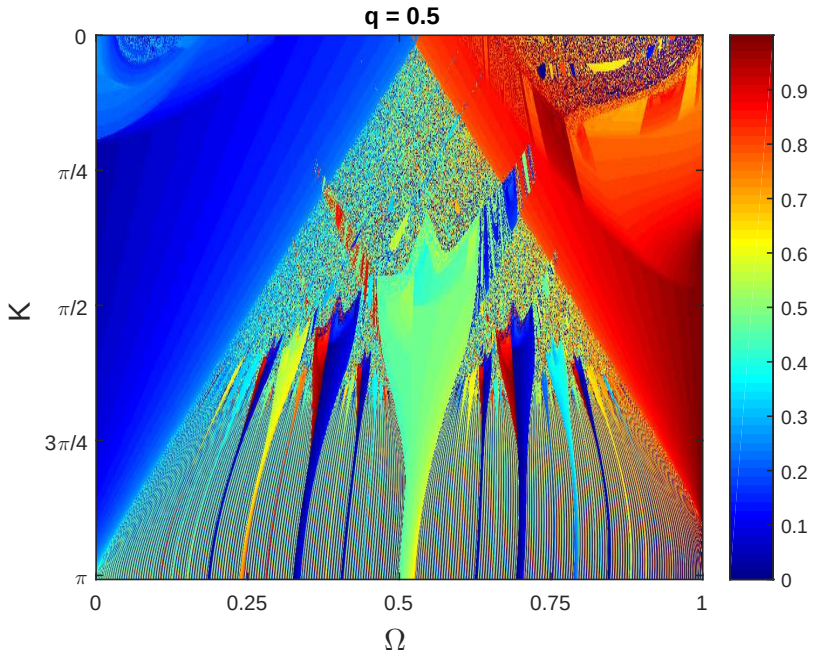

(b)

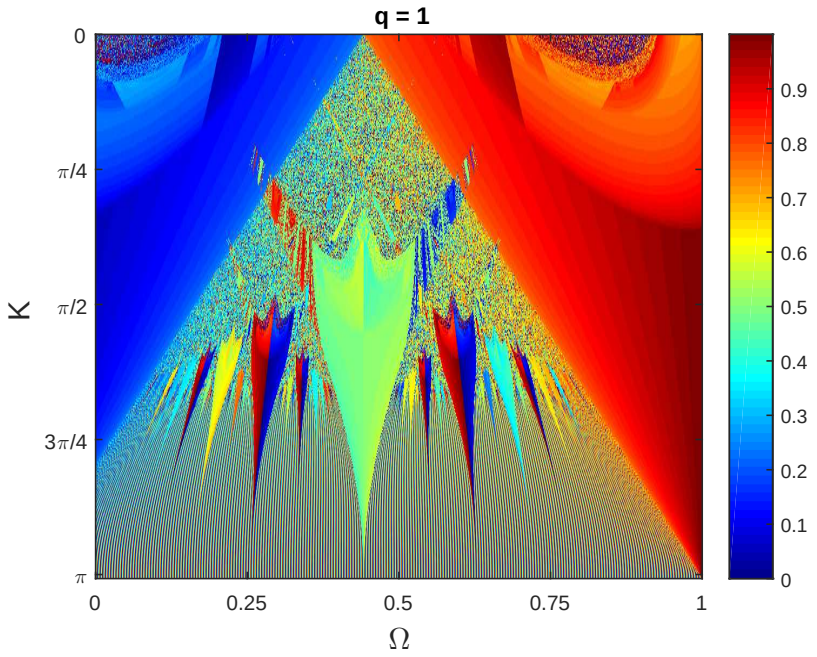

FIGURE 3.7. Arnold tongue for various values of q. The Arnold's tongue presents the regions of periodicity, quasi periodicity and chaos. The plot is between various values of Ω and K. (a) $q = 0.5$ (b)$q = 1$. The Arnold tongue at various values of q show slight distortion and a shift.

(a)

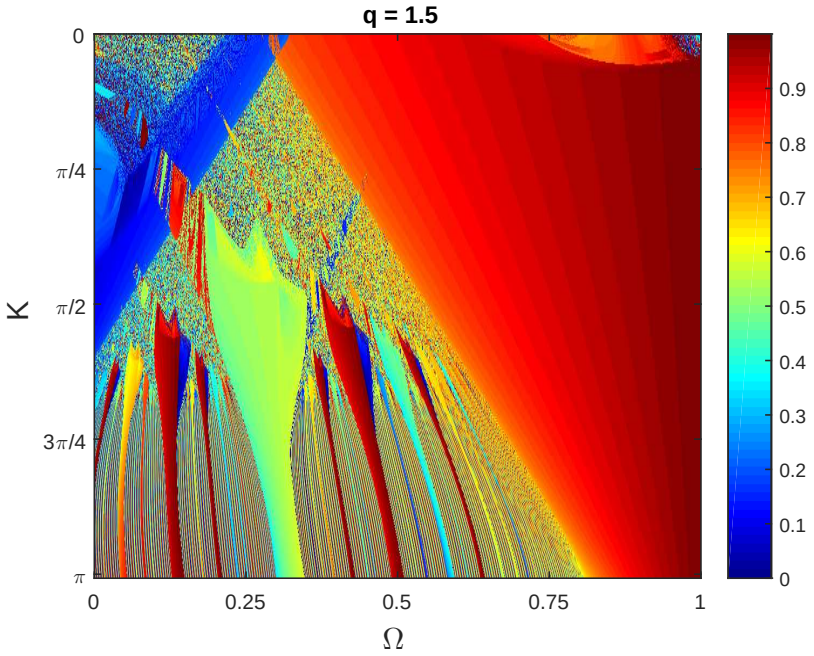

(b)

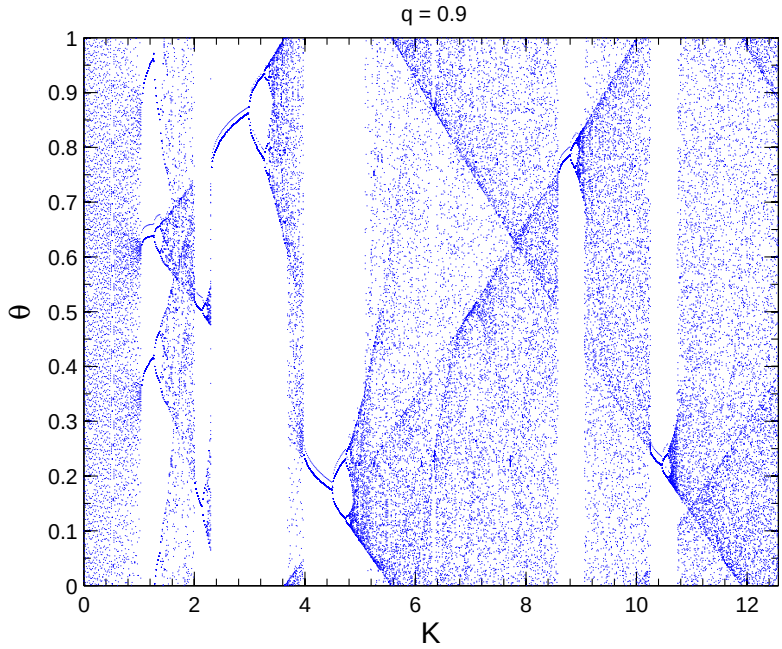

FIGURE 3.8. (a) Arnold tongue for various values of $q = 1.5$. The Arnold's tongue presents the regions of periodicity, quasi periodicity and chaos. The plot is between various values of Ω and K. Bifurcation diagram for various values of q. The bifurcation diagram is generated by using $\Omega = 0.65$. K is varied from 0 to 12. (b) The bifurcation diagram for circle map is generated by using $\Omega = 0.65$. K is varied from 0 to 12 and $q = 0.9$. From the bifurcation diagram, the replication of the cascade is seen.

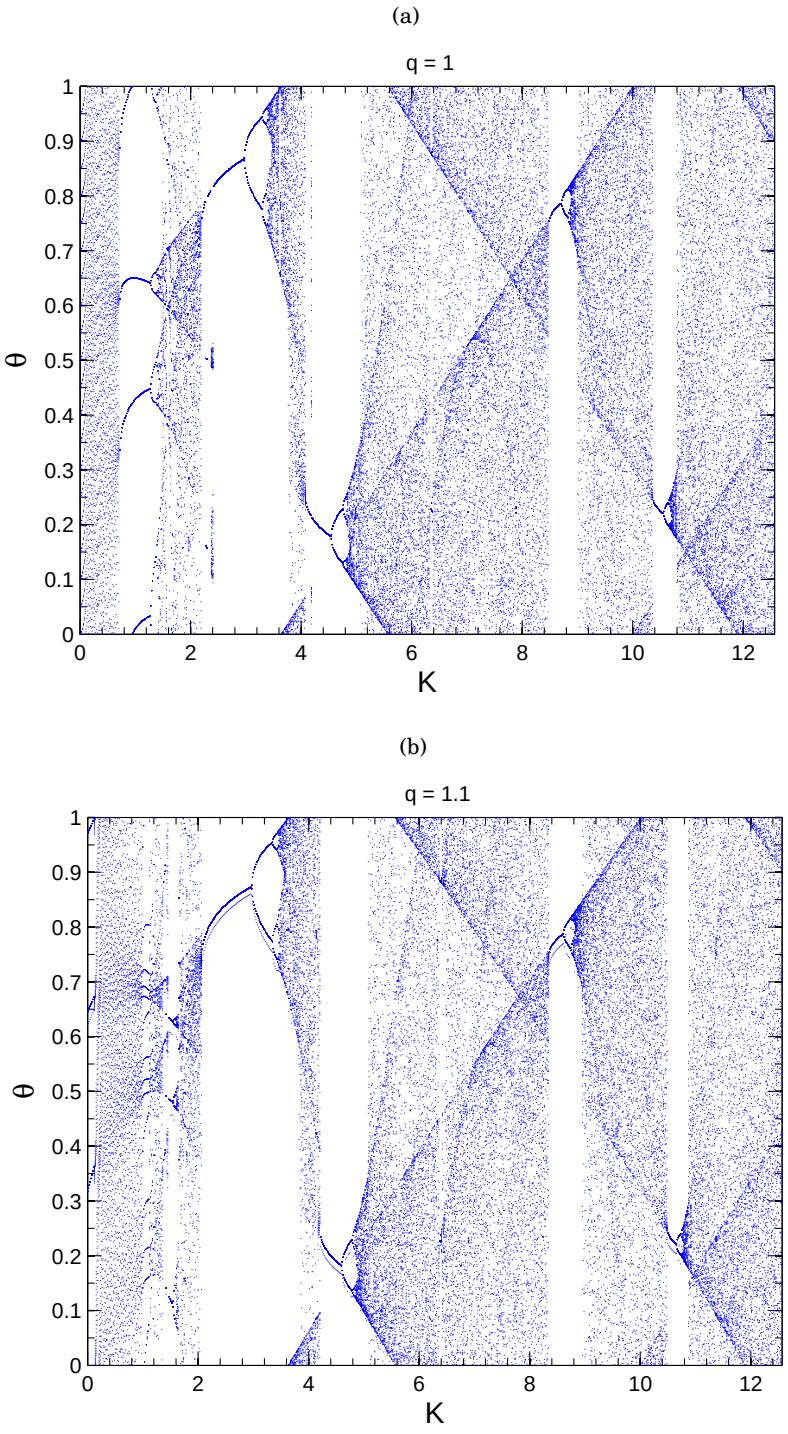

FIGURE 3.9. Bifurcation diagram for various values of q. The bifurcation diagram for circle map is generated by using $\Omega = 0.65$. K is varied from 0 to 12. (a) $q = 1$ (b) $q = 1.1$ (f). From the bifurcation diagram, the replication of the cascade is seen.

CHAPTER 4

DYNAMICS OF POPULATIONS: THE LARCH BUDMOTH CYCLES - OBSERVATIONS AND EARLIER WORK

4.1 Modeling ecological systems

Population dynamics come out of the complex interactions between various interacting species. To model the dynamics one needs to understand the kinds of interactions that go on in the system and one may also need to make some assumptions[57].

4.1.1 Assumptions while modeling an ecological system

Before modeling any systems, first, a thorough analysis is made on the constraints and observations made on the system. For any population dynamics model, we deal with numbers and hence the following assumptions help to describe the form of interactions [57]

1. The change in the population numbers happens only via birth, death, emigration and immigration.

2. Depending upon the available resources there is a maximum number for the population which the resource can support called the carrying capacity. Any dynamics results from the interaction of the organism with itself or with other species or the ecological niche in which it lives.

3. In a region of deficit resources the resource depletion is proportional to the resource density.

4. A consumer cannot get more energy than what is available. Hence the conversion rate decides the amount of energy that is passed on to the consumer.

5. Despite the availability of resources a consumer cannot consume continuously.

Type	Closeness	Aggression	Example
Predator	Low	High	Lion, Tiger
Parasitoid	High	High	HIV
Parasite	High	Low	Lice
Grazer	Low	Low	Cow, goat

TABLE 4.1. Classification of interaction between different species based on closeness and aggression

6. Reproduction is controlled by energy acquisition.

4.1.2 Various kinds of interaction

An interaction can be defined loosely by two quantities — the degree of closeness with the other individual and the degree of aggression. The interacting species can be classified into 4 main groups. The first group is that of the predators which are more ferocious, aggressive and most of the time end up killing their prey such as for instance, lions, tigers, humans who hunt, etc. Though aggressive, the predators do not have to be close to their prey [57]. The next group is that of parasitoids — these cling to their host, using their host for survival and finally end up killing the host [57]. Since parasitoids live inside or on the host, their closeness with their prey is high and the degree of aggression is also high as they end up killing the organism on which they survive. A typical example would be HIV (human immunodeficiency virus) that lives in the infected individual and kills the individual. The third group is that of parasites which live inside or on the body of the organism. it is however non-lethal [57]. A typical example would be lice living on humans which do not kill humans but depends on the blood of the host human for its survival. The final group is that of grazers which are neither close to their prey nor are they lethal. A typical example is a herbivore which is on the move, never killing any plants, though consuming from the plants once in a while [57]. Most of the nomadic interactions come under this type. The table (4.1) illustrates the various interactions [57].

Since a consumer relies on its prey, any fluctuation in prey numbers spatially or temporally affects the system immediately [57]. Response to temporal fluctuation, which is the functional response and response to spatial fluctuation, which is the aggregative response, happens on a shorter time scale [57]. However the numerical response which is on a slower time scale results due to changes in the numbers of the prey [57]. While functional and aggregative responses are individual responses, the numerical response is when the interacting species is considered as a whole[57]. Numerical response brings lag in the system. A typical example would be predators which reproduce once in a year and which respond to prey density only a year later. If the reproduction period in a particular year is over, irrespective of the availability of prey, they cannot alter the numbers. Hence, the effect of an increase in prey density after predator reproduction is reflected only in the next reproducing season[57].
Functional response reflects the rate at which the prey is removed for food. It is given as the number

S No	Types of response	Functional form	Remarks
1	Constant	c	Constant response
2	Linear	aN	No ceiling for functional response
3	Hyperbolic	$\frac{aN}{1+ahN}$	Saturating response
4	Exponential	$c(1-\exp^{\frac{-N}{a}})$	Saturating response - not in use
5	Sigmoid	$\frac{cN^2}{d^2+N^2}$	Searching rate as hyperbolic response
6	Sigmoid mechanistic	$\frac{bN^2}{1+gN+bhN^2}$	Searching rate as hyperbolic response
7	θ - sigmoid	$\frac{cN^\theta}{d^\theta+N^\theta}$	Controls nonlinearity
8	Predator interference	$\frac{aN}{1+awP}$	Includes predator interference
9	Predator interference (phenomenon)	$aNP^{-\theta}$	Not in use
10	Beddington	$\frac{aN}{1+awP+ahN}$	includes both handling time and wasting time with other predators
11	Hyperbolic Ratio Dependent	$\frac{cN}{dP+N}$	
12	Linear Ratio Dependent	$c\frac{cN}{P}$	

TABLE 4.2. Different types of functional response. The various variables and the parameters listed in this table are N is the prey density, P is the predator density, b is the maximum searching rate, c is the maximal killing rate, a predator searching rate, h handling time, w wasting time, g regulates how fast the search rate saturates with prey, d is the half saturation constant and θ is an exponent.

of prey hunted or the biomass of plants consumed in a unit time per predator. There are various types of response depending upon the species considered. A brief description of various types of functional response[57] can be found in table (4.2).

4.1.3 Population monitoring in ecology

When we consider a grazer system, a grazer seldom kills its food. It merely consumes some parts of the plant and moves on. It could be leaves or flowers or the sap or nectar. Hence, to monitor the herb, it is not a good idea to use the numbers of the prey. To mathematically model a herbivore-plant interaction, one considers the plant biomass. The biomass can be quantified in many ways — one could use the nitrogen content or the length of the plant leaves, the number of flowers that bloom, etc.

Similarly in case of a parasitoid which lives inside the body of the host, counting its actual numbers may not be possible practically. This difficulty is overcome by considering that a certain percentage of the host organism is the parasitoid. That percentage could be a function of parasitoid itself as in case of the Nicholson-Bailey model discussed in 4.2.5.

The host numbers are directly counted. If we consider an insect system, the quantification is done by considering how many insects live in a given area or in given biomass of plants etc.

4.1.4 Order of the equations

In any population system each interacting species is denoted by a variable. The population dynamics is captured by the equations which govern the system throughout its evolution[57]. Dynamics of populations can be modelled using ordinary differential equations or with difference equations. The differential equations describe a continuous time system while discrete systems are described by a difference equation. Be it discrete or continuous, given an equation it has an order. Without prior knowledge about the system, one can just infer a lot from the order of the equations.
In a zero order process the variable that denotes the population varies with respect to itself with a constant multiplying it. i.e., the growth rate is constant[57]. This has no ceiling or limiting factor and thus results in exponential growth[57]. In first order process the growth rate is a function of the variable, and in a second order process, the variable is a function of another variable, which is again a function of the original variable. The different order leads to different dynamics[57]. A zero order process either grows or declines exponentially, while a first order process has an equilibrium point, that is to say, it can halt a sudden increase or decrease of population[57]. A second order process can exhibit cycles and hence population cycles are possible[57]. A similar reasoning is also valid with maps[57]. However, in maps, since we deal with discrete time, the variables now are connected to the variable values in the past[57]. By going through the same analogy, in a zero order processes, the growth rate is constant, in a first order process, the growth rate is proportional to the value of variables in the previous time, while in a second order process two time lags are involved[57].
A difference between continuous and discrete time systems is that in a discrete system, cycles and chaotic dynamics are possible even in a first order process. It is noted through observations that a cycle generated by the second order process at the least covers 6 generations, while the one generated by first order has multiples of 2 generations[57].

4.2 Some simple ecological models

4.2.1 Logistic map

The logistic model is the first basic model that had a term halting population growth depending upon the value of its carrying capacity. This model did not have exponential growth or decay and hence was more comparable to what was observed in nature. Although this is much better than the constant growth rate that drove the system to zero or infinity exponentially, this is still not a very good model. Let N_t represent the population of an organism at time t, r the growth rate and K the carrying capacity. This logistic map can be used to model bacteria growing in a petri dish or for some very simple organisms. The equations are given by,

$$N_{t+1} = N_t r(1 - \frac{N_t}{K}) \tag{4.1}$$

which can be normalized as,

$$x_{t+1} = r x_t (1 - x_t) \tag{4.2}$$

where $x_t = N_t/K$.

The fixed point for this difference equation is at 0, $1 - \frac{1}{r}$. Depending on the value of r we may have one or two fixed points.

4.2.1.1 Linear Stability Analysis

Computing the first derivative at the fixed points helps us to decide on the stability of the system. The first derivative of the logistic function $F = rx_t(1 - x_t)$ is given by $F' = r - 2x_t$, which equals r at 0 and $r + \frac{2}{r} - 2$ at $1 - \frac{1}{r}$. For $r > 2$, the fixed point 0 is not a stable point. The system undergoes period-doubling and finally becomes chaotic as $r = 3.56946$.

4.2.2 Ricker Model

Let N_t denote the population of a species at time t. a represents the growth rate, b the intrinsic growth rate and K, the carrying capacity. The Ricker model for the species is given by,

$$N_{t+1} = N_t a \exp^{-bN_t} \tag{4.3}$$

Ricker developed the following equation 4.3 to model stocks in fisheries[58]. Ricker's model is an extension of a logistic model. This extension was needed as the logistic model could not explain beyond unicellular organism like yeast and bacterium that grew in the culture. It can be immediately seen that Ricker's Model does not show negative population when the current population exceeds the carrying capacity, which is not in the case in the case of the logistic model..
The equation 4.3 has two fixed points — one at $N_t = 0$ and the other at $N_t = \frac{ln(a)}{b}$. Depending on the values of a and b, stable solutions and oscillatory solutions can be obtained. This restricts the values of a to be greater than 0.

4.2.2.1 Linear Stability Analysis

At the two fixed points the value of the first derivative of the function R decides the stability. At $N_t = 0$, the derivative of the function

$$R' = a \exp(-bN_t)(1 - bN_t)|_{N_t=0} = a \tag{4.4}$$

This leads to the following [59][58]

1. $0 < a < 1$, 0 is stable, this implies extinction. Physically it means that the carrying capacity is too less to sustain a population.

2. $a > 1$, 0 is an unstable equilibrium, and small perturbations lead the system away from it. The second equilibrium point ($N_t = \frac{\ln(a)}{b}$) shows the following behavior. The derivative at this fixed point is
$$R'(\frac{\ln(a)}{b}) = a \exp(-bN_t)(1 - bP)|_{\frac{\ln(a)}{b}} = 1 - \ln(a) \tag{4.5}$$
The following observations are made on this system,

a) For $1 < a < e$ the fixed point is stable, all fixed points except 0 reach this monotonically.

b) For $e < a < e^2$, the solution is stable. All initial conditions other than 0 reach this point after oscillations.

c) For $a > e^2$, the fixed point is unstable.

4.2.3 Lotka-Volterra Models

This was independently modeled by Lotka and Volterra [60] and [61]. This basic model exhibited cyclic behavior and was used to explain the population dynamics seen between lynx and hares. In this model the rise in population of a species is taken as the difference between the births and deaths that occur in the time step t. Let R represent the rabbits, and L represent the lynx populations. The equations are given by

$$\frac{dR}{dt} = aR - bRL \tag{4.6}$$

$$\frac{dL}{dt} = cRL - dL \tag{4.7}$$

If there were no lynxes the population of rabbits would grow at the rate of a. In the presence of Lynx, the rabbit population is removed at the rate of bRL. A similar analysis of the equation of the lynx, explains the increase in population by cRL and decay of the population by dL during prey scarcity.

4.2.4 Linear stability analysis

The fixed points of the system are found from

$$aR - bRL = 0 \tag{4.8}$$

$$cRL - dL = 0 \tag{4.9}$$

Which gives the following possible solutions

1. $R = 0$ and $L = 0$
2. $R = 0$ and $L = \frac{a}{b}$
3. $R = \frac{d}{c}$ and $L = 0$
4. $R = \frac{d}{c}$ and $L = \frac{a}{b}$

Call these fixed points 1,2,3 and 4 respectively. The Jacobian of the system is given by

$$J = \begin{bmatrix} a - bL & -bR \\ cL & cR - d \end{bmatrix}$$

This basic system of equations explains the existence of cycles. Table(4.3) gives the values of Jacobian and nature of the fixed points (1 to 4). The models following this are analytically difficult

The Jacobian at different fixed points 1,2,3,4 are given in the table(4.3).

S.No	J	Eigenvalues	Nature of stability
1	$\begin{bmatrix} a & 0 \\ 0 & -d \end{bmatrix}$	$a, -d$	Saddle
2	$\begin{bmatrix} 0 & 0 \\ \frac{ca}{b} & -d \end{bmatrix}$	$0, d$	Unstable
3	$\begin{bmatrix} a & \frac{bd}{c} \\ 0 & 0 \end{bmatrix}$	$0, -a$	Stable
4	$\begin{bmatrix} 0 & \frac{-bd}{c} \\ \frac{ac}{b} & 0 \end{bmatrix}$	$\pm\sqrt{ac}$	Center

TABLE 4.3. Jacobian evaluated at the fixed points of a Lotka- Volterra type predator prey model

to solve but are more accurate. For instance, the Lotka-Volterra model can have a cycle of any size. It just depends on the initial condition. However, in reality, it is not the case. The observations of many population dynamics show a well-defined amplitude. This can come out from a model, only when there are limit cycles. The following models have limit cycles in them.

4.2.5 Nicholson and Bailey model

Nicholson and Bailey model[62] describes the interaction between the host and the parasite. Since parasitoids cannot be counted they are considered to be a fraction of the host number[62]. Let us denote the number of hosts attacked by the parasitoids at time t by H_t. Let a be the rate at which the parasitoid attacks the hosts. This model seems to be illogical as the number of hosts and parasitoids are assumed to be constant in one-time step, which in fact is not the case. One can overcome the difficulties by adding a multiplicative constant to the equation for parasitoid[62]. The host number can be considered to be a constant since the host has lived for some time before dying. The parasitoid is dependent on the host for most of its activities, so it doesn't kill the host immediately and thus we can safely assume that host densities H_t are constant in a given generation[62]. Using the above formulation Nicolson and Bailey constructed the following difference equations for capturing the dynamics of parasitoid P_t and host.

$$H_{t+1} = bH_t \exp(-aP_t) \tag{4.10}$$

$$P_{t+1} = cH_t(1 - \exp(-aP_t)) \tag{4.11}$$

The parameter b is the growth parameter, while c is the conversion rate. In a way c is the efficiency of the parasitoid. The higher the value of c, the higher is the parasitoid production.

4.2.6 Beddington Model

This model is formulated to explain the interaction between a parasite and host[63]. Let N_t and P_t respectively represent the host and the parasite that interact. The equations that describe the

interaction are as follows

$$N_{t+1} = \lambda N_t e^{\frac{-aP_t}{1+awP_t}} \tag{4.12}$$

$$P_{t+1} = N_t(1 - e^{\frac{-aP_t}{1+awP_t}}) \tag{4.13}$$

As in the Nicholson-Bailey model, it is assumed that the parasite is always a fraction of the total number of hosts that are available for the parasites to invade[63]. Here the model takes into the account the fact that there is always some time utilized by the parasite in consuming the prey and that the parasite will not cover the full area when it is searching for the prey[63]. (The rate of searching of the parasite is calculated per unit time and per unit area, which is why area comes in picture).

The searching efficiency E of the parasite is defined as

$$E = \frac{N_a}{NP} \tag{4.14}$$

where N_a is the number of prey victimized by the predator in a given area, in given time. N is the number of prey while P denotes the parasite number density. However, observations show us that at high predator or prey densities, there is a decline in E, which can be overcome by using a density dependent searching, using a functional response that declined as prey density increased, or by using a searching efficiency which was proportional to the predator[63]: $E = \mu P^{-m}$. This explained the decline when the predators rate was high. m is the intraspecific competition among the parasites and μ is the quest constant or the level of efficiency of one parasite. The number of hosts parasitized is proportional to the number of parasites, number of hosts that are in the given area and time taken to search for the hosts. Here an assumption is made that the parasite takes a unit time to consume the hosts and searches in a unit area[63]. There is also a time when the parasites could compete amongst themselves for the host (intraspecific competition). So the total time spent between 2 encounters with the host is the sum of the time taken to search the host (T_S) and the wasting time (T_w)[63].
The number of encounters between the parasites is defined as

$$N_e = bT_sR \tag{4.15}$$

where b is the rate of the encounter between parasites. R is the density of parasites, and T_s is the searching time. Therefore the total time wasted is given by

$$T_w = bT_sRt_w \tag{4.16}$$

where t_w is the time wasted per encounter[63]. Thus, total time that is wasted by the parasite is

$$T = T_s(1 + bRt_w) \tag{4.17}$$

Thus, the number of hosts that are attacked by the parasites is

$$N_a = \frac{NPaT}{1 + bt_wR} \quad . \tag{4.18}$$

The total time wasted t_w is equal to the sum of the time wasted in encounters with other parasites T_p and the time to handle the prey T_h. To distinguish these two, T_h and T_p is defined[63]. The total time wasted is

$$T_w = T_p + T_h \tag{4.19}$$

with $T_h = N_a t_h$ and $T_p = N_e t_w$. With this the number of hosts that are attacked becomes

$$N_a = \frac{aNPT}{1 + at_h N + bt_w R} \tag{4.20}$$

In a given time period, the rate of change of the prey numbers is given by,

$$\frac{dN}{dT} = -\frac{aNP}{1 + at_h N + bt_w R} \tag{4.21}$$

which can be reduced as

$$N_a = N(1 - e^{\frac{a(N_a t_h - PT)}{1 + bt_w R}}) \tag{4.22}$$

Since the attacked prey is converted into the parasite on consumption, this equation can be considered to represent the parasite population[63].

4.2.7 Grazing systems

Grazers are low in closeness and low in aggression. Herbivory induces plant defenses in the plants, which makes the plants less available for the consumers[57]. To model such systems we model the plant-induced defense D_t as a variable. We assume that plant defenses are proportional to the attack it faces[57]. Thus more the attack more is the defense. Since defenses cannot rise indefinitely, it is ceiled using a hyperbolic function[57]. In the absence of herbivory too the evolution of the plant must be considered. In this case, the defense slowly decays to zero. A quantity called the plant quality Q_t can be defined which represents the part of the plant that is consumed. This can be related to the plant defense through a relation: $D_t = 1 - Q_t$.

$$D_{t+1} = \frac{cN_t}{d + N_t} + \alpha D_t \tag{4.23}$$

In terms of the plant quality

$$Q_{t+1} = 1 - \alpha + \alpha Q_t - \frac{cN_t}{d + N_t} \tag{4.24}$$

Here c is the maximum killing rate. d is the half saturation constant for the uptake for the budmoth and α is the vulnerability of the plant to attack. Thus, the complete model describing the herbivore and the plant is given by

$$N_{t+1} = N_t \exp(r_0(Q_t - \frac{N_t}{k})) \tag{4.25}$$

$$Q_{t+1} = 1 - \alpha + \alpha Q_t - \frac{cN_t}{d + N_t} \tag{4.26}$$

4.3 Life cycle of the budmoth

The larch budmoth is an insect that infests larch trees. Larch trees are found in colder temperatures, and thus we always see them growing in the mountains. Larch trees are found all over the world — for instance in the Alps, in Cananda, in USA, in Japan and also in India. The larch budmoth infests the larch trees for food. The length of the larch needles and the budmoth population densities are seen to have a cyclic behavior which are in synchrony. The time period of this cycle is found to be approximately 8-9 years[64]. The budmoths in turn are infested by parasitoids which also exhibit cyclic behavior in their population densities. The cycles of the budmoth and the parasitoids are also mutually synchronized.

Just as every other insect the larch budmoth has 4 stages in its life— the egg, larva, pupa, and the adult. The larva stage itself has 5 stages within. Budmoths usually survive at the optimal heights of 1700 to 2000 meters above sea level. The adult moths start flying during the months of July to October and have a life span of more than a month. During the adult phase, egg-laying dominates most of their activity. A female moth usually deposits 20 to 280 eggs[65].
The female moths most of them time prefer to lay eggs underneath a lichen called *Parmelia exasperatula* which usually covers trees that are 3 years and older. They also lay eggs on cone-scales or bark scales. During the winters, there is a diapausing, which inhibits the eggs developing into larvae. This diapausing is altered by environmental conditions. The diapausing ceases and the first instar larvae emerge just as the fresh needles sprout from the larch buds. This timely synchrony helps the larvae to make the maximum use of the available resources. The first and the second instar larvae feed inside the needle cluster[65]. This offers them protection from adverse environmental conditions. The needle cases are seen in the larch branches when the fourth instar develops. The next stage, which is the most destructive stage is characterized by a webbing which runs along the branch axis[65].
After maturation, the budmoth larva becomes photo-phobic and leaves the sunshine to the litter below where it builds its pupation chamber and pupates[65]. A month later adult moths emerge out and the cycle continues[65].

4.4 Experiments and observations

The budmoth larvae rapidly defoliate vast areas of larch forests giving an ugly brown appearence to the regions which previously were lush green. This has had an adverse effect on the tourism industry also and led to dedicated studies of the larch trees and the budmoth insect pests especially in the Alpine region[64].

Between 1949 and 1986, several regions in the Alps were studied extensively to investigate the nature of the budmoth outbreaks. Five of the sites under study were more than 2000 ha in size[64]. and there were also several local sites which were about 100 ha in size [64]. The methods to study the larch budmoth were, life table studies, light traps, pheromone traps, physically counting the

actual numbers that survive in a sample tree, etc. [64]. Studies made in the seven major regions of the Alps showed that the most cyclic behavior of larch budmoth outbreaks occurred in the upper Engadine valley of the Swiss Alps only. Other places did not really have strong cycles, although there were outbreaks. In Engadine valley[64], the pattern of defoliation and its extent is also cyclical, which is not the case in other regions. In other regions say in Hautes-Alpes, France, the degree of defoliation is different in different cycles; there are also intermittent periods where there is no defoliation for over 20 years[64].

4.4.1 Observations

Strong outbreak cycles occurred in the high Alps where the elevation is between 1500 to 2000 meters above sea level. In the lower Alps where the altitudes are between 1200-1600 meters above sea level, there are cyclic fluctuations, but the amplitudes are much smaller[64]. In the regions of smaller amplitude, it is noted that the time period between outbreaks is longer by 1 to 2 years. Below an elevation of 1000 meters there are no fluctuations[64]. With a still lesser elevation, the fluctuations are irregular, such as along the river Rhine near Basel. In some larch stands in the deciduous forests there, the budmoth may have even become locally extinct[64].

4.4.2 Experiments done in the Alpine region

In the Swiss Alps, the natural conditions were altered to check on the progress of the cycles[66]. The budmoth populations were reduced by killing them using bacterial sprays during various parts of the population cycle[66]. Similarly, sparse populations were made denser by the addition of larvae from somewhere else and the system was allowed to evolve on its own[66].

It was noted that a decline of 60% in the population of budmoth larvae increased the time taken for occurrence of an outbreak by one year — hence the damage also appeared a year later, but subsequent decline in the population density and the growth rate were unaltered[66].
Reduction of peak populations by 80%, had no effect on the density during the subsequent years. This could possibly be due to movement of larch budmoths into the area under observation[66]. Increasing the budmoth population by introducing larvae from elsewhere advanced the outbreak and the damage by a year[66]. From the above-mentioned facts it is clear that the larch budmoth and the larch tree play a vital role in the cycling of the population and also supports the fact that the pathogens are also responsible for altering the population levels. Since the predator has similar life generations as the prey, it is very clear that the predator would have a second order effect on the prey. This is clear as the predator relaxes during the growth phase and intensifies its attack on its prey during the decline phase, which is typical of predator-prey cycles[66]. From [66] it is very clear that the cycles which are seen in the budmoth and the larch needle lengths can be switched off if there are too many parasitoids which completely removes the defoliators. This decouples the defoliator-parasitoid interaction and the cycles are halted. [66] suggests that parasitoids efficiency is somehow compromised and hence cycles go on in certain regions. Similarly addition of second parasitoid, incorporated by spraying bacillus spray, can halt the outbreak by an year or so[66].

4.4.3 Data collection technique in the Engadine valley Swiss Alps.

Individual larch trees were taken as a sample unit. 400 trees were selected and stratified based on topological features such as altitude, exposure to the sunshine. These are then weighted according to host tree density per unit area[64]. A sample of twigs, needles and branches weighing almost one kilogram is extracted from the larch tree branches. The number of larvae is counted and this provides the average density estimate for the entire region. This is then converted to actual numbers.

4.4.4 Data reconstructed using the tree ring analysis in the Alpine region

One of the longest available ecological time series is the larch budmoth outbreak record. Although the manual observational record is available for the relatively short time span of 50 years, it is really difficult to deduce anything from the same. The 50-year data does confirm an 8-9 year cycle in which the larch needle lengths and the budmoth population densities rise and fall. The longest record of the time series available till today is reconstructed from the dendrochronological analysis of the larch trees in the sub-Alpine region[67]. Since tree rings record the history through which the tree has survived, it essentially captures in the size of the rings, the conditions that were prevalent during the times. Extensive damage to foliage would reflect as morphological changes like narrower-than-normal thickness of the tree rings.

4.4.4.1 Data analysis

The health of a tree at various time periods is found by determining the wood density[67]. Wood density is visualized using x-rays. The variation of the brightness in the films show the variation of the wood density and hence is an indicator the health of the tree. Even annual seasonal patterns are recorded within the rings[67]. Severe defoliation results in severe loss of density in the X-ray films and those years are marked to have an outbreak of the budmoth. During an outbreak, photosynthetic activity also goes down which results in deficiencies and hence reduced growth, cell thickening, and thick tracheid formation[67].
Around 47513 wood profiles were used to construct the time series. Samples were collected from living trees and some of the wood used in the construction of old buildings located about 1600 meters above MSL[67]. These were accurately dated and found to belong to period between 832 to 2004 AD. The samples were analyzed for thick tracheid cell and low brightness in the X-ray imaging. These were further processed by various techniques [67] and the final outbreak data was constructed. The reconstructed data spans 1200 years making it the longest available ecological time series[67].

4.4.5 Data constructed from the tree ring analysis in the Tatra region, Slovakia

The Tatra mountains are in Slovakia, about 1000km distant from the Swiss Alps. The local foresters living in the Tatra mountains confirm the presence of larch budmoths in the region. However, no cyclic outbreaks are known to have occurred in the Tatra mountains[68]. Using dendrochronological

S.No	Name of the model	Equations
1	Kostitzin	$x_{k+1} = \frac{ax_k}{1+bx_k}$
2	Discrete Logistic Model	$x_{k+1} = ax_k(1-x_k)$
3	Skellam	$x_{k+1} = ax_k(1-\exp(-bx_k))$
4	Morris-Varley-Gadwell Model	$x_{k+1} = ax_k^{1-b}$
5	Moran-Ricker Model	$x_{k+1} = ax_k \exp(-bx_k)$

TABLE 4.4. Various one-dimensional model that were tried to fit with the data. The x_t in the above 5 models, represent the population of the budmoth at time t[70].

techniques, tree rings were analyzed to check for any outbreaks. The data collected was from the year 1671 till 2012. A non-host tree and host tree (larch) were selected and similar studies were done on samples from both. A sample from a non-host tree is required to subtract out the destruction of foliage if any due to the environment rather than due to the budmoth. These studies conclusively showed that there have been no cyclic outbreaks in the Tatra mountains. A possible reason for this could be the geographical differences between the two regions. Larch trees grow at altitudes of 800 to 2200 meters above mean sea level. Budmoth outbreaks occur on larches that grow at altitudes of 1500 to 2000 meters above msl. In the Tatra mountains of Slovakia, larch trees grow at much lower altitudes — between 850 to 1500m above msl[68] which are at slightly warmer conditions compared to the larches growing in the high Alps. The second noticeable difference between the Alps and the Tatra region is that in the Alpine region larch trees are densely packed, and it is this dense growth that enhances the larch outbreak [69]. More interesting dynamics occur when the larch trees are densely packed[69]. However, in the Tatra mountains, the distribution of larches is much sparser and hence the recurrence of the outbreaks is inhibited. The third possible difference between the Alps and the Tatra region could be related to the amount of the sunshine which is felt by the larch trees. With more cloud cover and heavy precipitation, the Tatra region does not expose the larch trees to the desired amount of sunlight during the growing phase of the plant when the buds sprout into foliage. In the Alpine region there is no such problem.

4.5 Modeling of Larch Budmoth cycles – previous attempts

4.5.1 One dimensional models

Other than the logistic map and Ricker map, there are other maps that can be used to model populations. The budmoth population is known to cycle every 8-9 years. In [70], one-dimensional maps were considered for modelling its dynamics. Five one-dimensional maps were used and the simulation results were compared with the original data set. Various lag terms were used and the simulations were carried out. The 5 models used are listed in table (4.4).

Of all these models, only the 5th model (Moran-Ricker model), gave the best match, and this was further modified by using lags[70]. It was found that using 4 lags in the 5th map gave results that were comparable to the original data. However, this model is empirical, with tight tuning of

parameters[70].

4.5.2 Host-Herbivore Model

Since budmoths depend on the larch needles for food, it was assumed that the interplay between them determined the cycles[57]. The dynamics was first modeled usign herbivore and plant interaction. Since it is a herbivore-plant interaction, the plant can be quantified using the length of the leaves[57]. The variables N_t and L_t represent the larch budmoth population density and the length of the larch needles[57]. The leaves when infested badly do not regrow well and indirectly indicate the health of the tree. It has been noted that the un-infested leaves have more protein and less fibre, while an infested tree has leaves which have more fibre content and less proteins[57].

The tree uses its reserves to repair the damage that is inflicted on the leaves infested by the budmoth. Because of this, the leaves that sprout in the next spring are deficient in nutrition. Increasing the fibre adds strength to the needles so that they are tough. This makes it a little more difficult for the budmoth larvae to devour the hard needles. It has been seen that after an infestation, the protein content in the needles drops from 6% to4% , while the fibre content increases from 12% to 18%. The average needle length is 15mm. Using this average value a normalised plant quality index (PQI) is defined[57]:

$$Q_t = \frac{L_t - 15}{15} \quad . \tag{4.27}$$

The equations for the budmoth and the plant quality index (PQI) are:

$$N_{t+1} = N_t \lambda \frac{Q_t}{\delta + Q_t} \exp(-gN_t) \tag{4.28}$$

$$Q_{t+1} = (1-\alpha)(1 - \frac{N_t}{\gamma + N_t}) + \alpha Q_t \tag{4.29}$$

where g is the intraspecific competition between the budmoths, δ is the half saturation constant of the PQI, γ is the half saturation constant for the budmoth and λ is the intrinsic growth rate. α denotes the plant vulnerability.

In the year 1990, there was a high mortality of eggs of the budmoth in the Engadine valleyof the Swiss Alps as a result of which[71] the larch trees were not affected; hence in the subsequent years, it was expected that the foliage would enhance budmoth growth. However the budmoth population failed to reach a maximum despite the availability of food[71]. Thus an increase or decrease in the food did not drive the cycle[71]. This observed fact indicated that the cycles are not driven by the interaction between the budmoths and larch but rather by something else.

4.5.3 Host-Parasitoid Model

There are more than 94 species of parasitoids[72], parasites and viruses that attack the budmoths and devour them, thus making it an important factor to consider their presence in a model for the budmoth population dynamics. The parasitoids are high in aggression and in closeness. Most of the time they kill the budmoth and hence the population density of the budmoth is always in

check. The interaction between the parasitoids and the budmoth is modeled using Nicholson-Bailey type interaction[57]. Here the budmoth population is governed by the Ricker type model, and the interaction with the parasitoids comes in via a Holling type II functional response[73]. In Holling type-II functional response, the functional response saturates when the food availability is large. This is to account for the fact consumption cannot be continuous and instantaneous. The functional form of Holling type II is given in the table(4.2), which is a hyperbolic form. Since parasitoids cannot be actually counted, they are considered to be a proportion of the budmoths, here given by a multiplicative factor ϕ. It was assumed that the parasitoid-budmoth interactions are responsible for the cycles we see. The equations that follow this section captures the parasitoid-budmoth dynamics.

$$N_{t+1} = \lambda N_t \exp(-N_t - \frac{aP_t}{1 + ahN_t + awP_t}) \tag{4.30}$$

$$P_{t+1} = \phi N_t (1 - \exp(-\frac{aP_t}{1 + ahN_t + awP_t})) \tag{4.31}$$

In the equations above N_t and P_t represents the budmoth population density and the parasitoid population density at time t[57]. a represents the searching rate of parasitoids in searching the budmoths; the wasting time w is the time spent in hunting the prey and consuming it, and h is the parasitoid handling time. Since parasitoids live inside the body of budmoth, we consider h to be vanishing throughout our work.

Still, this model couldn't precisely reproduce the observations. Although it is known that the parasitoid population increases and decreases based on the budmoth numbers, still parasitoids play a vital role in controlling the cycles[66]. The ability to stop the population increase is brought in by a first order effect whicle oscillations occur due to second order effect. Both the two dimensional models have the first and the second order effects which stop the population from raising indefinitely and to sustain oscillations. However both the models are deficient in explaining the actual observations made, compelling one to move towards a tritrophic model.

4.5.4 Tritrophic Model I

The first tritrophic model involving budmoth[57, 74], parasitoid, and the plant quality index was due to Turchin, who had used a 4-dimensional model. In this model along with the budmoth, parasitoid, and plant quality index, the intrinsic growth rate also varied, thus making it a 4-dimensional system. Observations proved that the plant quality index did not affect the carrying capacity but affected the growth rate[57]. Thus, the intrinsic growth rate depended upon the plant quality index and thus became a variable in the system. Table (4.5) gives the values of parameters that is used to

Parameter	Range	Parameter	Range
r_0	2.5 ± 0.2	a	2.5 ± 1
α	0.5 ± 0.1	w	0.17 ± 0.2
K	250 ± 50	c	0.7 ± 0.2
δ	0.22 ± 0.05	d	150 ± 150

TABLE 4.5. Parameter values used in Turchin's model

simulate the situation[57, 74]. The equations governing the system are

$$\begin{aligned} N_{t+1} &= N_t \exp\left(r_0(1-\exp(\frac{-Q_t}{\delta})) - \frac{r_0}{K}N_t - \frac{aP_t}{1+awP_t}\right) \\ P_{t+1} &= N_t\left(1-\exp(\frac{-aP_t}{1+awP_t})\right) \\ Q_{t+1} &= (1-\alpha) - \frac{cN_t}{d+N_t} + \alpha Q_t \\ \lambda_t &= \exp\left(r_0(1-\exp(\frac{-Q_t}{\delta}))\right) \end{aligned} \tag{4.32}$$

The parameters used in this model are:
r_0 which denotes the growth rate,
α which is the plant vulnerability parameter,
δ which determines the rate at which r_0 reaches the saturation,
γ, the half saturation constant for the budmoth,
a which denotes the parasitoid searching rate,
w, the parasitoid wasting time,
K, the carrying capacity,
c which controls the rate at which the PQI is lost due to budmoth infestation.

4.5.5 Tritrophic Model II

This model[75], also enunciated by Turchin is a three dimensional model, with N_t denoting the population of budmoths, P_t denoting the parasitoid population density and Q_t denoting the plant quality index. Here the intrinsic growth rate λ is multiplied with a Holling type-II feeding function[73]. The values of parameters are also not clearly stated in ref.[75]. However, from [76] and [57] the parameter values were obtained and deduced and this model was tested. The equations governing this model are,

$$N_{t+1} = N_t\lambda\frac{Q_t}{\delta+Q_t}\exp(-gN_t - \frac{aP_t}{1+ahN_t+awP_t})) \tag{4.33}$$

$$P_{t+1} = \phi N_t(1-\exp(-\frac{aP_t}{1+ahN_t+awP_t})) \tag{4.34}$$

$$Q_{t+1} = (1-\alpha)(1-\frac{N_t}{\gamma+N_t}) + \alpha Q_t \tag{4.35}$$

The parameters used in this model are
λ denotes the growth rate,

α which is the plant vulnerability parameter,
δ which determines the rate at which r_0 reaches the saturation,
γ, the half saturation constant for the budmoth,
a which denotes the parasitoid searching rate,
w, the parasitoid wasting time,
K, the carrying capacity,
h, the handling time of the parasitoid,
ϕ, the efficiency of parasitoid.
In this model the evolution of leaves had two parts. The first part is evolution of leaves which are not infested by the budmoth and second part is the one infested by the budmoth. This model when simulated did not yield significant variation in the plant quality index, which is quite in contrast with what is observed in nature[74]. The possible reason, could be because the second term that denotes the loss of PQI due to budmoth is assumed to be lost at a constant rate.

CHAPTER 5

A $q-$DEFORMED TRITROPHIC MODEL FOR THE LARCH BUDMOTH POPULATION CYCLES

The models mentioned in the previous chapters are the previous attempts made by others to reproduce the observed 9-year cycles of the budmoth outbreaks. A modification of Turchin's model[75] employing $q-$deformation of numbers was proposed by us and presented in [77]. In this model we introduced a density dependent removal of the larch needles plant quality index(PQI). This model is able to successfully simulate some of the observations.

5.1 $q-$ deformed tritrophic Model with density dependent removal of PQI

The ecological system is highly complex with a multitude of interactions. In general, ecological systems have parameters that are not invariant in time. These systems also have long range interactions and have a memory of the past events. In the larch budmoth (LBM) system, the budmoth infests the larch tree needles for food. The infestation in the previous year affects the infestation in the current year. Infestation depends on the nutrition content of the needles. A heavily infested tree uses its reserve to strengthen itself rather than for sprouting more foliage. For instance, after an infestation, the leaves are rich in fibre that makes it tough and strong. However such leaves lack protein and are less nutritious[57]. Due to this, the current infestation is much reduced compared to the past one, as the budmoth larvae have to deal with tougher and sturdier leaves which would be less palatable. Since the memory of the past events affects the current event, the system is highly non-ergodic. Loss of ergodicity skews the probability distribution. This could lead to enhancement of rare events and suppression of favorable events. This alteration is mainly due to the memory inherent in the system. In this system, usual classical statistical physics fails. This non-ergodic nature of the system motivates the use of $q-$deformed variables to explain the

dynamics.

A tritrophic model with a density dependent removal of PQI was first introduced by us in [77]. This was introduced so as to have a removal of PQI proportional to the budmoth numbers. When PQI is low, that is when the larch tree needles are less, the budmoth infestation is also less. The healthier the leaves, more is the infestation, until for very high PQI, the infestation becomes constant. This behaviour is captured by including the q-deformed variable for the plant quality index.

In this model the equations are made dimensionless by scaling the variables in the following way. Let N_t denote the population density of the budmoth at time t, P_t denote the density of parasitoid population infesting the budmoth and L_t denote the larch needle length [77, 57]. The normalised plant quality index (PQI) Q_t is used to quantify the variable for the larch needles as in eqn.4.27.

Using dimensionless scaling introduced in [76], we define new dimensionless variables x_t, y_t and z_t to respectively represent budmoth population density, parasitoid population density, and plant quality index as follows [76, 77]:

$$x_t = \beta N_t, \quad y_t = aP_t \ \ and \ \ z_t = Q_t \quad . \tag{5.1}$$

We deform the variables x,y,z using deformation parameters q_i , $(i = x, y, z)$ to incorporate the non-ergodic feature of the system. Since different species are involved, each of which responds in a different way to stimuli, the values of q_x, q_y and q_z need not be same. In this model for simplicity we keep x_t undeformed with $q_x = 1$, but we deform the y and z variables with $q_y \neq 1$ and $q_z \neq 1$. The deformed $y_{q,t}$ and z_{qt} are given by

$$y_{qt} = \frac{\rho_y y}{1+\mu_y y} \tag{5.2}$$

$$z_{qt} = \frac{\rho_z z}{1+\mu_z z} \tag{5.3}$$

$$\rho_i = \frac{1}{2-q_i} \tag{5.4}$$

$$\mu_i = \frac{q_i - 1}{2-q_i} \qquad i = y, z \tag{5.5}$$

We propose the following equations with the q-deformed variables to describe the larch budmoth system:

$$x_{t+1} = \lambda x_t \frac{\rho_z z_t}{1+\mu_z z_t} \exp\left(-x_t - \frac{\rho_y y_t}{1+\mu_y y_t}\right) \tag{5.6}$$

$$y_{t+1} = c x_t \left(1 - \exp(-\frac{\rho_y y_t}{1+\mu_y y})\right) \tag{5.7}$$

$$z_{t+1} = (1-\alpha)\left(1 - \frac{x_t}{m+x_t}\right) - \alpha x_t \frac{\rho_z z_t}{1+\mu_z z_t} \tag{5.8}$$

$$\rho_i = \frac{1}{2-q_i} \tag{5.9}$$

$$\mu_i = \frac{q_i - 1}{2-q_i} \tag{5.10}$$

The last term in the equation for z represents the density dependent removal of larch needles. When the needle length is very small, the rate of removal is proportional to the available leaves. However when the needles are fully grown, the removal rate is constant which denotes the fact that the budmoth cannot consume indefinitely just because the resources are abundantly available.
The feature of density-dependent removal of the larch needles which is physically observed in nature is not captured by Turchin's models.

The various parameters in the system are

1. α
   α is the vulnerability parameter[76]. Higher the value of α greater is the damage done to the larch tree needles. This is also called as the memory parameter. The equation governing the plant quality index resembles an autoregressive AR(1) process with α as the memory parameter. In an AR(1) process, the value of the variable at time $t+1$ is proportional to the value at time t. α varies from 0 to 1. $(1-\alpha)$ denotes the plant recovery rate. A higher value of α implies a poor recovery rate. At α=1, the value of PQI is zero. Consider the equation for the larch tree leaves. In an event of a forest fire or sudden loss of leaves, the PQI goes to zero. In that situation, the solution automatically forces α to equal 1 which implies that the leaves are completely damaged and $1-\alpha=0$, which means that the plant cannot recover. A small departure of α from one implies that plant recovery is at a very slow rate.

2. λ
   λ is the intrinsic growth rate of the budmoth[75]. The higher the growth rate the faster the budmoth population rise. It is found that the plant quality index affects the intrinsic growth rate rather than the carrying capacity of the bud moth. The main supporting evidence came from the observations made in the Engadine valley, Switzerland, where the budmoth outbreak cycle collapsed despite the resources/food[71].

3. m
   m appears in the equation for PQI[76]. It is the half-saturation constant of the budmoth. It dictates the rate at which the functional response reaches saturation. A smaller value of m implies a fast change in the functional response. That is the functional response rises steeply and reaches saturation while larger values of m imply a gradual transition, i.e., the response is almost linear and finally it saturates. This is related to the budmoth's efficiency in destroying the foliage. The rate of destruction becomes constant when the budmoth population is high, and m decides how the transition occurs. $m=\beta\gamma$, where γ is the half saturation constant and β is the intraspecific competition in the tritrophic model II.

4. c
   c is equal to the ratio of efficiency of the parasitoid in infesting the bud moth to the intraspecific competition among bud moth[76]. This is given as $\frac{ba}{\beta}$ where b is the number of surviving

parasitoids produced by a living parasitoid[76]. a is the handling time. i.e., it is the time taken to consume the prey. The greater the value more is the time taken to consume the prey. β, which is the intraspecific competition among the budmoths, can be high or low. A higher value of β implies a very high population of budmoth or very low availability of food (poor quality of PQI). The lower value of β implies availability of too many resources or low population of bud moth.

5. q_y

   By making a comparison between the equations (4.34 and 5.7), we identify q_y with the parasitoid wasting time[77]. In the equation for the parasitoid and the budmoth, the parasitoid is deformed using q_y. The deformation is included so as to avoid over-counting of the parasitoids. When $q_y = 1$, it is equivalent to assuming that the parasitoid is not wasting any time. That is to say, the time to consume the prey is not considered. But then the parasitoid requires the host for its survival and does not kill the host immediately, thus there is some time wasted by the parasitoid. To avoid the over-counting we deform the parasitoid population density with the parasitoid wasting time. The greater the value of q_y more is the time is wasted by the parasitoid to search for its prey. The parasitoid wasting time w is equal to $\frac{q_y-1}{2-q_y}$[77], which implies that the wasting time w can have a minimum of zero and maximum of infinity when q_y takes the value 1 and 2 respectively. Bearing in mind that the parasitoid wasting time is a positive quantity, we concur that q_y varies between 1 and 2. Larch bud moth larvae live inside the larch tree cone. During this stage these are dormant and motionless, so effectively the parasitoids are limited in spreading. Hence, q_y is larger than 1. In Beddington model q_y is equal to one. It is assumed that every attack the parasitoid makes on its prey is converted into increasing the parasitoid number, just as in the Lotka Volterra model, hence this results in higher estimates of the parasitoid number. To avoid the over-counting of individuals, a density dependent feeding function is introduced via $q-$deformations, and thus for this new model q_y is not equal to 1 and thus over counting is avoided. This feature is seen in both of Turchin's models.

6. q_z

   By comparing equations (4.33 and 5.8), it is evident that q_z is related to the intraspecific competition among the budmoths[77]. $q_z = 1 + \beta$, which is identified using $\rho_z = \frac{1}{\beta\delta}$ and $\mu_z = \frac{1}{\delta}$[77]. Theoretically, the intraspecific competition can vary from 0 to ∞. However restricting δ to be positive limits the value of β between 0 and 1, thus making q_z vary between 1 and 2. Again this is incorporated to take into account the wasteful feeding by budmoth larvae. If q_z equals 1, as in Turchin's model, this would correspond to the assumption that the rise in bud moth numbers is proportional to food available. By setting $q_z \neq 1$, we take into account the wasteful feeding of the larvae. The second term in the equation for the plant quality index is different from that in Turchin's model. In Turchin's model, the decay of damaged leaves was considered constant. However, wasteful feeding also damages the larch trees, and despite the

fact that the needles are not fully damaged, the needles take a longer time to regrow, since the tree uses its resources to repair itself, thereby taking a longer time to flourish again. This is captured in our model.

5.1.1 Linear stability analysis

Linear stability analysis is performed by doing a Taylor series expansion of the governing equations. The Jacobian of the system, governs the systems behavior near the fixed point (x^*, y^*, z^*). The Jacobian matrix is given by,

$$\begin{bmatrix} \lambda z_q^* \exp(-x^* - y_q^*) & \frac{-x^*\lambda\rho_y \exp(-x-y_q^*)}{(1+\mu_y y^*)^2} & \frac{-x^*\lambda\rho_y \exp(-x^*-y_q^*)}{(1+\mu_z z^*)^2} \\ c(1-\exp(y_q^*)) & -c\frac{\rho_y \exp(-y_q^*)}{(1+\mu_y y^*)^2} & 0 \\ \frac{\alpha m}{(m+x^*)^2} & 0 & \frac{\alpha x^* \rho_z}{(1+\mu_z z^*)^2} \end{bmatrix}$$

There are three kinds of fixed points. (i)The trivial solution is when there is no bud moth and parasitoid, only leaf stays; (ii) the parasitoid free solution, wherein there is no parasitoid, only larch tree and the budmoth coexists; (iii) Finally the nontrivial solution has non-zero values for all the three species.

Trivial Solution

This trivial solution which denotes non zero value for the PQI is given by $(0,0,(1-\alpha))$. The Jacobian at $(0,0,(1-\alpha))$ is given by,

$$\begin{bmatrix} \lambda(1-\alpha) & 0 & 0 \\ 0 - c\rho_y & 0 & \\ \frac{\alpha-1}{m} + \frac{\alpha(1-\alpha)\rho_z}{1=(1-\alpha)\mu_z} & 0 & 0 \end{bmatrix}$$

The eigenvalues of this Jacobian at the fixed points are 0, $-c\rho_y$ and $\lambda(1-\alpha)$. If the real parts of all the eigenvalues are less than 1, then the fixed point is said to be stable. Thus for this trivial solution to be stable, it requires that $|c\rho_y| < 1$ and $|\lambda(1-\alpha)| < 1$. That is to say for a low value of c and for $\lambda < \frac{1}{1-\alpha}$, the fixed point is stable. This physically implies that when the intrinsic growth rate of the budmoth is too low and if the parasitoid is also not efficient in devouring the budmoth, then the system cannot have cycles. This consistent with the observations. It is noted that if the parasitoid and the budmoth are decoupled then cycles do not exist [66]. Similarly, if the budmoth cannot grow, there will not be a significant rise in populations. When both λ and $c\rho_y$ increase, the fixed point loses is stability and cycles are born. One of the eigenvalues is zero for this system, this indicates that the system possesses an unstable manifold.

5.2 Results

Our $q-$deformed model produces cycles. It is known that the bud moth exhibits an average of 8-9 year cycles [67]. Our $q-$deformed model also produced cycles of various time periods, depending on the value of the parameters. From the figures (5.1(a)-5.1(c)), one can see that all the three interacting species are synchronized and have the same time period. The parasitoid alone has a

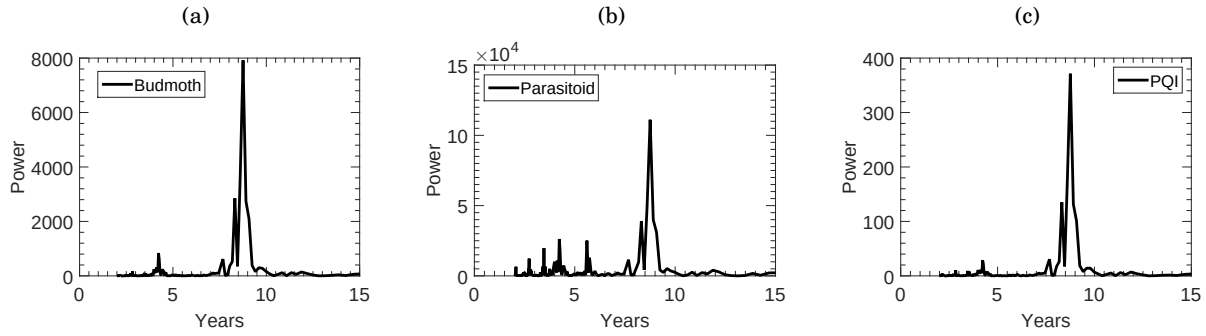

FIGURE 5.1. The power spectrum is generated from the time series using FFT. The values of the parameters chosen to generated the power spectrum are $\lambda = 8$, $\alpha = 0.5$, $m = 13$, $c = 12$, $q_y = 1.13$ and $q_z = 1.34$. The figures show the power spectrum of (a) budmoth (b)parasitoid (c) PQI

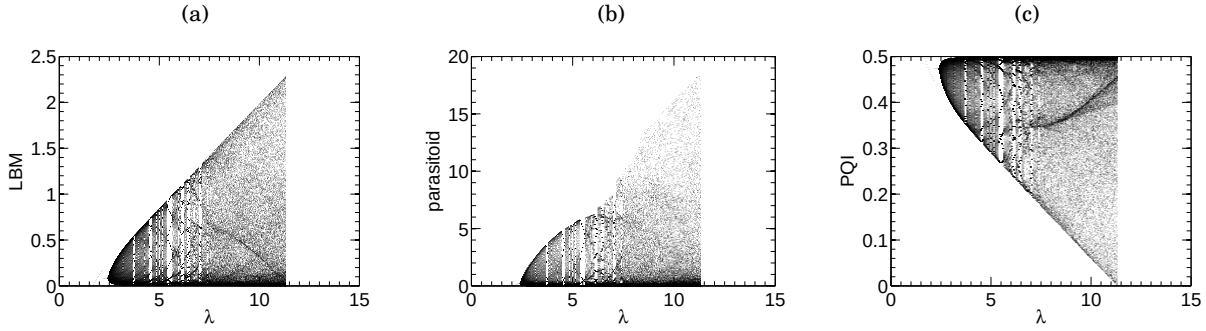

FIGURE 5.2. The bifurcation diagram is generated with respect to the parameter λ with all other parameters set at $\alpha = 0.5$, $m = 13$, $c = 12$, $q_y = 1.13$ and $q_z = 1.34$. (a) budmoth (b)parasitoid (c) PQI

strong sub-harmonic at half the dominant time period (refer to figure (5.1(b))). This is not seen in the other two species.

The system exhibits Neimark-Sacker bifurcation as the parameter value is varied. The figure below shows Neimark-Sacker bifurcation with respect to λ ($\lambda = 2.1$) with other parameters fixed at $\alpha = 0.5$, $m = 13$, $c = 12$, $q_y = 1.13$ and $q_z = 1.34$.

In the bifurcation diagram, it is evident that for low values of λ cycles do not occur. As λ is increased Neimark-Sacker bifurcation occurs, which creates limit cycles. The figures(5.2(a)-5.2(c)), shows the limit cycles at higher values of $\lambda(\lambda > 2.1)$. The bifurcation diagram with respect to q_z, q_y and α is presented in figures (5.3(a)-5.3(i)). The parameters q_y, q_z are deformation parameters related to parasitoid wasting time and the intraspecific competition among the bud moth. As the parameters change, one can see interesting dynamics in the system. The system goes from being chaotic to periodic as the parameter q_y is changed. In these figures (5.3(a)-5.3(c)), it is evident that the larch budmoth, the plant quality index and the parasitoid exhibit the same kind of dynamics as the parameters are changed. The system is highly synchronized. The figures (5.3(a)-5.3(c)),

show the bifurcation diagram with respect to parameter q_y. The three figures respectively denote the budmoth, parasitoid, and the PQI populations. We see a reverse Neimark-Sacker bifurcation with respect to parameter q_y This is seen at $q_y = 1.345$. A higher value of q_y implies that the parasitoid is wasting more time and thus is less efficient in attacking the budmoth. This results in weakening of the larch budmoth and the parasitoid interaction, which finally halts the cycles. This is again consistent with the observations that are made in the Alpine region[66]. The figures (5.3(d)-5.3(f),) show the bifurcation diagram with respect to parameter q_z which is related to intraspecific competition[77]. The cycles exist till $q = 1.6$, after which we see no solutions. When the intraspecific competition is too high, the budmoth population collapses and goes to extinction. The figures (5.3(g)-5.3(i),) show the bifurcation diagram with respect to parameter α which is realted to the plant vulnerability. Higher the value of α, more is the damage to the plant quality index. As α increases the population of all the three species collapses to zero. At $\alpha = 0$, the plant is safe, and thus it is fully grown. As α increases, the plant becomes more susceptible to the attack by the budmoth. There are some paired cascades in all the species at the values of $0.05 \leq \alpha \leq 0.35$. When α is very high, i.e, close to 1, the plant quality index vanishes which brings down the larch budmoth population. This brings the parasitoid population also to zero[77].

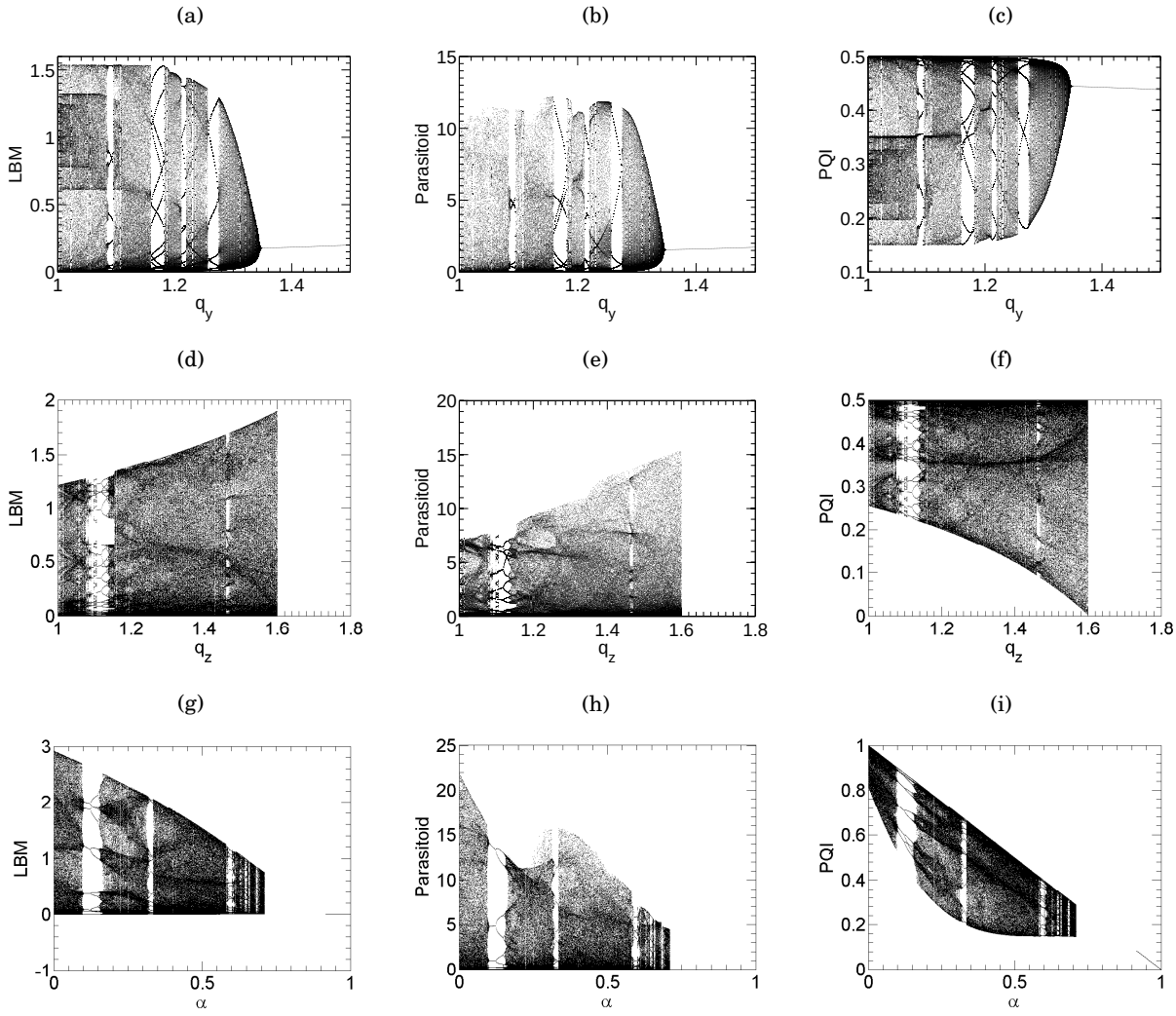

FIGURE 5.3. The bifurcation diagram is generated with the parameters values $\alpha = 0.5$, $m = 13$, $c = 12$, $q_y = 1.13$, $\lambda = 8$ and $q_z = 1.34$. (a) LBM vs q_y (b)parasitoid vs q_y (c) PQI vs q_y (d) LBM vs q_z (e)parasitoid vs q_z (f) PQI vs q_z (g) LBM vs α (h)parasitoid vs α (i) PQI vs α

CHAPTER 6

CAPTURING CLIMATE CHANGE EFFECTS ON BUDMOTH CYCLES WITH A $q-$DEFORMED MODEL

In the previous chapter, we motivated the readers towards our new $q-$deformed model that would solve some of the deficiencies of the models existing in the literature of the larch budmoth system such as the evolution of the partially eaten leaves.

Climatic and environmental changes have a direct impact on plant growth and the ecological systems centered around them. Yet, none of the mathematical models existing in the literature of the larch budmoth system have shown how climate and environmental effects can be directly included in the model and how these can affect the population dynamics. In this chapter we describe how we successfully included environmental/climate effects for the budmoth population dynamics for the first time in the literature[78].

Turchin's tritrophic model I was simulated and it gave the periodicity of 9 years as cited in [57]. However, the model is very finely adjusted with parameters which are tightly tuned to give the desired cycles and the error bars cited in [57] are large. A small perturbation in any of the parameters gives rise to completely different cycles. To produce cycles of different lengths, many changes are required in the model.

The parameter values for Turchin's II model[75] had not been specified by him. We extracted the values from [76, 57] and simulated it and found that it gave very different time periods. The variation in the plant quality index is also minimal and it required the value of α to be very low to produce even a very small variation. Our $q-$deformed tritrophic model with density dependent removal of PQI has a better variation compared to the models described in [75, 57]. There is another problem with this model. In the equation that governs the PQI, the description is not complete. Firstly, in Turchin's tritrophic models I and II a constant decay of damaged leaves was considered, while in model III a density-dependent removal of leaves was considered. However, the model III is not complete as we did not take into consideration the leaves which were damaged partially by the

budmoths. These damaged needles, do not recover unless environmental conditions are favorable. These damaged needles lack nutrition and thereby do not attract anymore budmoth larvae to feed upon them. Thus, the plant quality index must have three governing terms — one that governs the evolution of leaves that are not infested by budmoth, the second term that governs the evolution of needles that were damaged in wasteful feeding, and the third term that governs the current removal of leaves by the budmoth.
Secondly the above-mentioned models could produce only cycles. The parameters used in the model are all species-specific. For instance α, δ, from the models I and II and q_z in model III are related to PQI, the parameters r_0, d, K in the model-I ,γ in model II and λ, m in our q-deformed model are related to the budmoth and a,w,h in the model I and II and c in our q-deformed model are related to the parasitoid. To produce a different cycle one needs these values to change which could happen only if different species come into play or evolution occurs that changes the parameter values. However, evolution cannot occur at small time scales. Thus, we have a model which can only give 9-year cycles and nothing else.

In the 1200 year dendrochronological data[67] other cycles too, apart from the 9-year cycles have been observed. Thus one is drawn to conclude that there are other parameters apart from the species-specific ones, which play an important role in controlling the length of cycles. We recall that in the Swiss Alps the 9-year cyclic outbreaks which had been occuring over the centuries collapsed after 1981. We hypothesize that the main reason for the breakdown of the cyclic outbreaks of the budmoth are environmental factors. It is only the environment which has not remained constant or invariant over the years.
Anthropogenic activities alter our climate. The environment around us always affects us. Global warming has affected many taxa of species. Due to environmental changes, some species have become endangered and some have become extinct locally [79]. A classical example for this event is the coral reefs that are bleached due to increase in the acidity of the oceans due to absorption of more carbon dioxide. Bleached corals do not support any life and hence all the organisms that depend on corals have started to vanish. Just as an oasis in the desert supports life, corals in the sea are local regions which support a diversity of life. Due to global warming these have now become dead structures. Another effect of global warming is the shift of organisms to higher latitudes and altitudes, in search of cooler temperatures. In the last 150 years, global warming has made the earth, so warm that the Arctic regions are now conducive for plants to grow upon. The Arctic regions were once too cold to support any plants now appear green due to vegetation that have begun to grow there. Most of the animals living within the arctic circles relied on hunting the fishes and other organisms that lived there. However the recent change in the landscape due to growth of vegetation would slowly bring in other creatures too, thus endangering territories of the native animals. An example is the entry of the red fox into the arctic circle, which is the territory of the Arctic fox [80]. Alpine plants are shifting northward due to increase in temperature [81]. Change in the domain of one species has affected the food web of the entire ecological niche. Sometimes the effect could be very severe, resulting in the local extinction of all species

that interacted with the one that shifted. This is not something new. Even today in China, due to the absence of pollinators (bees), human pollinators are used, who climb every tree to collect pollen and then deposit it in the stigma of some other flower [82] [83]. If this was not done, there will not be any fruits, and that would imply food scarcity and local business is also affected. Bees got eradicated from China as their natural habitat began to shrink, due to deforestation that was done to increase farm land. Use of pesticides also killed most of the insect pollinators. In the UK also there are reports of six bee species becoming extinct and some others becoming endangered [84].

The changes in the environment thus cause movement of habitat and territory, which take a very long time to notice. But disruptions in population cycles happen very fast and are observable in a few generations. Collapses of population cycles have been noted in many species. Due to unavailability of long time series, modelling and analyzing the other systems has not been possible. However, insect pest outbreaks get recorded in the tree rings and using dendrochronological studies, it is possible to reconstruct the health of trees for many years. Such a study on the larch trees which provided an uninterrupted data of larch budmoth outbreaks spanning 1200 years also reveals a shift in the elevation of the occurence of the outbreaks. The possibility of environmental changes being the cause for the collapse of te larch budmoth cycles after 1200 years of regular periodicity was suggested in [85]. Our work [78] proves this in a mathematical model for the first time in literature. The larch tree and the budmoth are both affected by the environment. The leaves that are infested by the budmoth do not recover to their fullest if environmental conditions are bad. Similarly, the diapausing of larch budmoth eggs occurs at 2^o C. When the egg is exposed to high temperatures, diapausing occurs for a longer time. Due to this longer diapausing the egg mortality increases. It has been found that diapausing for 180 days causes 14 to 19 percent egg mortality, while 270 days diapausing results in 36 percent [86]. Thus higher temperature increases the diapausing stage, which results in more budmoth deaths.
From the analysis of 1200 year data, it is very clear that after 1981, no outbreak has occurred till today[71]. The next budmoth outbreak after 1981 was expected in 1990 but it did not occur. Clearly after 1980, something has led to the collapse of the cycles[87]. It is also noted that it is during these times there are regime shifts taking place globally. Notable temperature warming in the upper troposphere over Switzerland after 1980, has been reported in [88] resulting in a shift globally of the climate to warmer states within short time-span. We suggest in [78], that the collapse of budmoth cyclic outbreaks in the Swiss Alps has resulted because of a climatic tipping point reached in 1980's.

With these considerations we have performed simulations after including environmental parameters in our model which is discussed below.

6.1 Effect of the environment on the larch budmoth cycles

Environmental effects can be incorporated in many ways. Larch foliage flourish well when exposed to sunlight during the growing phase when the larch buds sprout in early spring at which time the

first instar larvae of the budmoth emerge. Clear weather favors growth in this stage. Changes in the temperatures also affect the budmoths. If the temperature is higher, then eggs diapause for a longer time and this increases the mortality of eggs. Thus, if winter temperatures are too high the eggs will die. However, the eggs that mature to become larvae will enjoy good food, especially if the next summer was cloud cover free and allowed bright sunshine. In general, it is noted that the increase in temperature favors the budmoth population increase. Thus, we introduce the environmental parameters h and s as coefficients multiplying the evolution of damaged leaves and the current infestation term respectively[78]. The equations in our model contain 8 parameters. Although for a model it may be very bad to have many parameters, for simulations every detail is necessary so that the simulations match the observations[89]. Indeed, our 8 parameter model does explain many things.

6.2 $q-$deformed tritrophic model with environmental parameters

Let N_t denote the population density of larch budmoth at time t, P_t denote the number of parasitoids infesting the budmoth and L_t denote the needle length of the larch tree. We use the dimensionless scaling introduced by Jang and Johnson[76] in their study using Turchin's 2-dimensional model equations (4.33,4.34,4.35) [76]: $N_t\beta = x_t, \quad aP_t = y_t, \quad \frac{L_t-15}{15} = z_t$. We describe the tritrophic larch budmoth system incorporating climate/environmental parameters h and s with the following equations:

$$x_{t+1} = \lambda x_t \frac{\rho_z z_t}{1+\mu_z z_t} exp\left(-x_t - \frac{\rho_y y_t}{1+\mu_y y_t}\right) \tag{6.1}$$

$$y_{t+1} = c x_t \left(1 - exp(-\frac{\rho_y y_t}{1+\mu_y y})\right) \tag{6.2}$$

$$z_{t+1} = (1-\alpha)\left(1 - \frac{x_t}{m+x_t}\right) + \alpha(h - s x_t)\frac{\rho_z z_t}{1+\mu_z z_t} \tag{6.3}$$

$$\rho_i = \frac{1}{2-q_i} \tag{6.4}$$

$$\mu_i = \frac{q_i - 1}{2-q_i} \tag{6.5}$$

6.3 The Environmental/Climate parameters h and s

All the parameters used in this model, have the same meaning as before(tritrophic model III). However, we have introduced 2 more parameters to mimic the role of environment on the system. These two parameters are denoted by h and s[78].

The parameter climate h varies from 0 to 1[78] with 0 corresponding to a less favorable environment condition and 1 corresponding to favorable conditions that support plant growth. This could be related to the amount of sunshine and precipitation. h directly affects the plant quality index[78]. It is noted that h is present only in the second term and not the other terms. Such a choice is made

for the reason that the first term which is the evolution of leaves that are not infested by budmoth is not going to grow more than maximum if environmental conditions are good. Similarly the third term is the current infestation by the budmoth, which is not affected by the environmental factors. However the second term is the evolution of damaged leaves, which when environmental conditions are good, grow well.
This parameter s is also introduced by us. This denotes the strength of the interaction between the PQI and the budmoth[78]. s varies from 0 to 1[78]. A higher value of s implies effective removal of PQI. s can also be viewed as the effect of environment on the budmoth although there may be lots of other things also to contribute to it. It may be related to the inverse of temperature. s=0 could be related to high temperatures while s = 1 could represent low temperatures[78]. s appears in the equation of the larch tree leaves. This can be seen in the third term that denotes the current infestation. We have made this deduction based on the fact that higher winter temperatures cause more mortality in the budmoth eggs. The higher mortality is caused due to longer diapausing, which compromises the quality of eggs. In the case of higher mortality the larch tree is saved, while a lower mortality implies devouring of the foliage. Since the eggs are destroyed, s doesn't affect the existing budmoth larvae, which continue to feast upon the existing larch foliage. However it is the next generation which is affected by environment. Thus the number of larvae coming out of these eggs are less in the next generation, there by damage to the tree is less. This is the reason why we had introduced s in the equation for the larch tree rather than the budmoth itself. The effect of environment on the budmoth is seen via the effect on larch tree, which is affected directly by the environment (h) or indirectly by the budmoth (s). This effect of s is second order as the effect on the budmoth is through PQI and not direct. In other words its effect is seen only one generation later[78].

6.4 Stability Analysis

One of the tools to understand a nonlinear system is to study the behavior of the linearized version of the nonlinear system. Here too there three kinds of fixed points (x^*, y^*, z^*): the trivial solution, the parasitoid-free solution and the non-trivial solution.

1. Trivial Solution $(0, 0, z^*)$:
   The trivial solution physically represents the situation where the larch budmoth and the parasitoid are absent,with just the plant sticking around. The solutions for the same are given below for q_z=1 and for $q_z \neq 1$.

   Fixed points for $q_z = 1$:

$$x^* = 0 \;\; y^* = 0 \;\; and \;\; z^* = \frac{1-\alpha}{1-\alpha h} \tag{6.6}$$

Fixed points for $q_z \neq 1$:

$$x^* = 0 \;\; y^* = 0 \;\; and \;\; z^* = \frac{1}{2} - b \pm \sqrt{b^2 - a} \tag{6.7}$$

$$b = 1 - (1-\alpha)\mu_z - \alpha h \rho_z \tag{6.8}$$

$$a = 4\mu_z(\alpha - 1) \tag{6.9}$$

Since α is between 0 and 1, a is always negative. Since z^* denotes the plant quality index, its value is restricted to be positive, thereby we discard the negative solution and consider only the positive one.

2. Parasitoid-free Solution $(x^*, 0, z^*)$:
   Parasitoid-free solution as the name suggests is a situation where there are only two interacting species.
   Fixed points for $q_z = 1$:
   From the equations for the budmoth, one gets the following relation between $z*$ and x^*,

$$z^* = \frac{1}{\lambda \exp(-x^*)} \tag{6.10}$$

   From the equations for the plant quality index we get

$$z^* = \frac{m(1-\alpha)}{(m+x^*)(1-\alpha(h-sx^*))} \tag{6.11}$$

   Equating the two equations we get,

$$x^{*2} + \frac{1 + m\alpha s - \alpha h}{\alpha s} x^* + \frac{m - m\alpha h}{\alpha s} = \frac{m(1-\alpha)\lambda}{\alpha s} \exp(-x^*) \tag{6.12}$$

   Solving the equations gives the the variable x^* from which z^* can be found.
   Fixed points for $q_z \neq 1$:
   From the equations for the budmoth, the expression for the deformed z_q is found to be,

$$\frac{\rho_z z*}{1 + \mu_z z*} = \frac{1}{\lambda \exp(-x^*)} \tag{6.13}$$

   The above expression can be used in place of the deformed z_q variable in the equation for the plant quality index.

$$z^* = \frac{(1-\alpha)m}{m+x} + \frac{\alpha(h - sx)}{\lambda \exp(x^*)} \tag{6.14}$$

3. Non-trivial equilibria (x^*, y^*, z^*)
   For $q_y \neq 1$ and $q_z \neq 1$, the fixed points are given by

$$z^* = \frac{(1-\alpha)m}{m+x} + \frac{\alpha(h - sx)}{\lambda \exp(x^* - (1 - \frac{y^*}{cx^*}))} \tag{6.15}$$

   The expression $(1 - \frac{y^*}{cx^*})$ is retrieved from the equation for the parasitoid.

6.4.1 Jacobian for the tritrophic system

The Jacobian matrix is constructed using the first derivatives of the equations. The construction allows us to study the linearized system about the fixed point. Here f is the map and f_1, f_2 etc., are the number of equations depending on the number of variables in the system that is considered.

$$J = \frac{d\mathbf{f}}{d\mathbf{x}} = \begin{bmatrix} \frac{\partial \mathbf{f}}{\partial x_1} & \cdots & \frac{\partial \mathbf{f}}{\partial x_n} \end{bmatrix} = \begin{bmatrix} \frac{\partial f_1}{\partial x_1} & \cdots & \frac{\partial f_1}{\partial x_n} \\ \vdots & \ddots & \vdots \\ \frac{\partial f_m}{\partial x_1} & \cdots & \frac{\partial f_m}{\partial x_n} \end{bmatrix}$$

Since this is a 3-dimensional system, we have a 3x3 matrix with 9 entries. From this matrix, the eigenvalues are found, which pinpoints the stability of the particular fixed point. One can also find the stability of the fixed point without finding the eigenvalue by using the Routh-Hurwitz criteria[51]. Consider a matrix given by

$\begin{bmatrix} A & B & C \\ D & E & F \\ G & H & I \end{bmatrix}$ To find the eigenvalues of this matrix, the characteristic equations are to be solved.

The characteristic equations of the Jacobian matrix is given by,

$$a_0\lambda^3 + a_1\lambda^2 + a_2\lambda + a_3 = 0 \tag{6.16}$$

where the coefficients are given by,

$$\begin{aligned} a_0 &= -1 \\ a_1 &= A + E + I \\ a_2 &= -AE + BD - AI + CG - EI + FH \\ a_3 &= -AFH + AEI - BDI + BFG + CDH - CEG \end{aligned} \tag{6.17}$$

The entries of the Jacobian matrix are as follows:

$$A = \frac{\rho_z z^*}{1+\mu_z z^*}\lambda \exp(-x^* - \frac{\rho_y y^*}{1+\mu_y y^*})(1-x^*) \tag{6.18}$$

$$B = -\lambda \frac{\rho_z z^*}{1+\mu_z z^*} x^* \exp(-x^* - \frac{\rho_y y^*}{)} 1 + \mu_y y^* \frac{\rho_y}{(1+\mu_y y^*)^2} \tag{6.19}$$

$$C = \lambda x \exp(-x^* - \frac{\rho_y y^*}{1+\mu_y y^*}) \frac{\rho_z}{(1+\mu_z z^*)^2} \tag{6.20}$$

$$D = c(1 - \exp(-\frac{\rho_y y^*}{1+\mu_y y^*})) \tag{6.21}$$

$$E = cx(1 - \exp(-\frac{\rho_y y^*}{1+\mu_y y^*})) \frac{\rho_y y^*}{(1+\mu_y y^*)^2} \tag{6.22}$$

$$F = 0 \tag{6.23}$$

$$G = \frac{-\alpha z^* s \rho_z}{1+\mu_z z^*} - (1-\alpha)\frac{m}{(m+x)^2} \tag{6.24}$$

$$H = 0 \tag{6.25}$$

$$I = \frac{\alpha(h - s x^*)\rho_z}{(1+\mu_z)^2} \tag{6.26}$$

1. Trivial Solution

   The trivial solution represents a situation where both the budmoth and the parasitoid are absent. In such a scenario, most of the entries of the Jacobian matrix are zero. i.e., $B = C = D = E = F = H$ Using these the entries of the Jacobian matrix are,

$$\begin{aligned} A &= \frac{\rho_z z^*}{1+\mu_z z^*}\lambda \exp(-x^* - \frac{\rho_y y^*}{1+\mu_y y^*})(1-x^*) && (6.27)\\ B &= 0 && (6.28)\\ C &= 0 && (6.29)\\ D &= 0 && (6.30)\\ E &= 0 && (6.31)\\ F &= 0 && (6.32)\\ G &= \frac{-\alpha z^* s\rho_z}{1+\mu_z z^*} - \frac{(1-\alpha)}{m} && (6.33)\\ H &= 0 && (6.34)\\ I &= \frac{\alpha h \rho_z}{(1+\mu_z)^2} && (6.35) \end{aligned}$$

   The coefficients are given by

$$\begin{aligned} a_0 &= -1\\ a_1 &= A + I\\ a_2 &= -AI\\ a_3 &= 0 && (6.36) \end{aligned}$$

   Using this Routh array is found to be,

$$\begin{bmatrix} -1 & -AI \\ A+I & 0 \\ -AI & 0 \\ 0 & 0 \end{bmatrix}$$

   A and I are positive as they deal with entries that denote populations. Observing the entries in the first column of the Routh array, it is very clear that there are two sign changes, thus trivial solution is clearly unstable. Using Routh array one confirms the existence of the periodic solutions also[50, 51]

2. Parasitoid-free solution

   The entries in the Jacobian which are zero are, $D = F = H = 0$. The coefficients of the charac-

teristic equations are

$$\begin{aligned} a_0 &= -1 \\ a_1 &= A+E+I \\ a_2 &= CG-AE-AI-EI \\ a_3 &= AEI-CEG \end{aligned} \tag{6.37}$$

Using this, the Routh array is found to be,

$$\begin{bmatrix} -1 & CG-AE-AI-EI \\ A+E+I & AEI-CEG \\ -\frac{A^2E+A^2I+AE^2+2AEI+AI^2-CGA+E^2I+EI^2-CGI}{A+E+I} & 0 \\ AEI-CEG & 0 \end{bmatrix}$$

3. Non trivial Solution
   For the non trivial solution, the only entries that are zero in the Jacobian matrix are F and H. which results in the following coefficients for the characteristic equations,

$$\begin{aligned} a_0 &= -1 \\ a_1 &= A+E+I \\ a_2 &= -AE+BD+CG-AI+EI \\ a_3 &= -CEG+AEI-BDI \end{aligned} \tag{6.38}$$

Using these values the Routh array is found to be,

$$\begin{bmatrix} -1 & BD-AE+CG-AI-EI \\ A+E+I & AEI-CEG-BDI \\ -\frac{AE^2+A^2E+AI^2+A^2I+EI^2+E^2I-ABD-ACG-BDE+2AEI-CGI}{A+E+I} & 0 \\ AEI-CEG-BDI & 0 \end{bmatrix}$$

Further analysis is done numerically, as analytically solving the system is very difficult.

6.5 Results of the numerical study performed on our $q-$ deformed model

Here we discuss the outcome of our model. The robustness of the model is discussed as various parameters are changed. We try to simulate the effects of the environment/climate using the parameters h and s. We then check the correctness of our model by comparing our results with the data recorded from dendrochronological studies spanning 1200 years from the Swiss Alps[67].

6.6 Cycles of the Alpine region

As mentioned in the introduction [64] gives complete detail of larch budmoth outbreak in the Alpine region. It is noted the predominant outbreak and defoliation occurs in the altitude of 1200-1600

S.No	PQI	Parasitoid	LBM
1	α	c	λ
2	h	q_y	q_z
3	-	-	m
4	-	-	s

[1]

TABLE 6.1. Parameter and the species they affect

meters from the sea level. For altitudes below 1000 meters from sea level, it is observed that the densities don't reach high enough to cause an observable defoliation. However the populations at lower altitudes also cyclically rise and fall with a longer time period. Along the Rhine river, the larch budmoth oscillates irregularly and in some regions budmoth could be locally extinct.
From the tree ring analysis, 123 outbreaks spanning over 1200 years have been collected. The relative frequencies were presented in Figure 1[67].
From the work in [64] and [67] it is clear that different regions have different parameter values. With 8 parameters, it is really difficult to specify the parameter values only from observations. However, one can make some deductions on what parameters can change easily.
First, we shall classify the parameters based on the species they affect (refer to table (6.1).

In the Alpine region we consider budmoth, parasitoids, and PQI to interact among themselves. Since it is the same region, we start with an assumption that all parameters except s, h and λ are constant[78]. This is because h and s are climate/environmental factors and hence they can vary in time. The intrinsic growth rate λ of the budmoth larve is affected by the food resources (larch needles) available, which varies in time showing that λ can vary.
The reasons for other parameters to be constant is because they are all organism-specific and only evolution can change them, which is a very slow process compared to the available 1200 year dendrochronological data.

6.6.1 The simulation

Varying the three parameters the system is numerically simulated. As the time series are produced, the transients are removed and the most dominant time period is recovered after an performing a fast fourrier transform[78]. The histogram generated from our model of the relative frequencies of occurrence of budmoth outbreaks is presented here for comparison with observations made in 1200 years in the Alpine region. Figures(6.1(a),6.1(b)) respectively denote the histograms generated from the data recovered from the Alpine region and the histograms generated from our $q-$deformed tritrophic model. The histogram from the Alpine data shows a predominant peak at 9 years followed by 8 and 10[78]. Our model has also reproduced the same trend as noted in the figure(6.1(b)). The relative frequencies of the top three dominant frequencies match well[78].

Histograms generated from Turchin's models I and II, $q-$deformed 2-D parasitoid-budmoth

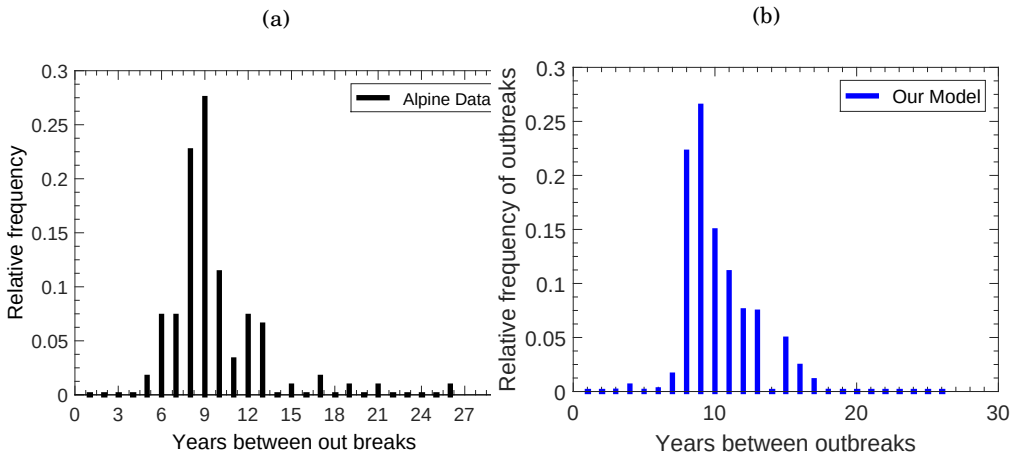

FIGURE 6.1. (a)Alpine region (Data from [67]) (b) Our Model see (Iyengar, S.V., Balakrishnan, J. and Kurths, J., *Sci. Rep.*, **6**, 27845 (2016).)

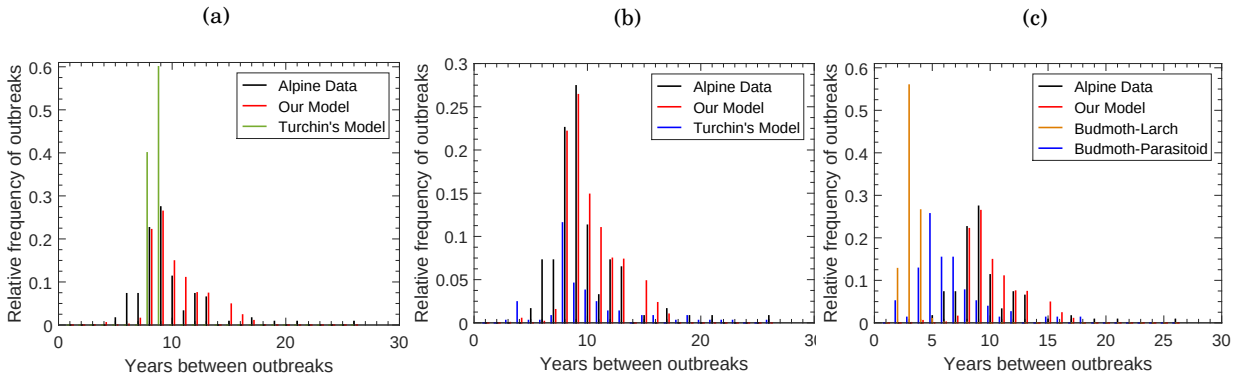

FIGURE 6.2. Comparision of historgrams form [67], Our model and other models(a) Tritrophic model I (b)Tritrophic model II (c) $q-$deformed budmoth-parasitoid model and $q-$deformed budmoth larch model see (Iyengar, S.V., Balakrishnan, J. and Kurths, J., *Sci. Rep.*, **6**, 27845 (2016).)

model and the $q-$deformed 2-D budmoth-plant model are all presented here for comparison (Fig.(**??**)). Turchin's models I and II were fine-tuned to obtain the 9 year cycle. Turchin's model I could give only 8 and 9 year cycles, but with no match with the observed magnitude of occurrences (figure(6.2(a))), while Turchin's model II gave other time periods but again with poor match of the relative frequencies with observations (refer to figure(6.2(b))). Since the tritrophic model was suggested only as an alternative to the 2-D models which failed to predict observations, it is worthwhile to test the $q-$deformed version and compare the results with the Alpine data. Although both the 2-D model (parasitoid-budmoth and budmoth-plant) exhibited cycles, there is no match with the histograms produced from the Alpine data (Fig.(6.2(c))). This confirms that the system is defiantly not two-dimensional.

6.6.2 Results

1. It is clearly evident that our $q-$deformed model has captured what is observed in nature for over 1200 years[78].

2. The relative frequencies of the three dominant frequencies predicted by our $q-$deformed model match with what is observed in nature[78].

3. 1200 year Alpine data was published in the year 2006[67]. The last observed outbreak was recorded in the year 1981. The authors of [67] assumed that there was an outbreak in 2006 to generate the histograms, hence, the histograms denoting the observations made over 1200 years assume a 25-year cycle (1981-2006) which did not materialize actually. Since we have not made that assumption, our simulations do not show the (incorrect) 25-year cycle[67, 78].

4. Till today a budmoth outbreak in the Alpine region has not been reported after 1981. Our model predicts the existence of 40 years and 100 years cycles, i.e., we predict that the next outbreak would occur in 2021. The values for which the 40 and 100 year cycle occur are $h = 0.7$, $s = 0.84$, $\lambda = 1.23$ and $h = 0.76$, $s = 0.53$, $\lambda = 1.13$ respectively, with all other parameters values fixed at $\alpha = 0.5$, $q - y = 1.13$, $q_z = 1.34$, $c = 12$ and $m = 13$[78].

5. In the histograms one can see a discrepancy for the lower time periods between our model's prediction and the Alpine data. In the 1200 data, one can see an enhancement of 6 and 7-year cycles which is not seen in our simulation. It is also noted that the 6 and 7-year cycle occurred a lot of time during the period from 1000 to 1400 AD. While simulating our model, we gave equal probabilities to the values s, h and λ can take. However [67] clearly shows a peaking of 6 and 7-year cycles between 1000 AD and 1400 AD. For reasons unknown to us nature has preferred to be in this state for a long enough time. More analysis needs to be done on the same. It is noted that the little ice age occurred after 1400 AD. Before that it was warm, higher temperature would mean smaller s. More quantification needs to be done after field research work[67, 78].

6. From the figures (6.2(a) 6.2(b) 6.2(c)), it is very clear that the $q-$deformed tritrophic model, matches with the 1200 year data. The 2-dimensional models and the two of the models of Turchin's do not even come close to the 1200 year data.

7. From the figures (6.1(a) and 6.1(b)), the matching of the 3 dominant peaks and their relative frequencies of $q-$deformed tritrophic model with the 1200 year data is clearly visible.

6.7 Tatra region

The Carpathian mountains in Slovakia, are home to larch trees. Local loggers and villagers have confirmed the dwelling of larch budmoth on those trees. However, tree ring analysis done on the trees extracted from those regions, confirms the absence of damage events, which would correspond

to the outbreak of budmoth, which results in the defoliation of the larch tree[78].
Here too we have modeled the system using our tritrophic model and have succeeded.
We make a similar analysis of how the parameter could differ in Tatra. From [68] it is clear that along with the environment possibly c, m, q_z and q_z could be different. The reasons being m and q_z are related to intraspecific competition, which is different in Tatra compared to Alpine, as larch trees in Tatra are sparse. In [64] it is also noted that beyond the Rhine river there are irregular fluctuations and sometimes even absence of the budmoth outbreaks.
The climate/environmental factor h has different values in the Alpine and the Tatra region which is under constant cloud cover making it less favorable for growth of larch.
s may be related to the inverse of temperature, and we note from [68], that cycles have not been there in Tatra for more than 400 years, and since global warming etc., are recent activity, we suggest that absence of cycles in Tatra is not because of current anthropogenic activity, but rather a characteristic of the place itself and thus we choose not to vary s. q_y and c are related to parasitoid. One is the parasitoid wasting time and other parasitoid's efficiency devouring the budmoth.
λ also varies. However, it is numerically found that m and q_z do not affect the system much. The videos containing the bifurcation diagram confirm that and this is also expected because we are considering the same larch budmoth species, so physical attributes of species do not change from place to place. (The bifurcation videos will be discussed in the following section, where effect of two parameters on the system is seen.) q_y is a parasitoid wasting time, unless we consider a completely different parasitoid there is no reason this should change, hence for simulation we keep it as a constant. In [66] experiments have revealed that spraying of bacteria on the budmoth larvae affected the cycles. Hence, we chose the parameter c, and varied it and we did find out that, cycles do not exist if values of c are lower. However, the quantification needs to be done. Hence, with 3 different parameters, i.e., h,λ and c, our model simulations matches with the Tatra region. Similarly, h in Tatra is different from what is observed in the Alpine region. c is related to intraspecific competition, which is quite high in Tatra due to sparseness in trees.

From our simulations it is very clear, that despite environmental conditions being good, there are no cycles if λ and c are too low, as evident from figure (6.3(a)). However slightly increasing the intrinsic growth rate λ to 6.5, limit cycles are born for higher values of h, as evident in figure (6.3(b)). For very low values of λ as in figures (6.3(c), 6.3(d)), a high value of c and h are required to kick start the cycles. Lower the value of c, higher is the value of h that is required to kick start a cycle. For higher values of λ and c limit cycles are formed at lower values of h. This complex interaction between the budmoth and the parasitoid is also seen here. Given a value of c, as λ increases, the limit cycles are born for a lower value of h (refer to figure (6.3(d) and 6.3(e))), showing that for a given infesting ability a better growth rate allows the budmoth population to grow well. Similarly for a given growth rate λ, as c increases, the value of h for which limit cycles are created decreases. i.e., limit cycles are born at lower value of h as c increases (refer to figures (6.3(b) and 6.3(f))). This is because the parasitoid keeps the budmoth population at check, so that they do not over-exploit the resources that might lead to their extinction. Thus a lower value of c and λ, gives no cycle,

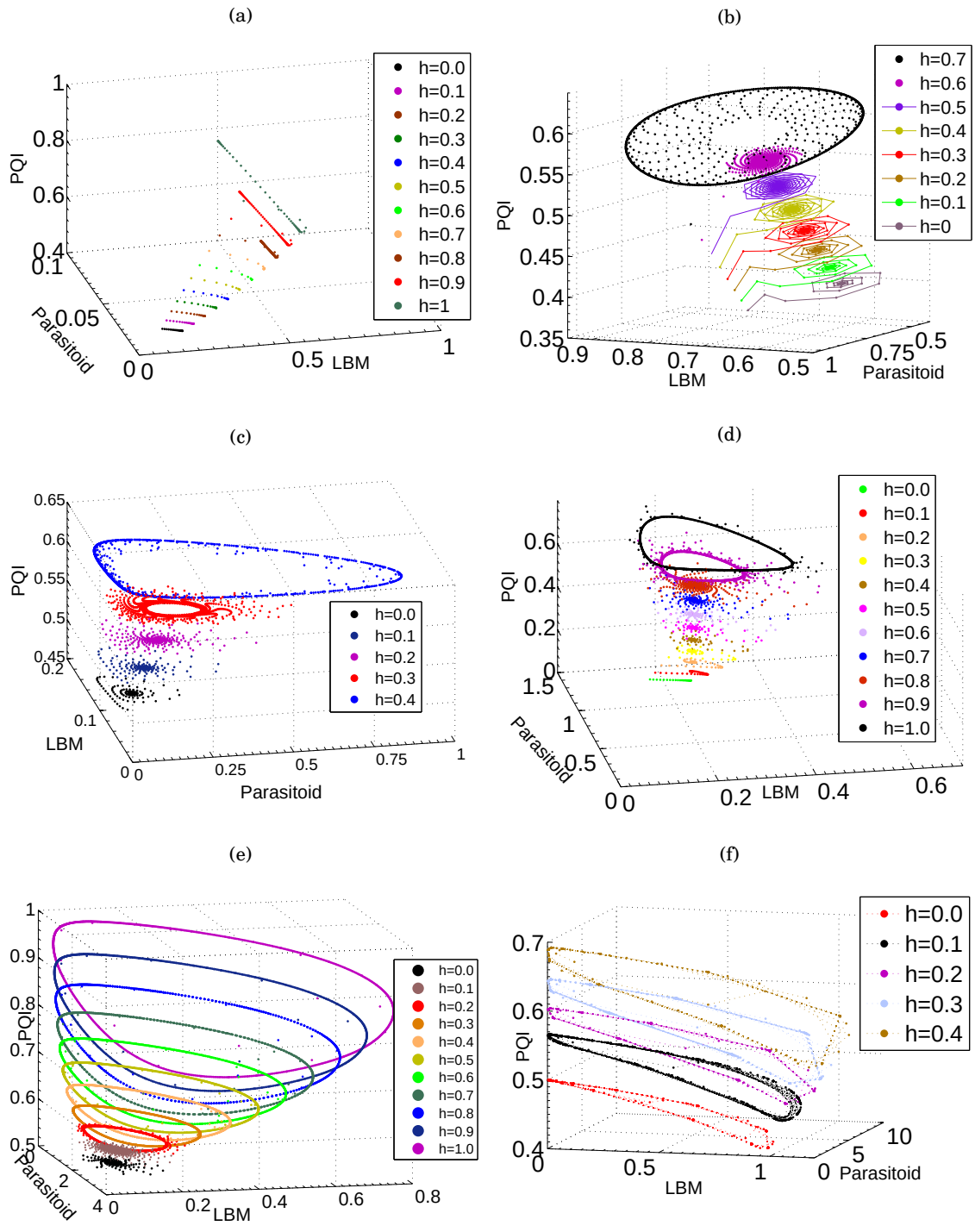

FIGURE 6.3. Simulations of q–deformed tritrophic model with $s = 0.5$, $\alpha = 0.5$, $q_y = 1.13$, $q_z = 1.34$ and $m = 13$. The various figures are generated with different values of λ, c and h. In all of the figures h is varied after fixing the value of c and λ. (Iyengar, S.V., Balakrishnan, J. and Kurths, J., *Sci. Rep.*, **6**, 27845 (2016).)(a)$c = 2$ and $\lambda = 2$ (b)$c = 2$ and $\lambda = 6.5$ (c)$c = 12$ and $\lambda = 2$ (d)$c = 6$ and $\lambda = 2$(e)$c = 6$ and $\lambda = 3$ (f)$c = 12$ and $\lambda = 5$

and we conclude that Tatra region possibly has a low value of c, due to sparseness in trees. This statement remains true for all values h[78].

6.8 Effect of various parameters on the system's time period

Mathematically it would be really interesting to check how the system behaves in different parameter regimes, although all those regimes may not in reality happen. Being a nonlinear system and with 8 parameters, pinpointing how the time period is in general affected may not be easy. However the trend of the time period as one of the parameter is varied can be easily studied by keeping the other parameters at a constant value. Based on our simulations we are inclined to believe that the following values of parameters represent the Alpine region. The parameter values that characterize the alpine region are, $c = 12$, $m = 13$, $q_y = 1.13$, $q_z = 1.34$ and $\alpha = 0.5$. h and s can vary from 0 to 1. We set them at $h = s = 0.5$ and $\lambda = 8$. The time period is obtained from the FFT of the time series which provides us with the power at each frequency. The frequency at which the maximum power is delivered is inverted to obtain the time period. There could also be other harmonics and other peaks. However, we choose only the dominant one and assign the corresponding time period as the time period of the system[90]. In the figure(6.4(a)) the general trends of varying one parameter at a time are seen. λ is the intrinsic growth rate. Higher the growth rate, faster is the growth of the budmoth population. The growing budmoth depletes the plant, which collapses the budmoth population, thereby giving itself some time to regrow. This fresh growth of the foliage again starts rising the budmoth population and this continues. Depending on the value of λ, the rate of rising and falling changes. Higher the growth rate, faster is the rise and fall, resulting in shorter time period. Thus higher values of λ result in shorter time periods. Similar observations are made as the parameter h is changed[90]. Just as λ represents the growth of the budmoth, h here dictates the growth of larch needles. When the environmental conditions are better, h values are higher which results in more foliage which again increases the budmoth population and this goes on. The other climate parameter we have introduced, s, may be related to the inverse of temperature. s does not seem to affect the system much, except at large fluctuations at very high values[90]. m controls the rate at which the budmoth feeds on the larch leaves. It has been noted that the m does not significantly alter the time period. The system fluctuates around the 9 year time period, and the fluctuations are also small[90]. Similar observations are also made with respect to parameter q_z[90] which is related to the intraspecific competition. c is the efficiency of the parasitoid in attacking the budmoth. A Higher value of c implies an efficient predation by the parasitoid. Thus the budmoth is never able to grow fully, as the parasitoids keep it at check which results in long time period[90] for the outbreaks. α is related to plant vulnerability. More vulnerable the plant is, more is the infestation, thus a longer time for the plant to regrow. Greater the value of α more is the time taken by the plant to regrow, and thus makes the time period very long[90]. q_y is related to the time wasted by the parasitoid in searching for its host. A higher value of q_y indicates that budmoth is free from a parasitoid attack. Since budmoth population is then not in check, they consume the larch leaves

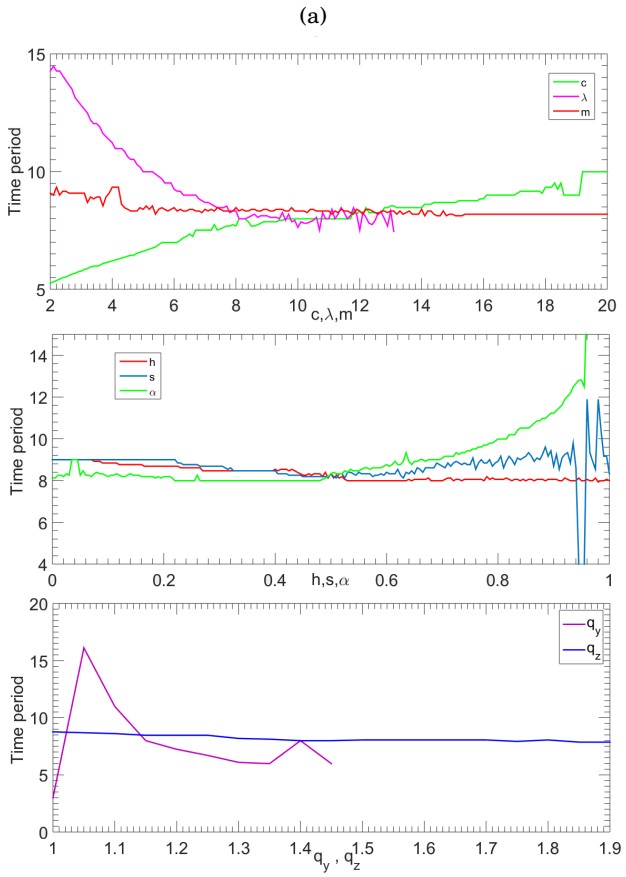

FIGURE 6.4. Variation of time period as one of the parameter is changed, keeping all other at a constant value. The values of the other parameters are $c = 12$, $m = 13$, $q_y = 1.13$, $q_z = 1.34$, $\alpha = 0.5$, $h = 0.5$, $s = 0.5$ and $\lambda = 8$.

at their will. Greater the consumption, faster is the depletion of the foliage causing a rapid fall in budmoth numbers due to the fast depletion of food resources, thus resulting in smaller cycles[90].

From the figure(6.4(a)), it is very clear that the $q-$deformed model is robust, and maintains the 9-year periodicity unless the value is too extreme. This robustness is not found in other models discussed in literature so far.

6.9 $h = 0$ a special case that explains observations in the French Alps.

When $h = 0$, we consider a scenario where the larch leaves don't recover. This happens when the leaves are permanently damaged. This permanent damage is seen in French Alps, where larch tree are damaged for timber and land. For $h = 0$ or close to zero and for different values of c, we are able to simulate the observations made in French Alps[91]. However, c being different implies a different parasitoid in action. Further studies need to quantify that. When we set $s = 1$ along with $h = 0$, the

tritrophic model III is recovered. This seems to explain the observations seen in the French Alpine region. But this model requires a different value of c, which loosely indicates that the parasitoid driving the cycles in the French region is different.

6.10 Neimark Sacker Bifurcation

Neimark-Sacker bifurcation leads to the creation of limit cycles in a system. This is similar to Andronov-Hopf bifurcation that happens in continuous systems. In discrete systems, it is termed as the Neimark-Sacker bifurcation. In this system, a fixed point becomes a stable spiral and loses its stability to become an unstable spiral with limit cycle forming around it, as the parameter is varied[90]. Therefore the budmoth population density, larch needle lengths (PQI), and the parasitoid population density exhibit cycles. There are 8 parameters in the system it has been noted that Neimark-Sacker bifurcation happens with respect to the change of all parameters[90]. In the bifurcation videos, one can see Neimark-Sacker and reverse Neimark-Sacker bifurcation occurring as the parameters are changed. Figures (6.5(a) and 6.5(b)) show the Neimark-Sacker bifurcation with respect to parameters λ and c. It is evident from both the figures that below a particular value of the parameter, the limit cycles cannot be sustained. Figure6.5(a), shows the trajectory of particles from the start to end while figure(6.5(b)), records the last 500 points visited in the phase space. Although it is good to discard the transients (say the first 1000 or 1500 iterations), the choice to plot the transients also is purposefully made to see the spiral behavior, which wouldn't be visible if one chooses to plot the last 500 points. The figure(6.5(b)) is devoid of transients and thus shows a fixed point becoming a limit cycle as the parameter is increased. Plotting the transients would have enabled viewing the spiral behavior; this however spoils the clarity of the picture.

6.11 Hydra effect

Any model we design must capture that effect which has already been reported. For instance, in a population model, populations cannot go negative, they cannot go to infinity. There are some restrictions. Similarly, it is also observed that populations under stress and when in the verge of extinctions increase their population so as to propagate and prevent extinction. For instance In [92, 93] there is a discussion on how greater mortality results in an increase in population. This is also known as the "Hydra Effect". The name "Hydra" was coined due to inspiration from Greek mythology, where a slayed demon instead of dying grew two more heads from one that is lost. In a bifurcation diagram, this is seen as a paired cascade [40] or a bubble [94]. A paired cascade and bubble both mean the same phenomena, while paired cascade is more technical, the bubble is more understandable. A bubble or a paired cascade is a closed structure which is created via a period doubling and a period halving. The degree of period doubling and period halving depends on the values of the parameter that govern the system. In [94] there is a discussion on a one-dimensional map (using a Ricker like a model), wherein there is harvesting. Due to harvesting, there is bubbling

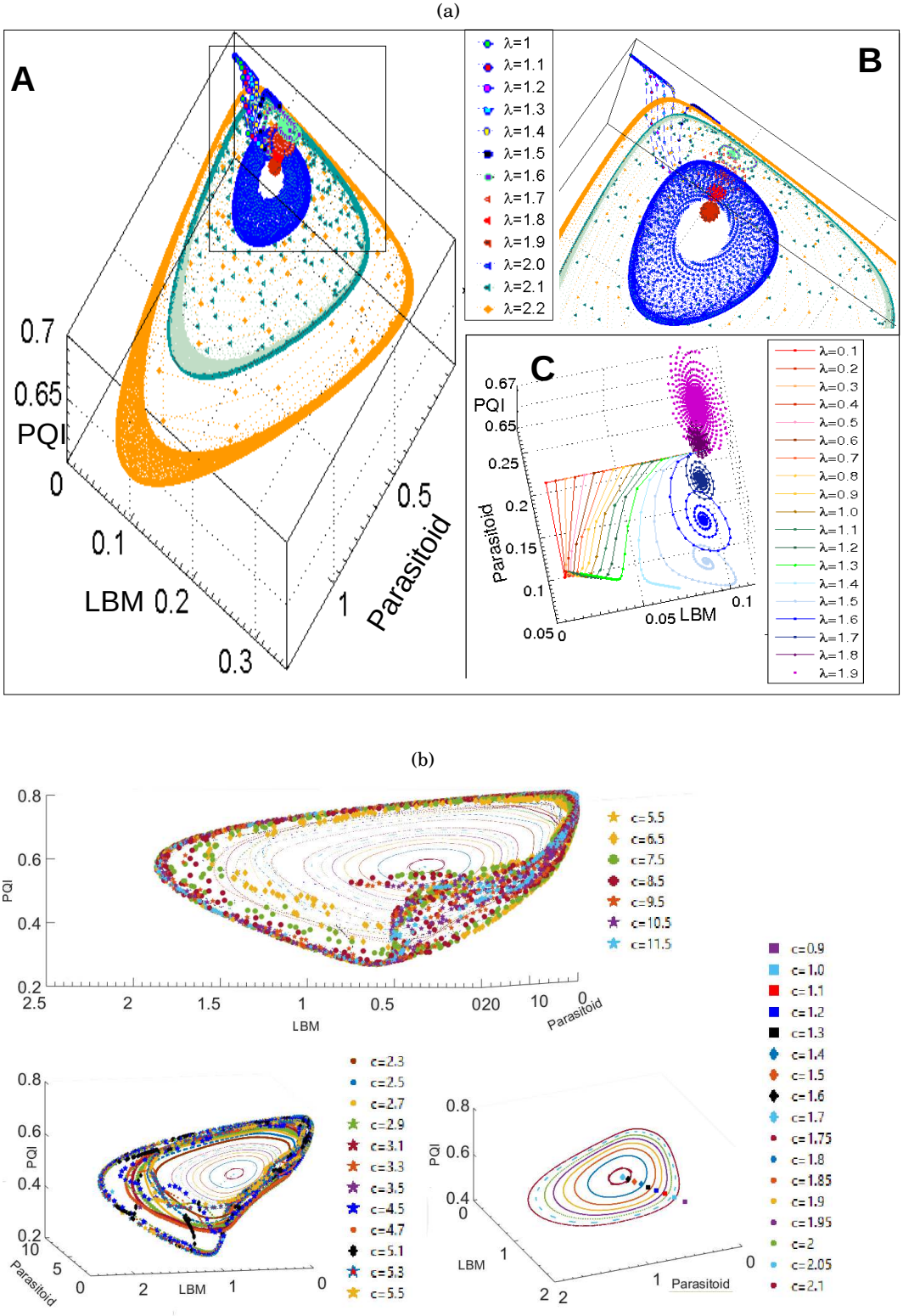

FIGURE 6.5. The values of the parameters chosen to generate this bifurcation diagram are $\alpha = 0.5$, $s = 0.5$, $q_y = 1.13$, $q_z = 1.34$, $m = 13$, (a)$c = 12$ and $h = 0.5$ (b) $\lambda = 8$ and $h = 0.7$. The choice of $h = 0.7$ is just for clarity of the picture, as limit cycles become larger as h increases. Similar behavior is noted when $h = 0.5$.

in the system. Depending upon the value of the parameter (harvesting in [94]), the closed structure can be a simple bubble which is formed by one period doubling and one period halving or a complex bubble which is formed via many periods-doublings followed by the same number of period halving and a chaotic bubble, when the bubble structure encloses a chaotic region which occurred due to many period-doublings. In [95], dynamics of flour beetle is discussed. In certain parameter regime the paired cascades comprising of one period doubling and one-period halving, forming a closed loop like structure, are observed, which is the first observations of paired cascade in a 3D system, as reported in [94]. However, in flour beetle dynamics, there is no further complex or chaotic bubble. The work on [94] Ricker like model is also the first time a paired cascade is reported in a one-dimensional model. Our model, which is a 3D model has paired cascades, which, depending on the parameter value can be a simple bubble or a complex bubble or a chaotic bubble. In [96], discussions are made on how the loss of monotonicity, (due to harvesting in the case of [94, 96]) introduces paired cascades. A simple Ricker map is chosen for this study. The number of period doubling and period halving depended on the value of the growth rate used in the Ricker map. Our model is also showing this feature, which shows that under extreme stressful conditions the budmoth system tries to escape extinction[90]. This could also be a possible reason why the budmoth outbreaks sustained for almost 1200 years[67]. In figure(6.8(f)) a bubble or a paired cascade is visible. As α is increased the period doubling is reversed and chaos is lost. h controls the degree of period-doubling and period-halving. For a value of h lesser than 0.536, the system shows lesser period-doubling and halving, while a value of h greater than 0.536 produces more period-doubling and period-halving, which leads to the merging of all chaotic regions of bubbles forming a band-like structure[78].

6.12 Effect of changing two parameters

The $q-$deformed tritrophic model is very robust and is able to produce the 8-9 year cycle when one of the parameters is changed, keeping the other constant. To study the effect of a change in two parameters of the system at the same time, we introduce a novel technique of looking at the change in bifurcation diagram (generated with respect to the first parameter) as the second parameter varies. The various frames are compiled as a video. The method to generate these videos are given in the Appendix. Each frame contains the details on bifurcation diagram created with respect to a particular parameter[90]. On top of the video is the second parameter which is varied frame by frame. Since there are 8 parameters, there are 56 combinations of two parameters, that can change. The results of all the 56 combinations are listed in a tabular format, given in table(6.3). The table (6.2) contains the key to read the table(6.3). In the tables, the column represents the variable which is in the y axis, while the rows represent the second parameter.

6.12.1 Results of varying two parameters

1. The larch budmoth, the parasitoid, and the larch tree leaves show complete synchrony in their dynamics, irrespective of the change in the parameter[90].

2. The system exhibits limit cycle only when parameter values are above a certain threshold. Below this threshold only one fixed point is seen[90].

3. Interesting phenomenon such as the interior crisis, boundary crisis, paired cascades, creation of source and sink like regions are seen in the phase space[90].

4. In general once the system parameter is above(below) the Neimark-Sacker(Reverse Neimark-Sacker) bifurcation point, the system exhibits oscillatory behavior only. However, this behavior can be perfectly periodic or quasi-periodic or even chaotic[90].

5. The other minor details can be seen in the table (6.3)[90].

6.13 Recurrence quantification analysis

Recurrence quantification analysis is a novel way to understand a system from its time series. Recurrence plot is generated by recording the recurrences from the time series. A recurrence plot (RP) is a plot of points, that is based on recurrences. Depending on the pattern, density and distribution of points, many properties of the time series can be deciphered[97]. For more details refer to Appendix. The list of invariants can be found in the table(6.4). The invariants used to study a time series are the Recurrence Rate (RR) and Determinism (DET). Since the system has 8 parameters, it is very difficult to know the general behavior and thus we fix the values of all parameters but one, and vary the parameter and record how the invariant quantities change as a function of the chosen parameter.
The figures (6.6(a)-6.7(d)) show the variation of CRQA (cross recurrence quantification analysis) invariants with respect to change in various parameters. It is evident from the figures that the invariants do not change much, indicating that for these set of parameters the system is highly periodic and the system is robust. The system has a lower RR indicating it is a fast varying signal, higher DET indicates a strongly periodic signal. V_{max} is very low indicating absence of intermittent states.

PD /PH	Period doubling (1 into 2)/ Period halving (2 into 1)
NS/RNS	Neimark Sacker bifurcation / Reverse Neimark Sacker bifurcation
PP /QP	Periodic pattern /Quasi-periodic
SRC/SNK	The region from where fixed points spread out (source)/annihilate (sink)
SB	Simple Bubble (closed structure formed by a PD,PH)
CB	Complex Bubble (formed via a few PD and PH)
Z	Any of the 8 parameters with respect to which the Bfd is generated
Z_c	The value of Z at which NS occurs
ChB	Chaotic Bubble (many PD,PH chaos inside bubble)
Z_{max}	The value of Z at which BC occurs
CR/Ch	Chaotic region (fine distribution of points)/Chaos
DB/IB	Distorted Bubble/ Interlaced bubbles (many bubbles join)
BC	Boundary Crisis (sudden disappearance of points after a Z)
Bfd	Bifurcation Diagram
IC	Interior Crisis (expansion or compression of size of attractor)
λ	intrinsic growth rate ($0 \leq \lambda \leq 12$)
$\uparrow$ / $\downarrow$	increases /decreases
α	Plant vulnerability ($0 \leq \alpha \leq 1$)
h/s	Environmental factors ($0 \leq h, s \leq 1$)
$\rightarrow$ /$\leftarrow$	Bfd shifting towards right/left (higher/lower values)
c	efficiency of parasitoid ($0 \leq c \leq 15$)
$Z_>/Z_<$/X	greater/lesser values of parameter /No drastic change from the original configuration
m	Budmoth's efficiency of infesting($0 \leq m \leq 20$)
q_z/q_y	intraspecific competition / parasitoid wasting time ($1 \leq q_z, q_y \leq 2$)
PW /CR /SB /ChB/CB/exp	Periodic Window /Chaotic Region / Simple Bubble / Chaotic Bubble /Complex Bubble/expands
PW to CR	PW becomes SB, turns into CB and becomes ChB. Finally, CR of all bubbles form CR of the Bfd
Pop_{max}	maximum population attained by the species
OD	Oscillation death

TABLE 6.2. Abbrevations and conventions used in Table (6.3)

	α	h	s	m	λ	c	q_y	q_z
α	-	$Pop_{max}\uparrow$ Satellites PW to CR	SNK $s=0.5$ $Pop_{max}\downarrow$ SB to CR CR to SB	Satellites SNK $8<m<15$	$Pop_{max}\uparrow$ $\lambda_c\uparrow$ SNK λ =8 $\lambda_{max}\downarrow$	$c_c\uparrow$ CR to PW $Pop_{max}\downarrow$ PW to CR	RNS $\uparrow$ $Pop_{max}\downarrow$ PW to CR CR to PW	$\rightarrow$ SNK at $q_z=1.5$
h	CR to PW SNK at RNS	-	CR to PW satellites	PW to CR CR to PW $Pop_{max}\uparrow$	RNS $\downarrow$ $\lambda_{max}\downarrow$ $\leftarrow$	$\rightarrow$ slow $Pop_{max}\uparrow$	X	$\leftarrow$ satellites
s	RNS at $\alpha=0.9$ $\rightarrow$ SNK at RNS pt CR to PW PW to CR	$\leftarrow$ PW to CR CR to PW $h_{max}\downarrow$	-	IB CR to PW	PW to CR CR to PW $\lambda_{max}\downarrow$ NS $\lambda=2.5$	NS slow $\rightarrow$ PW to CR CR to PW	X	SNK at $q_z=1.75$ PW to CR $q_{zc}\downarrow$
m	RNS $\alpha=0.9$ SNK $\alpha=0.9$ CR to PW PW to CR	$Pop_{max}\uparrow$ PW to CR	X	-	RNS $Pop_{max}\uparrow$ X	RNS $\downarrow$ $Pop_{max}\uparrow$ Satellites	RNS $\downarrow$ $Pop_{max}\uparrow$ X	$s_c\uparrow$ X
λ	RNS $\uparrow$ $Pop_{max}\uparrow$ SRC $\alpha=0.25$ PW to CR CR to PW	$Pop_{max}\uparrow$ $h_c\downarrow$ $\leftarrow$ CR to PW satellites	$s_c\uparrow$ $Pop_{max}\uparrow$ PW to CR CR to PW	CR to PW $m_c\downarrow$ $Pop_{max}\uparrow$ PW to CR	-	$c_c\downarrow$ $\rightarrow$ SB to CR	RNS $q_{yc}\uparrow$ $Pop_{max}\uparrow$ satellites	$q_{zc}\downarrow$ $\leftarrow$ CR to PW
c	SRC at RNS pt $\leftarrow$ MS satellites SNK at $\alpha=0.3$	$Pop_{max}\uparrow$ PW to CR	$c_c\downarrow$ QP SNK $s=0.5$	CB at $c=1.8$ Bubble exp SB to CR QP	$\lambda_c\downarrow$ Satellites PW to CR	-	RNS $\uparrow$ PW to CR	SRC at $q_z=1.5$ PW to CR NS
q_y	RNS $\alpha=0.9$ OD $q_y=1.42$ PW to CR before before q_y=1.42.	MS PW CR OD at $q_y=1.35$	$s_c\uparrow$ OD at $q_y=1.35$ PW CR CB CW	PW CR Satellites $\leftarrow$	SNK SB to CR PR to SB $\lambda_{max}\uparrow$	$\rightarrow$ OD at $q_y=1.35$	-	$\leftarrow$ SB to CR CR to SB RNS $\downarrow$
q_z	RNS at $\alpha=0.9$ $\rightarrow\alpha_c\downarrow$	X	PW TO CR $Pop_{max}\uparrow$	$Pop_{max}\uparrow$ X	NS $\leftarrow$	$Pop_{max}\uparrow$ CR to PW	$Pop_{max}\uparrow$	-

TABLE 6.3. Effect of variation of two parameter on the larch budmoth system

SNo	Quantity (Full form)	What they denote
1	RR (recurrence rate)	density of points. Slowly varying signal will have higher RR
2	DET (determinism)	Periodic signal will more determinism
3	<L> (mean diagonal line length)	Measure of prediction time
4	Lmax (maximal diagonal line length)	Measure of divergence of two trajectories. higher L_{max} smaller is the divergence.
5	ENTR (entropy of the diagonal line lengths)	Low for uncorrelated events
6	LAM (laminarity)	Indicator of intermittent regimes
7	TT (trapping time)	Measure of prediction time in an intermittent state
8	Vmax (maximal vertical line length)	Measure of divergence from an intermittent state.
9	T1 (recurrence time of 1st type)	Time between states that are with in a ϵ of state i. gives information of stationary in the signal.
10	T2 (recurrence time of 2nd type)	Time between two recurrence measured by constructing a Poincarè plane. Gives information dimension.

TABLE 6.4. Invariants from an RP

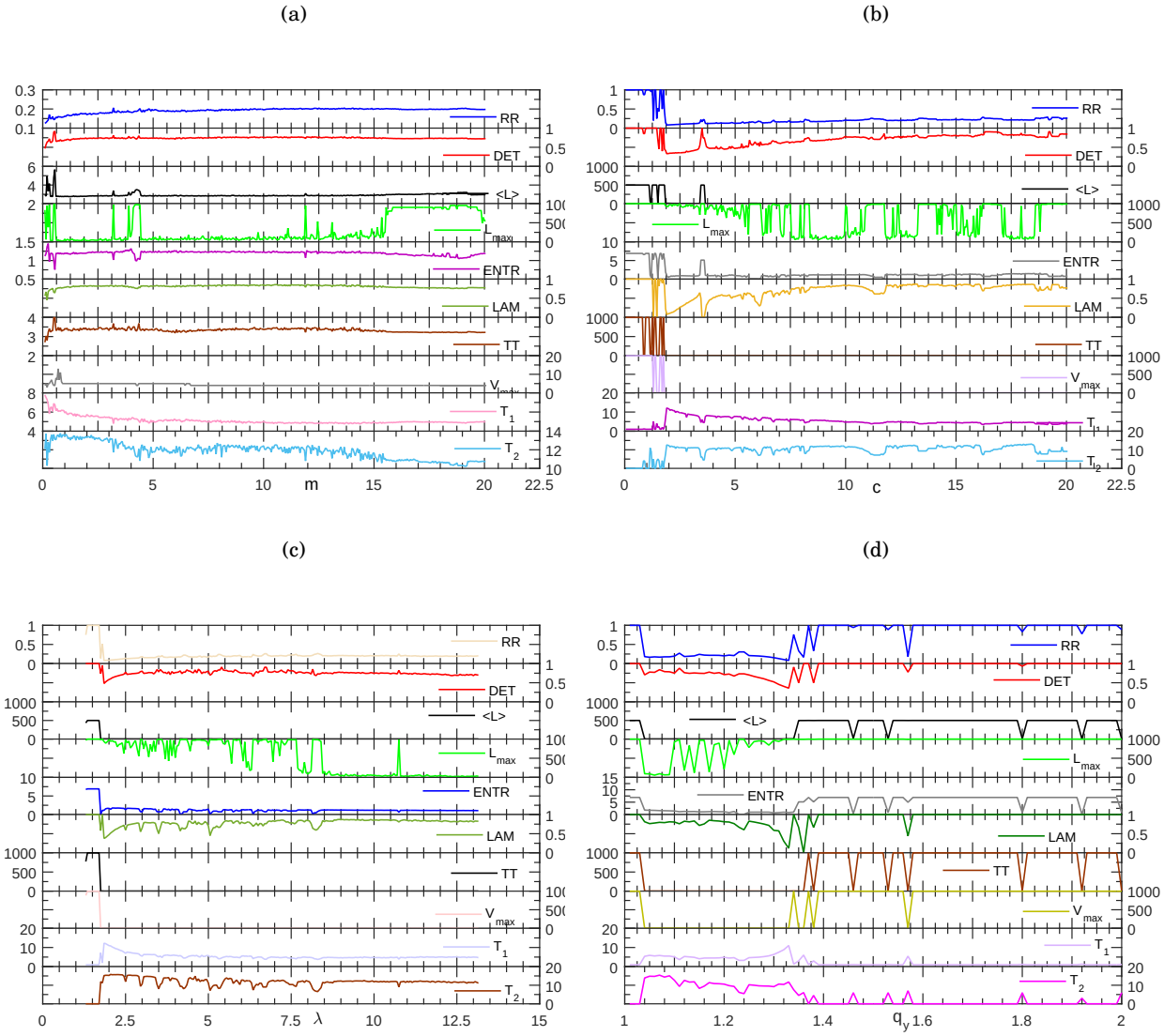

FIGURE 6.6. CRQA measurements as a function of various parameters. The parameter values chosen to generate the figures are $h = 0.5$, $s = 0.5$, $\alpha = 0.5$, $m = 13$, $q_y = 1, 13$, $q - z = 1.34$, $c = 12$, $\lambda = 8$. The various figures show CRQA with respect to (a)m (b)c (c)λ (d)q_y

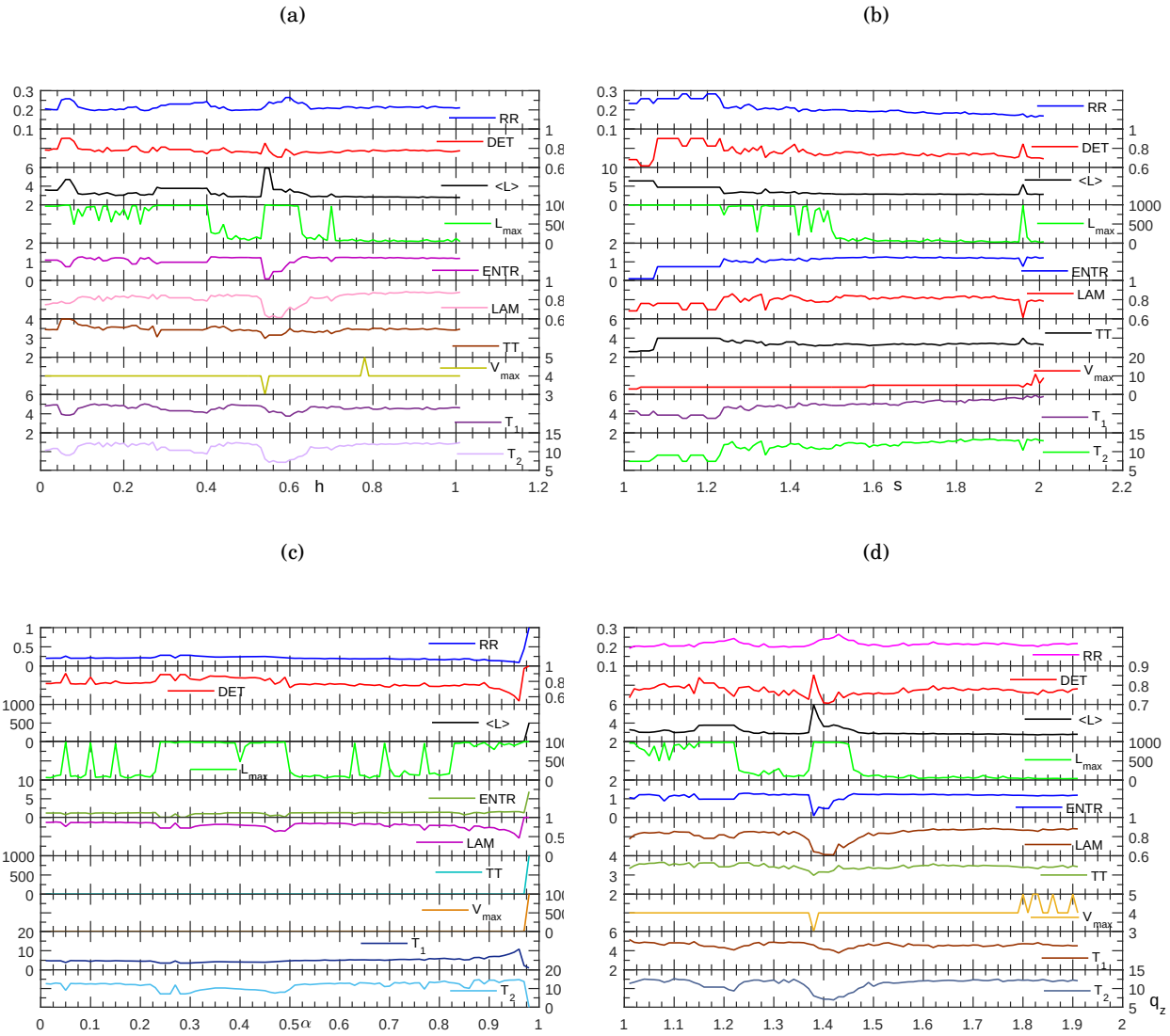

FIGURE 6.7. CRQA measurements as a function of various parameters. The parameter values chosen to generate the figures are $h = 0.5$, $s = 0.5$, $\alpha = 0.5$, $m = 13$, $q_y = 1, 13$, $q - z = 1.34$, $c = 12$, $\lambda = 8$. The various figures show CRQA with respect to (a)h (b)s (c)α (d)q_z

6.14 Interesting features

The figures (6.8(c) and 6.8(d)), show bifurcation diagrams with respect to parameter s, at different values of h and α. The videos generated by changing two parameters, reveal the presence of sink and source like regions (attracting and repelling regions). These sources and sink could be representing stability boundaries of basins in phase space[78]. These may possibly be related to climatic tipping points. The figures (6.8(a),6.8(b) and 6.8(e)), show the 2-dimensional, 3-dimensional and 1-dimensional bifurcation diagram with respect to parameter q_z. The three dimensional

bifurcation diagram, which, shows the entire attractor is color coded based on the value of c[90]. Usual bifurcation diagrams as in figures (6.8(e) and 6.8(a)), one of the axis is the parameter itself. However in figure (6.8(b)), colour represents the parameter. When $c = 7$, one can see 7 limit cycles of various sizes close by. The system hops from one limit cycle to other[90].

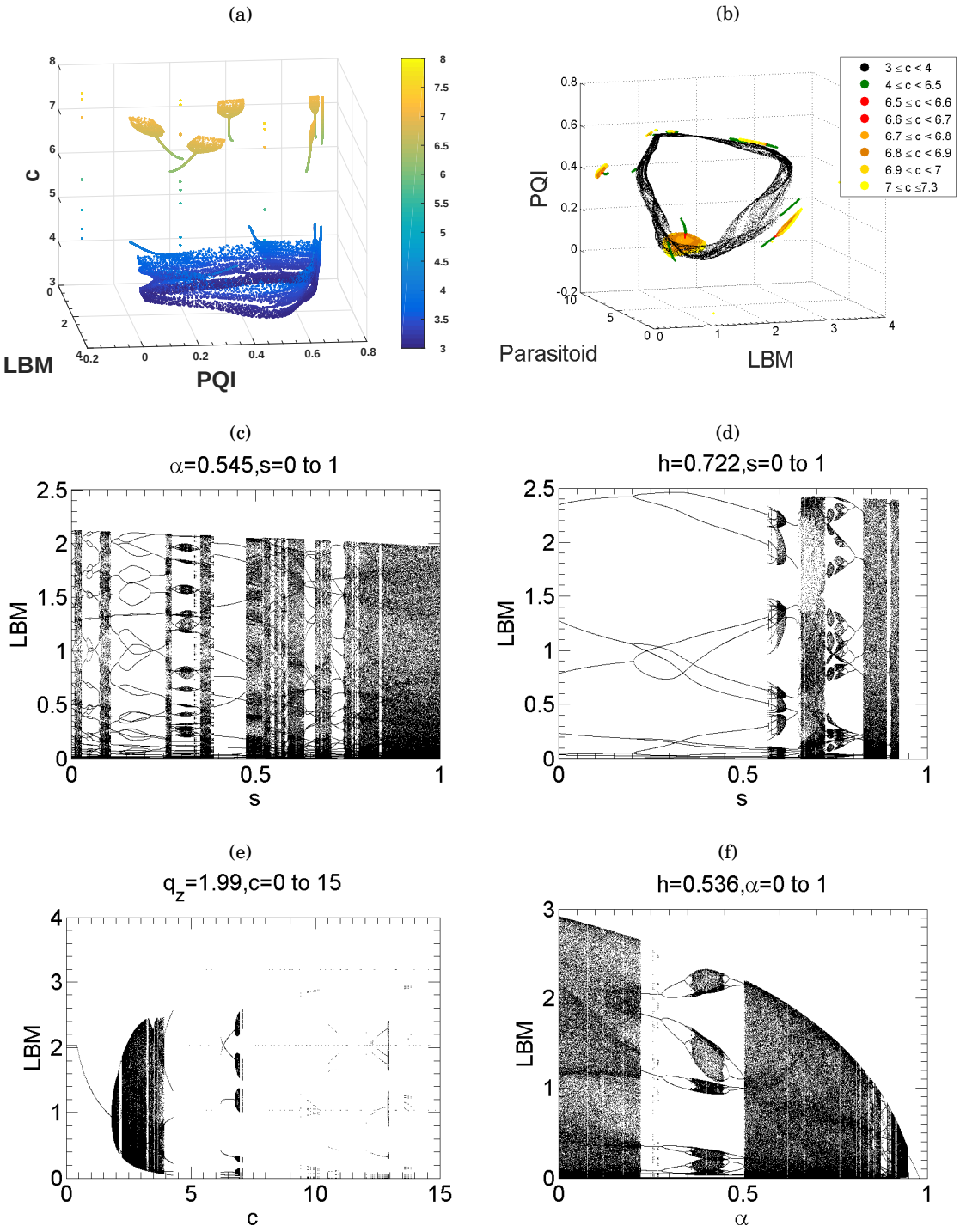

FIGURE 6.8. Simulations of q–deformed tritrophic model with $s = 0.5$, $\alpha = 0.5$, $q_y = 1.13$, $q_z = 1.34$, $m = 13$, $c = 12$, $h = 0.5$ and $\lambda = 8$. The various figures are generated with different values of parameters keeping all others at the above mentioned values. (Iyengar, S.V., Balakrishnan, J. and Kurths, J., *Sci. Rep.*, **6**, 27845 (2016).) (a)Full attractor (3D)with $q_z = 1.99$ (b)2-D bifurcation diagram with respect to c with $q_z = 1.99$, PQI-LBM attractor. (c) bifurcation diagram (LBM vs s with $\alpha = 0.545$, $m = 15$ and $c = 10$ (d)Bifurcation diagram (LBM vs s with $h = 0.722$, $m = 15$ and $c = 10$ (e) Bifurcation diagram (LBM vs c) with $q_z = 1.99$. (f) A representation of chaotic bubble with $h = 0.536$

CHAPTER 7

INTRODUCTION OF A SECOND PARASITOID SPECIES IN THE $q-$DEFORMED TRITROPHIC MODEL

Analytical solutions of equations of a model alone may not suffice to forecast the future. Still the equations can be used to understand the general behavior of the system. Numerical simulations on the other hand are mainly done to forecast the future and hence these carry the maximum possible details. Our analysis in the previous chapter on the our $q-$deformed tritrophic model had 3 interacting species. With 8 parameters, simulations were carried out and we were able to make definite predictions. To make the system more general, so as to mimic the ones we see in nature, an additional equation that governs the evolution of another parasitoid species is added. The motivation to do the same arises from live experiments reported in [66], wherein bacillus were sprayed on live budmoth larvae and time for the pest outbreak was recorded. It was observed that such an addition of another parasitoid species/bacillus to an existing larch branch advanced the insect outbreak by a year. We show below that introduction of a new species in our $q-$deformed model mimics this experimentally observed increase in the time period of the budmoth outbreak cycle.

This model is a simple one and the biological effect of adding another parasitoid is to reduce the number of budmoth larvae. For simplicity, *no interaction is assumed between the two parasitoids*. The two parasitoids enter the budmoth equation in the exponential part. It is also very well known that more than 94 species[72] of parasitoids attack the budmoth [72]. Since a single organism can host many parasitoid species in it, we generalize our three-dimensional model proposed with climate parameters in the previous chapter, to include another species of parasitoid. Let us denote the second parasitoid by v_t, where t denotes the time. κ is a new parameter that decides the strength of the interacting parasitoids. For $\kappa < 1$, parasitoid 1 is stronger, For $\kappa > 1$ parasitoid 2 is stronger. By strength, we mean the fecundity and virulence of the parasitoid. Higher fecundity and higher

virulence make the parasitoid a better hunter.

The other parameters hold the same meaning as in the previous chapter. The new equations are given by,

$$\begin{aligned}
x_{t+1} &= \frac{\rho_z z_t}{1+\mu_z z_t}\lambda x_t \exp\left(-x_t - \frac{\rho_y y_t}{1+\mu_y y_t} - \frac{\rho_v v_t}{1+\mu_v v_t}\right) \\
y_{t+1} &= c x_t \left(1 - \exp(-\frac{\rho_y y_t}{1+\mu_y y_t})\right) \\
v_{t+1} &= \kappa c x_t \left(1 - \exp(-\frac{\rho_v v_t}{1+\mu_v v_t})\right) \\
z_{t+1} &= (1-\alpha)\left(1 - \frac{x_t}{m+x_t}\right) \\
&\quad + \alpha(h - s x_t)\frac{\rho_z z_t}{1+\mu_z z_t} \\
\mu_i &= \frac{q_i - 1}{2 - q_i} \quad \rho_i = \frac{1}{2-q_i}
\end{aligned} \tag{7.1}$$

7.1 Fixed points

As before we find there are three types of fixed points in the system:(i) the trivial, (ii)the parasitoid-free solution and (iii)the non-trivial solution. The trivial and the parasitoid free-solutions are the same as in the $q-$deformed tritrophic model explained in 5.1.1. When one of the parasitoids is absent, we have the original tritrophic system. The non-trivial solution, wherein all the four interacting species are present is given by (x^*, y^*, v^*, z^*) where

$$z^* = \frac{(1-\alpha)m}{m+x} + \frac{\alpha(h-sx)}{\lambda \exp(x^* - (1 - \frac{y^*}{cx^*}) - (1 - \frac{v^*}{\kappa c x^*}))} \tag{7.2}$$

The expressions $(1 - \frac{y^*}{cx^*})$ and $(1 - \frac{v^*}{\kappa c x^*}))$ were obtained from the equations governing the evolution of the parasitoids.

7.1.1 Linear Stability analysis

The Jacobian matrix of the 4 dimensional system is given by,

$$\begin{bmatrix} A & B & C & D \\ E & F & G & H \\ I & J & K & L \\ M & N & O & P \end{bmatrix}$$

To find the eigenvalues of this matrix, the characteristic equation has to be solved. The characteristic equation of the Jacobian matrix is given by,

$$a_0\lambda^4 + a_1\lambda^3 + a_2\lambda^2 + a_3\lambda + a_4 = 0 \tag{7.3}$$

where the coefficients are given by,

$$\begin{aligned}
a_0 &= -1 \\
a_1 &= A+F+K+P \\
a_2 &= BE-AF-AK+CI-AP-FK+GJ+DM-FP+HN-KP+LO \\
a_3 &= AFK-AGJ-BEK+BGI+CEJ-CFI+AFP-AHN+BHM-BEP- \\
&\quad DFM+DEN+AKP+CLM-ALO-CIP-DKM+DIO+FKP-GJP \\
&\quad +GLN-HKN-FLO+HJO \\
a_4 &= AGJP-AFKP-AGLN+AHKN+BGLM-BHKM-CFLM \\
&\quad +CHJM+AFLO-AHJO+BEKP-BGIP-CEJP+CELN \\
&\quad +CFIP-CHIN+DFKM-DGJM-BELO+BHIO- \\
&\quad DEKN+DGIN+DEJO-DFIO
\end{aligned} \tag{7.4}$$

where the entries of the Jacobian Matrix are,

$$A = \frac{\rho_z z^*}{1+\ mu_z z^*}\lambda(1-x^*)\exp(-x^*-\frac{\rho_y y^*}{1+\mu_y y^*}-\frac{\rho_v v^*}{1+\mu_v v^*}) \tag{7.5}$$

$$B = -x^*\exp(-x^*-\frac{\rho_y y^*}{1+\mu_y y^*}-\frac{\rho_v v^*}{1+\mu_v v^*})\lambda\frac{\rho_z z^*}{1+\mu_z z^*}\frac{\rho_y}{(1+\mu_y y^*)^2} \tag{7.6}$$

$$C = -x^*\exp(-x^*-\frac{\rho_y y^*}{1+\mu_y y^*}-\frac{\rho_v v^*}{1+\mu_v v^*})\lambda\frac{\rho_z z^*}{1+\mu_z z^*}\frac{\rho_v}{(1+\mu_v v^*)^2} \tag{7.7}$$

$$D = \lambda x^*\exp(-x^*-\frac{\rho_y y^*}{1+\mu_y y^*}-\frac{\rho_v v^*}{1+\mu_v v^*})\frac{\rho_z}{(1+\mu_z z^*)^2} \tag{7.8}$$

$$E = c(1-\exp(-\frac{\rho_y y^*}{1+\mu_y y^*})) \tag{7.9}$$

$$F = cx^*\exp(-\frac{\rho_y y^*}{1+\mu_y y^*})\frac{\rho_y}{1+\mu_y y^2} \tag{7.10}$$

$$G = 0 \tag{7.11}$$

$$H = 0 \tag{7.12}$$

$$I = \kappa c(1-\exp(-\frac{\rho_v v^*}{1+\mu_v v^*})) \tag{7.13}$$

$$J = 0 \tag{7.14}$$

$$K = cx^*\exp(-\frac{\rho_v v^*}{1+\mu_v v^*})\frac{\rho_v}{1+\mu_v v^2} \tag{7.15}$$

$$
\begin{aligned}
L &= 0 && (7.16)\\
M &= -\frac{(1-\alpha)m}{(m+x^*)^2} - \frac{\alpha s \rho_z z^*}{1+\mu_z z^*} && (7.17)\\
N &= 0 && (7.18)\\
O &= 0 && (7.19)\\
P &= \frac{\alpha(h-sx^*)\rho_z}{(1+\mu_z z^*)^2} && (7.20)
\end{aligned}
$$

7.1.1.1 Trivial solution $(0,0,0,z^*)$

The trivial solution deal with a situation where there is only one species — the larch tree. In such a scenario, most of the entries in the Jacobian matrix become zero giving a fairly simple analysis. We have $B = C = D = E = F = G = H = I = J = K = L = N = O = 0$. The other non-zero entries are

$$
\begin{aligned}
A &= \frac{\rho_z z^* \lambda}{1+\mu_z z^*} && (7.21)\\
M &= -\frac{1-\alpha}{m} - \frac{\alpha s \rho_z z}{1+\mu_z z^*} && (7.22)\\
P &= \frac{\alpha h \rho_z}{(1+\mu_z z^*)^2} && (7.23)
\end{aligned}
$$

The coefficients of the characteristic equations are now much simpler, which are given by,

$$
\begin{aligned}
a_0 &= -1\\
a_1 &= A+P\\
a_2 &= -AP\\
a_3 &= 0\\
a_4 &= 0 && (7.24)
\end{aligned}
$$

The Routh array helps to understand the stability of the fixed points without actually solving the characteristic equations. The Routh array is given by

$$
\begin{bmatrix}
-1 & -A*P & 0\\
A+P & 0 & \\
-A*P & 0 & 0\\
-2A*P & 0 & 0\\
0 & 0 & 0
\end{bmatrix}
$$

Since we deal with populations all the quantities that enter the Routh array, i.e., A and P are positive. In the Routh array we see there are two sign changes which implies that this fixed point is unstable. It must be noted that we have not solved for the fixed points at all. The same result is applicable for q_z=1.

7.1.1.2 The parasitoid-free solution $(x^*, 0, 0, z^*)$

In absence of both the parasitoids, $E = G = H = I = J = L = N = O = 0$, while the non zero entries are:

$$A = \frac{\rho_z z^*}{1+\mu_z z^*}\lambda(1-x^*)\exp(-x^*) \tag{7.25}$$

$$B = -x^*\exp(-x^*)\lambda\frac{\rho_z z^*}{1+\mu_z z^*}\frac{\rho_y}{(1+\mu_y y^*)^2} \tag{7.26}$$

$$C = -x^*\exp(-x^*)\lambda\frac{\rho_z z^*}{1+\mu_z z^*}\frac{\rho_v}{(1+\mu_v v^*)^2} \tag{7.27}$$

$$D = \lambda x^*\exp(-x^*)\frac{\rho_z}{(1+\mu_z z^*)^2} \tag{7.28}$$

$$F = cx^*\exp(-\frac{\rho_y y^*}{1+\mu_y y^*})\frac{\rho_y}{1+\mu_y y^2} \tag{7.29}$$

$$K = cx^*\exp(-\frac{\rho_v v^*}{1+\mu_v v^*})\frac{\rho_v}{1+\mu_v v^2} \tag{7.30}$$

$$M = -\frac{(1-\alpha)m}{(m+x^*)^2} - \frac{\alpha s\rho_z z^*}{1+\mu_z z^*} \tag{7.31}$$

$$P = \frac{\alpha(h-sx^*)\rho_z}{(1+\mu_z z^*)^2} \tag{7.32}$$

The corresponding coefficients are

$$\begin{aligned} a_0 &= -1 \\ a_1 &= A+F+K+P \\ a_2 &= -AF-AK-AP-FK+DM-FP-KP \\ a_3 &= AFK+AFP-DFM+AKP-DKM+FKP \\ a_4 &= -AFKP+DFKM \end{aligned} \tag{7.33}$$

The Routh array coefficients are given by

$$\begin{bmatrix} -1 & (A+P)(F+K)+AP+FK-DM & FK(AP-DM) & FK(AP-DM) \\ -A-F-K-P & -(AP-DM)(F+K)-FK(A+P) & 0 & \\ r_{3,1} & FK(AP-DM) & 0 & \\ r_{4,1} & 0 & 0 & \\ FK(AP-DM) & 0 & 0 & \end{bmatrix}$$

where the various coefficients are given by

$$r_{3,1} = \frac{(A^2F+A^2K+A^2P+AF^2+2AFK+2AFP+AK^2+2AKP+AP^2}{(A+F+K+P)} \tag{7.34}$$

$$\frac{-DMA+F^2K+F^2P+FK^2+2FKP+FP^2+K^2P+KP^2-DMP)}{(A+F+K+P)} \tag{7.35}$$

$$r_{4,1} = \frac{R_1}{R_2} \tag{7.36}$$

Here R_1 and R_2 are given by

$$\begin{aligned}
R_1 &= A^3F^2K + A^3F^2P + A^3FK^2 + 2A^3FKP + A^3FP^2 + A^3K^2P + A^3KP^2 - A^2DF^2M - 2A^2DFKM \\
&\quad -2A^2DFMP - A^2DK^2M - 2A^2DKMP + A^2F^3K + A^2F^3P + 4A^2F^2KP + 2A^2F^2P^2 + A^2FK^3 \\
&\quad +4A^2FK^2P + 4A^2FKP^2 + A^2FP^3 + A^2K^3P + 2A^2K^2P^2 + A^2KP^3 + AD^2FM^2 + AD^2KM^2 \\
&\quad -2ADK^2MP - ADF^3M - ADF^2KM - 2ADF^2MP - ADFK^2M - 4ADFKMP - 2ADFMP^2 \\
&\quad -ADK^3M - 2ADKMP^2 + AF^3K^2 + 2AF^3KP + AF^3P^2 + AF^2K^3 + 4AF^2K^2P \\
&\quad +4AF^2KP^2 + AF^2P^3 + 2AFK^3P4AFK^2P^2 + 2AFKP^3 + AK^3P^2 + AK^2P^3 + D^2FM^2P + \\
&\quad D^2KM^2P - DF^3MP - DF^2KMP - DF^2MP^2 - DFK^2MP - 2DFKMP^2 - DK^3MP - DK^2MP^2 \\
&\quad +F^3K^2P + F^2K^3P + 2F^2K^2P^2 + F^2KP^3 + FK^3P^2 + FK^2P^3 + 2A^2F^2K^2 + F^3KP^2 \\
R_2 &= A^2F + A^2K + A^2P + AF^2 + 2AFK + 2AFP + AK^2 + 2AKP + AP^2 - DMA + F^2K + F^2P + FK^2 + \\
&\quad 2FKP + FP^2 + K^2P + KP^2 - DMP
\end{aligned} \tag{7.37}$$

7.1.1.3 Nontrivial solution (x^*, y^*, v^*, z^*)

The coefficients of the characteristic equations are given by

$$\begin{aligned}
a_0 &= -1 \\
a_1 &= A + F + K + P \\
a_2 &= BE - AF - AK + CI - AP - FK + DM - FP - KP \\
a_3 &= AFK - BEK - CFI + AFP - BEP - DFM + AKP - CIP - DKM + FKP \\
a_4 &= BEKP - AFKP + CFIP + DFKM
\end{aligned} \tag{7.38}$$

The Routh array however is more complicated and definite conclusions cannot be reached unless we switch to numerical methods.
The Routh array is given by,

$$\begin{bmatrix}
a_0 & a_2 & a_4 \\
a_1 & a_3 & 0 \\
-(a_0a_3 - a1a2)/a_1 & a_4 & 0 \\
(a_4a_1^2 - a_2a_1a_3 + a_0a_3^2)/(a_0a_3 - a_1a_2) & 0 & 0 \\
a_4 & 0 & 0
\end{bmatrix}$$

7.2 Existence of limit cycles

The Routh-Hurwitz criterion[51] [50] can also be used to check the existence of limit cycles in the system. Since solving our 4-dimensional $q-$deformed model analytically is difficult, numerical methods were employed to check the criterion. The model is iterated for 10,000-time steps and the fixed point is determined. The fixed point is then fed into the Jacobian from which the Routh array is constructed. The limit cycles are formed when the condition $c_4(c_2c_3 - c_4) - c_5c_2^2 = 0$. Under this circumstance, the frequency $\omega^2 = \frac{c_4}{c_2}$[51] [50].

Fixed points (x^*, y^*, z^*, v^*)	RH-coeff	Stability	λ κ
$0, 0, 0, 0.6936$	All positive	Stable	$\lambda = 1$
$0.01, 0.001, 0, 0.6936$	One negative	Unstable	$\lambda = 8, \kappa = 0.3$
$0.01, 0, 0.001, 0.6936$	One negative	Unstable	$\lambda = 8, \kappa = 1.8$
$0.001, 0.2, 0.1, 0.6936$	One negative	Unstable	$\lambda = 8, \kappa = 1.08$
$0.001, 0.2, 0.1, 0.6936$	One negative	Unstable	$\lambda = 9, \kappa = 1.08$
$0.001, 0.2, 0.1, 0.6936$	One negative	Unstable	$\lambda = 5, \kappa = 1.2$
$0.001, 0.2, 0.1, 0.6936$	One negative	Unstable	$\lambda = 8, \kappa = 0.9$
$0.001, 0.2, 0.1, 0.6936$	One negative	Unstable	$\lambda = 7, \kappa = 1.3$
$0.5, 0.2, 0.1, 0.6936$	One negative	Unstable	$\lambda = 8, \kappa = 1.0$

TABLE 7.1. Rout-Hurwitz criterion for $h = 0.5$, $s = 0.5$, $\alpha = 0.5$, $m = 13$, $c = 12$, $q_y = 1.13$, $q_v = 1.13$ and $q_z = 1.34$.

For both the three-dimensional and the four-dimensional systems, numerical computation of Routh-Hurwitz criterion confirms the presence of limit cycle.

The matrix of the four-dimensional systems which is used for simulations is given below:

$$\begin{bmatrix} a_0 & a_2 & a_4 \\ a_1 & a_3 & 0 \\ -(a_0a_3 - a1a2)/a_1 & a_4 & 0 \\ (a_4a_1^2 - a_2a_1a_3 + a_0a_3^2)/(a_0a_3 - a_1a_2) & 0 & 0 \\ a_4 & 0 & 0 \end{bmatrix}$$

The table(7.1) is a representative of various simulations carried out to find the Routh coefficients. From the table (7.1) it is very clear that the limit cycles do not form when $\lambda = 1$. The reason being that Neimark-Sacker bifurcation as not occurred. As we change, λ, the fixed point looses its stability and a limit cycle is born. When this occurs the coefficients of the Routh array change sign which is evident in the table (7.1). The similar behavior is noted when one of the parasitoids is absent (3-dimensional model).

7.3 Results of the numerical study of the four dimensional model

The four dimensional model which includes the effect of another parasitoid has been fruitful. Including the parasitoid has increased the time period of the outbreak cycles, just as observed in the live experiments performed on larch budmoths as reported in [66]. This model has few more interesting features to offer. Mathematically, these four variables can be considered as 4 oscillators, which are synchronized precisely. In these four oscillators, two of them (the parasitoids) are exactly the same except for their strength which is dictated by κ. Coupled oscillators are known to show interesting behavior as the coupling strengths are varied[98]. Most of the coupled oscillator systems dealt with in the literature are coupled directly with each other, or through diffusive couplings[98]. However, in the system which we consider with 4 species (2 parasitoids), the coupling is indirect. Both parasitoids have no direct coupling with each other. They are coupled to each other via another

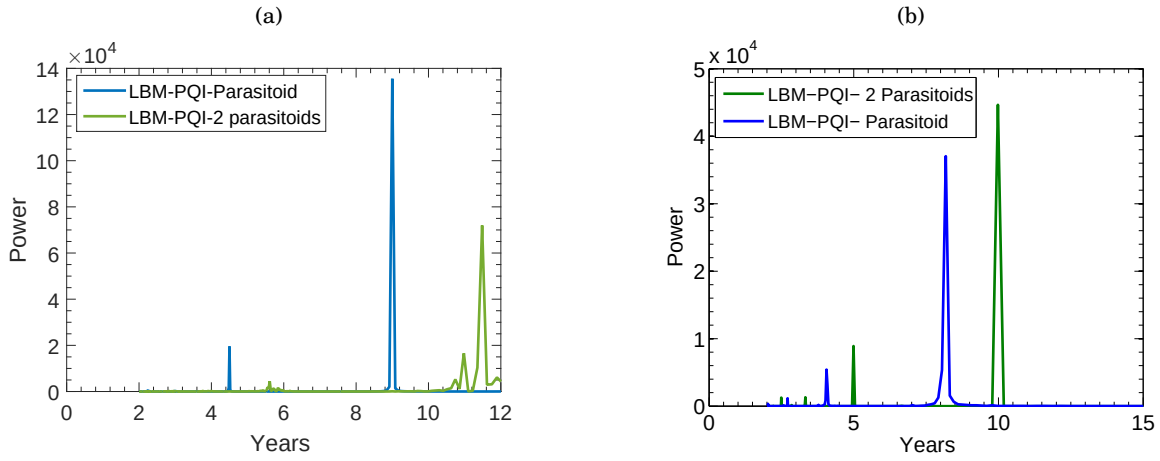

FIGURE 7.1. Variation of time period as the second parameter is introduced. the values of other parameters are $c = 12$, $m = 13$, $q_y = q_v = 1.13$, $q_z = 1.34$, $\alpha = 0.5$, $h = 0.5$, $s = 0.5$, $\kappa = 1.95$ (a) $\lambda = 6.5$ (b)=$\lambda = 8$.

oscillator which is the budmoth. Thus, we see interesting behavior in coupled oscillators which are not directly coupled but are coupled via the third oscillator, which is affected by both the oscillators. PQI, which is the fourth oscillator, is related to the budmoth and hence is not affected by the parasitoids. In the form, we have considered there was no explicit direct competition between the two parasitoids. Despite the indirect coupling of the q−deformed numbers, this system exhibits a variety of behaviors, observed numerically.

7.3.1 Effect on time period

Adding another parasiotid on the budmoth delays the outbreak[66]. Depending on the value of κ the delay can be very large too. In figures(7.1(a) and 7.1(b)), the effect of adding second parasitoid to the original system is clearly visible[90].

7.3.2 Oscillation Death

Oscillation death is a phenomenon that occurs in the coupled system when the phase space is shared between the steady state and limit cycles[98]. A specific choice of the coupling constant leads to oscillation death, where all the four variables become static[98]. The budmoth and plant quality index settle on a non-zero value, while the parasitoids settle at zero[90]. This is clearly visible in figure(7.2(a)). Oscillation death occurs when the phase space is shared between fixed points and the limit cycles. This final state which is inhomogeneous sustains both oscillations and oscillation death. Thus depending on the initial conditions, the system may land into either of the solutions (oscillation death or steady state). Thus, the system has co-existence of attractors (figure(7.2(a)))[90].

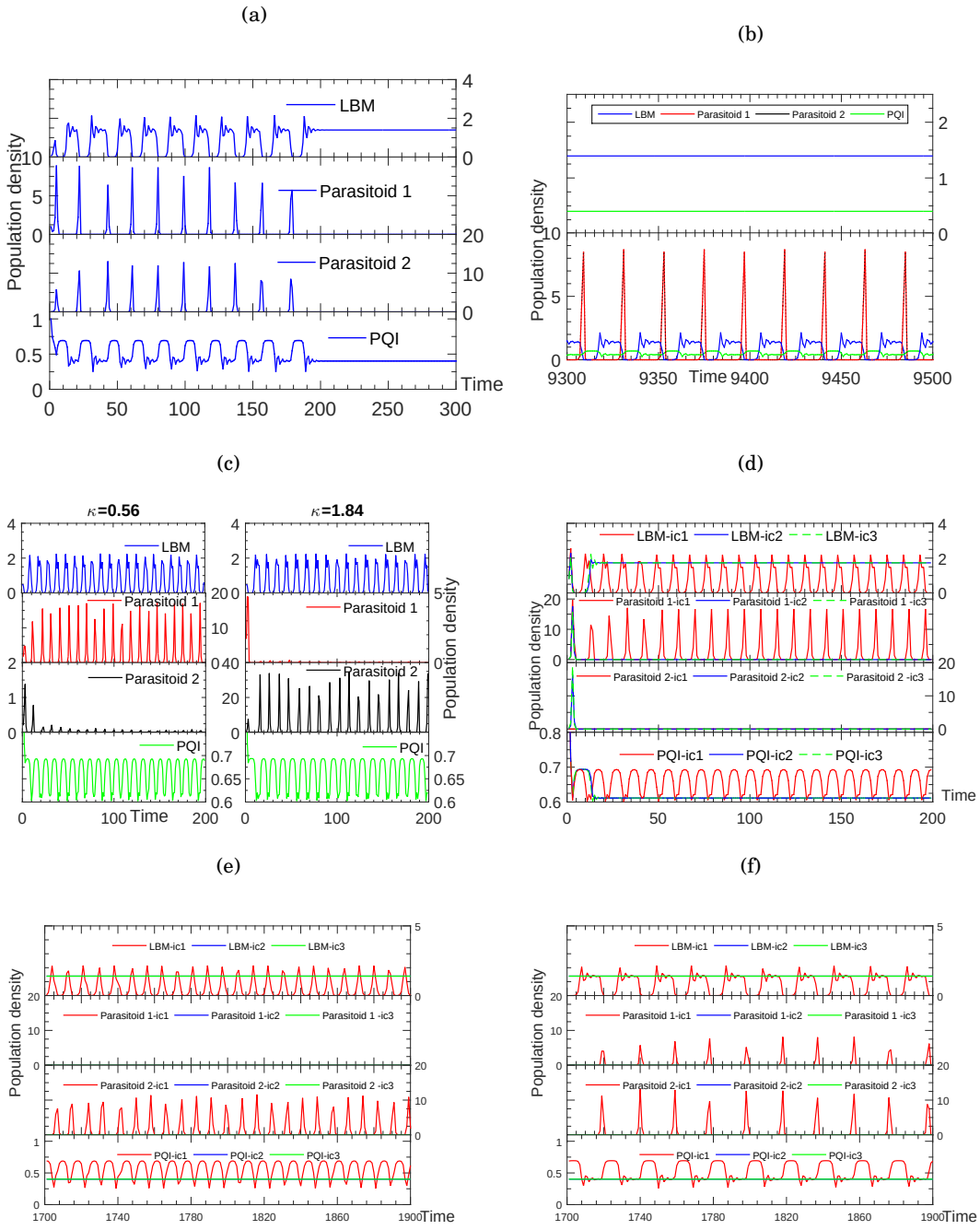

FIGURE 7.2. The values of the parameters for generating this time series are $\alpha = 0.5$, $h = 0.5$, $s = 0.5$, $m = 13$, $c = 12$, $\lambda = 8$, $q_y = q_v = 1.13$, $q_z = 1.34$, (a)Oscillation death for $\kappa = 1.07$,$x_0 = 0.05$,$y_0 = 1$,$z_0 = 1$ and $v_0 = 0.1$. (b)Co-existence of attractors with $\kappa = 1$ with two initial conditions $x_0 = 0.05$, $z_0 = 1$, $y_0 = 2$ and $v_0 = 0.1$ (top) and $x_0 = 2.6450$,$y_0 = 0.2135$, $z_0 = 0.2082$ and $v_0 = 1.4653$.(c)Partial amplitude death with $\kappa = 0.56$ (left), $\kappa = 1.84$ (right) with $x_0 = 0.05$, $z_0 = 1$, $y_0 = 2$ and $v_0 = 0.1$. (d) Addition of second parasitoid brings in oscillation death.$\kappa = 0.95$,$x_0 = 0.8$, $y_0 = 0.1$ and $z_0 = 1$ with colors denoting different values of v_0, Red: $v_0 = 0$, Blue:$v_0 = 0.1$ and Green:$v_0 = 0.2$(e) Co-existence of spiking with oscillation death.$\kappa = 1.06$, $x_0 = 0.05$, $z_0 = 1$, Red: $y_0 = 2$ and $v_0 = 0.1$, Blue: $y_0 = 2$ and $v_0 = 0.3$ and Green: $y_0 = 1$ and $v_0 = 0.1$(f)Co-existence of bursting with oscillation death $\kappa = 1.08$, $x_0 = 0.05$, $z_0 = 1$ Red: $y_0 = 2$ and $v_0 = 0.1$, Blue: $y_0 = 2$ and $v_0 = 0.3$ and Green: $y_0 = 1$ and $v_0 = 0.1$

7.3.3 Bursting

In this four dimensional model, bursting is seen for certain values of κ[90]. The bursting is seen in budmoth and the plant quality index[90]. It is also noted that changing the value of κ a very little changes the bursting back to periodic spiking[90]. Figures (7.2(f)) and 7.2(e)), show the behavior of the system for $\kappa = 1.08$ and $\kappa = 1.06$ respectively. The spiking behavior seen at $\kappa = 1.06$ is lost and the budmoth and the plant being to burst as $\kappa = 1.08$. Figure (7.2(b)) shows bursting co-existing with a fixed point for $\kappa = 1$. A small change in the value of κ creates a transition from spiking to bursting. it is also very clear that both the parasitoids have to be present for bursting to occur. When one of them is absent, we get the spiking behavior, which is also the original 3-D model. The system shows extreme sensitivity to initial conditions[90].

7.3.4 Partial amplitude death

This four dimensional system also shows partial amplitude death wherein oscillations are sustained in some of the variables, while others die out. In the four dimensional model it is seen that for $h = 0.5$, $s = 0.5$, $\lambda = 8$, $m = 13$,$q_y = 1.13$,$q_z = 1.34$,$\alpha = 0.5$ and $c = 12$, partial amplitude death is seen when $\kappa \leq 0.56$ and $\kappa \geq 1.84$ (figure(7.2(c))). Below and above this threshold, one of the parasitoids amongst the two becomes more virulent and stronger. The stronger and the virulent parasitoid reduces the host numbers more efficiently, thereby wiping out the other parasitoid. The other parasitoid is unable to survive on low host numbers, however, the virulent parasitoid is able to survive on low host numbers. The efficiency of the parasitoids in infesting the host is denoted by c which is directly proportional to the number of surviving offspring produced by the parasitoid. That is to say that the virulent parasitoid has a higher fecundity. This is also a clear indication wherein the 2 species do not compete or interact directly, but then are affecting each other so much that their survival is challenged. This is manifested as partial amplitude death shown in the figure(7.2(c))[90].

7.3.5 Co-existence of attractors

The system, shows co existence of attractors[90], by which different initial conditions are attracted to different basins. Since certain conditions show oscillation death, while some go on with sustained oscillation, it is possible that different places in the world started with different initial condition. For instance absence of population cycles in Tatra mountains in Slovakia could have started from a different initial condition and ended up in a steady state[90]. On the other hand the Alps, which are known for strong 8-9 year cycle could have started from another initial condition. The presence of the second parasitoid increases the time period of the observed cycles. It has been noted in the French Alps that the cycles have been quite longer than the usual 9 year cycles[91]. The most plausible reason could be the presence of second parasitoid[90].

7.3.6 Neimark-Sacker bifurcation

Similar to the three dimensional system the four dimensional system also shows creation of limit cycles via Neimark-Sacker (NS) bifurcation. The figures (7.3(a)-7.3(c)) show the creation of limit cycles for various values of κ[90]. Figure(7.3(a)) shows the NS bifurcation when one of the parasitoids is zero. The figure(7.3(b)) shows the same when the virulence of both the parasitoids are equal and finally the figure (7.3(c)) shows NS bifurcation when the second parasitoid is stronger[90].

7.3.7 Effect of κ on the system

κ is the indicator of the strength of the parasitoids. It is seen that the system undergoes an oscillation death at $\kappa = 1$ (Fig.(7.4(a))). Mathematically κ is the coupling between the two oscillators. As mentioned in the literature [98], the coupling constant controls oscillation death which is also seen in the system. When both the parasitoids have the same strength, perhaps they wipe out each other. This results in the loss of parasitism which halts the budmoth cycles[90]. This is also consistent with observations made in the Alpine valley, which led to the conclusion that the parasitoids are needed to drive the cycles [66]. (It must be mentioned that larch tree and the budmoth (2D system) also show cycles, but they require a very high value of λ. Same is true for the parasitoid-budmoth model.) For higher values of κ, chaotic bubbles are formed from simple bubbles. As κ increases it is also noted that the population of the second parasitoid increases and the first parasitoid goes down[90].

(a)

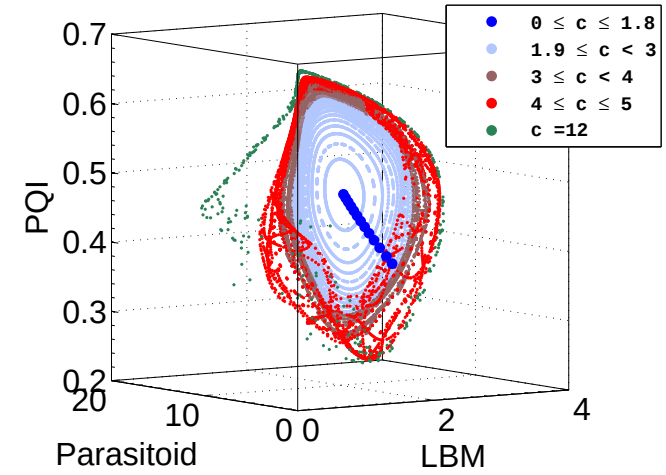

(b)

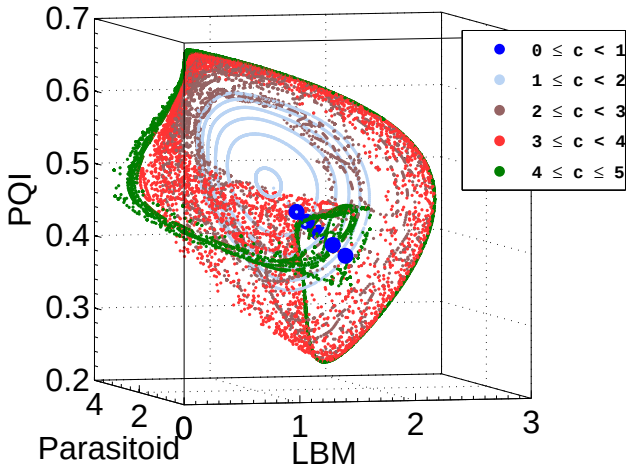

(c)

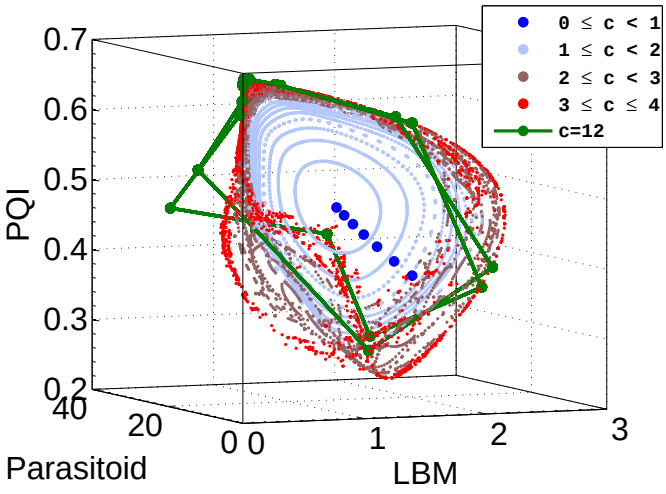

FIGURE 7.3. 3-D phase portraits of three species showing Neimark-Sacker bifurcation for various values of κ, with other parameters fixed at $h = 0.5$, $s = 0.5$, $\alpha = 0.5$, $m = 13$, $q - y = 1.13$, $q - v = 1.13$, $q_z = 1.34$, $\lambda = 8$ and various values of c (a)$\kappa = 0$ (b)$\kappa = 1$ (c)$\kappa = 1.95$

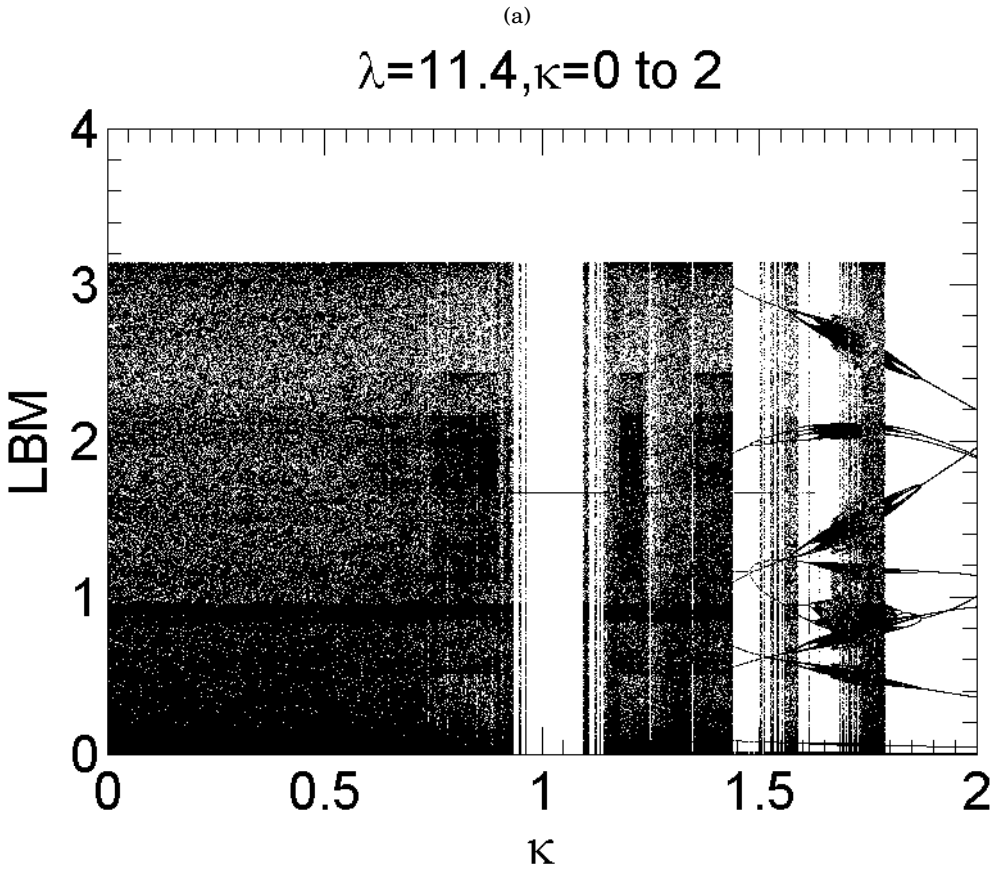

FIGURE 7.4. Bifurcation diagram with respect to κ as λ is changed. At around $\kappa = 1$ oscillation death occurs which is clearly seen.

CHAPTER 8

CONCLUSIONS

The failure of classical physics in explaining some well known phenomena has paved the way for newer theories to emerge and the generalization of older theories. Tsallis' statistics has been useful in situations where there is no ergodicity, where there are long-range interactions, where memories of past events are present and where the phase space has a fractal nature. The Tsallis form of entropy and generalized statistics have been applied to many fields after its discovery.
In this thesis we have presented our results on the use of q-deformation of numbers and Tsallis statistics in real-life. We began with an exposition on q-deformations and followed it with its application to various maps. We then discussed a tritrophic ecological system and the observation of population cycles over several centuries. We then showed how our model of this system gives very good results in agreement with observations and also explains some puzzling features of these cycles and makes some useful predictions.

In Chapter 2 we began with an enumeration of examples of systems where ordinary statistics have failed and Tsallis statistics was used instead. These examples made it very clear that when there is memory of the past, or when there is no ergodicity, when we have system-governing parameters that are fluctuating, or when there are co-existence of attractors, normal statistical mechanics fails to explain the system behaviour satisfactorily. These shortcomings were overcome by the use of Tsallis statistics.
In Chapter 3, as a first, preliminary exercise, $q-$deformed numbers were used in four well-known maps to study their behavior under $q-$deformations. The maps discussed in this thesis are the Duffing map, the Ikeda map, the Tinkerbell map and the circle map. Under $q-$ deformations, the maps show different behaviour[37].

In the Duffing map, $q-$ deformations caused a reduction in the size of the attractor. The system

is chaotic and the attractor size is largest for $q = 1$. As q is varied from -2 to 2, the system undergoes a change in the size of the attractor, a phenomenon that is referred to as an interior crisis. Satellites are created for some parameter values of q, which are again indicators of interior crises. The Duffing map can be used to model the motion of particles in an accelerator. The use of q-deformation could possibly help to include the effects of many physical processes which are usually neglected for simplicity in an analytical treatment of the phenomenon. These could be, for example, the existence of higher order multipole moments and interaction of incoming particles with the radiation emitted by an accelerated particle. The main purpose of an accelerator is to accelerate a particle to very high speeds, requiring the particle to stay inside the accelerator for a long enough time. The ordinate and abscissa (x, y) of the Duffing map would correspond to the position and momentum of a particle inside the accelerator. The spread in particle position and momentum, which is also known as the emittance, should be less. This corresponds to the attractor of the Duffing map being smaller. The original map is maximally chaotic at $q = 1$. If a transition is made in the value of q to other values, the attractor size would be less, with less spread in the position and velocity of the particle[37].

The Ikeda map when subjected to varying q, shows interior crises for values of $q > 1$. For $q < 1$, the Ikeda attractor is smaller. The Ikeda map is used to describe the electric field inside an optical cavity. A proper choice of the nonlinear absorber can make it spell a variety of behavior. The ordinate and abscissa of the Ikeda map are related to the in-phase and the out-phase components of the electric fields that are generated by laser going on a round trip. For values of $q > 1.5$, the attractor is almost confined to two lines appearing to run almost perpendicular to each other. Thus, we see that very high values of q lead to constant values of x and y, indicating that the laser fields do not fluctuate and give a steady input. The nonlinearity in the system arises due to properties of the absorber used in the optical cavity. We suggest that engineering of such an absorber could give a non-fluctuating steady output with higher magnitudes[37].

The circle map can be used in situations where a system responds to a stimulus or where systems have multiple response frequencies. A Poincarè section reduces a time series with multiple frequencies to a circle map. Most of the systems we know of in daily life are driven by external stimuli – a truly isolated system is very rare. For instance, a flower blooming in the morning is controlled by sunlight which has a periodicity of a day. Taking another example, that of a heart with a pace-maker: the heartbeat is the response of the heart muscle to the stimulus generated by the electrical signal from the pace-maker. A circle map can be used to study any such system that has an external forcing. This makes it very significant as a general study of this map could help us understand many physical phenomena. It was found that this system is robust with not much significant change under q-deformations. Under q deformation, the system shows “period-twinning", or replication of a period doubling cascade from an already existing cascade[37]. This is evident from the bifurcation diagram.
For different parameter values for a circle map, the winding number was calculated and plotted.

Regions in parameter space that correspond to periodic behavior are called Arnold tongues. Such a plot of the winding number shows the shift in the domains of periodicity, quasi-periodicity and chaos as q varied[37]. There is no drastic change in this map when subjected to q-deformations. It is perhaps the reason why most of the natural driver-responder systems are quite stable.

The Tinkerbell map, when subjected to $q-$deformations shows exotic behavior. As q is varied from 0 to 1, limit cycles are born via Neimark-Sacker bifurcation. The map also shows paired cascades between $0.945 \leq q \leq 0.97$. As q increases, interior crises occurs that increase the size of the attractors. From $3.2 \leq q \leq 3.3$, multiple limit cycles are seen lying next to each other. Two of these limit cycles undergo a Neimark-Sacker bifurcation, while the third one undergoes a reverse Neimark-Sacker bifurcation.
The Tinkerbell map can be used in encryption and decryption of messages. An earlier work [52] in this field implemented encryption and decryption by varying the four parameters and the two initial conditions. Including q-deformation would add more parameters, thereby making the key space richer and hence making it that much more difficult for breaking into a message. Since the system exhibits many distinct types of behaviour depending on the value of q, a message could be encrypted in a variety of ways[48].

Earlier work done on one dimensional maps and two dimensional maps (logistic, Gaussian, and Henon maps) [33, 34, 35, 36] have shown coexistence of attractors and change in the nature of orbit (periodic/ chaotic/ quasi-periodic, stable/ unstable) qualitatively. The 2-dimensional bifurcation diagram shows interesting features like paired cascades, multiple limit cycles, exterior crises, presences of satellites, etc.
After reproducing the results seen in a one dimensional map, our attempts on q- deforming the various 2 dimensional maps were also fruitful[37, 48]. Many interesting phenomena such as the formation of paired cascades, Neimark-Sacker bifurcation, interior crises, cascade replication, satellite formation, etc. were observed, as mentioned above.

We then studied a tritrophic ecological system which has shown periodic population cycles over a period of several centuries. This system consists of larch trees, the insect infesting it known as the larch budmoth, as well as the parasitoid which, in turn, treats the budmoth larvae as its hosts. The observed 9-year cycle for the larch budmoth population in a large part of the Alps has been a matter of historical record over twelve centuries, and has also been the subject of study by various researchers. Details of this ecological system and past work on this was covered in Chapter 4.

The usual methods of modelling an ecological system till today assume no interactions with environment. However, since in reality, anthropogenic activities are affecting the environment, the parameters governing the system-behaviour keep changing both temporally and spatially. Nor is the phase space ergodic. Since we are dealing with living organisms, memory too plays a vital

role. Ecological systems are known to have co-existence of attractors. The complexity of the system increases as the number of parameters increase.

The overall objective of the next part of our work, explained in Chapter 5[77], was to model the well-known population cycle of the larch budmoth, detailed in Chapter 4.
Although there have been other mathematical models by other researchers which could give the observed 9 year cycle, these were strictly rigid with no flexibility to include the variations introduced into the system due to changes in the environmental conditions. Nor have these models any explanation for the absence of these cycles in other larch forests (in the Carpathian mountains).
In general, the effects of environment on an eco-system are very well documented. For instance, pumping of excess CO_2 into the atmosphere has resulted in global warming which has affected the entire planet. Many ecological niches have collapsed due to this. Climate research over the past few decades have shown that there has been a distinct regime-change in ecosystems after 1980. Studies on varied ecological systems have shown that some population cycles have collapsed suddenly, with no apparent reason. The larch budmoth, larch tree and parasitoid system too, seem to have been affected by environmental changes: the 9-year cycle which should have next appeared in 1990 in the larch forests of the Engadine valley in the Alps, failed to occur.

Our model, which we discussed in Chapter 6, is the first to make a direct connection between the environment and population cycles in a mathematical model[78]. Almost all ecological models prevalent currently do not have any parameters that represent the environment. Since environmental changes affect different organisms differently, we require different parameters for different species.
There are three interacting species in the system we have considered. However, the parasitoid lives on the host (budmoth) and thus any effect of the environment on the budmoth affects the parasitoid as well – the parasitoid itself is not separately affected by the environment. We have introduced two parameters, s and h, to capture environmental effects on the budmoth and the larch tree. Both parameters are seen in the equation of the plant quality index,PQI, which is a measure of how healthy the plant is (and which is practically quantified by the length of the larch leaves). Parameter h affects the plant quality index by altering the rate of re-growth of damaged foliage, and can be taken as a measure of the precipitation and the amount of sunshine received in the region. Incidentally, all previous models did not even consider the further growth of damaged leaves, let alone climatic and environmental factors like precipitation or sunshine.
Parameter s, that appears in the equation corresponding to the plant growth, is taken to directly affect the budmoths. We have interpreted this to be related to the inverse of the ambient temperature. This interpretation is based on the fact that higher winter temperatures result in higher mortality in the budmoth eggs. In case of higher budmoth mortality, the larch tree is saved, while a lower mortality implies devouring of the foliage. Since the eggs are destroyed, s does not affect the existing budmoth larvae. This was the reason why we introduced s into the equation for the

larch tree rather than the budmoth itself. The effect of environment on the budmoth is seen via the effect on larch tree, which is affected directly by the environment (h) or indirectly by the budmoth (s). The correct identification of these parameters has made this model a practical one and which can be observationally verified, and the parameters quantitatively calibrated in future from what is observed in nature.

The main difference between our model and earlier models is that the older, existing models did not take into consideration the unequal probabilities of budmoth infestation of the leaves. The system is actually not ergodic. Secondly, with changing environmental parameters, the system is actually not in equilibrium, with the dynamics of the population cycle also changing.

Third, the system has memory of past years' growth. This is evident in the equation for the larch tree. The value of PQI in the previous year affects the current year's growth (including environmental factors). Thus the presence of memory skews the probabilities. This brings in $q-$deformations into the system.

Earlier models did not differentiate between fresh foliage and the foliage damaged due to infestation in previous years. However, documentation and observations in the Alpine region have clearly revealed that fresh foliage is more nutritious with higher protein content, while the damaged leaves are more fibrous and less nutritious. The budmoths hence indulge in wasteful feeding, moving to more nutritious fresh leaves leaving behind the damaged leaves, which are left at the mercy of the environment to flourish or perish. q-deformation mimics this phenomenon, and our model is able to explain the observations more precisely[77].

The inclusion of $q-$deformation and environmental factors has made our model an accurate one which is able to reproduce observations seen in dendrochronological records spanning 1200 years. The 3 dominant peaks and their relative frequencies produced by our $q-$deformed model in the histograms depicting relative frequencies of occurrences of budmoth outbreaks, match with observations seen in these data.

The system is robust in producing the 8-9 year cycle with even small changes in parameter values. The histograms clearly show that population cycles that are seen in the Alpine region require the presence of a tritrophic system of larch, budmoth as well as parasitoid, for the observed population outbreak cycles to be present: with just the larches and budmoths alone, one would not get the periodicity seen.

The population cycles of the larch budmoth which are experimentally observed, arise in our mathematical model as a result of limit cycles produced through Neimark-Sacker bifurcations.

Observations made in the Engadine Valley of the Swiss Alps have shown the presence of various outbreak cycles, ranging from 3 to 18 years, but with the main predominant cycle being that of 8-9 years. Depending upon the parameter values in our mathematical model, that is, depending upon the climatic conditions being represented, we have successfully captured both this possible range of outbreaks, as well as the predominant 8-9 year cycle. Our model also predicts a 40 year and a 100 year cycle, although the probability of occurrence of these latter cycles is very small, with

low relative frequencies. After 1981, there as been no outbreak till today. If the LBM cycles have slipped into these 40 or 100 year cycle regimes, the next outbreak will recur in another 5 years or 65 years[78].

We have also found parameter regimes which can sustain no cycles. The Carpathian mountains in the Tatra region of Slovakia, which is also home to larch trees, have no reported outbreaks. Since our model has no cycles in certain parameter regimes, it is plausible that the Tatra larches could belong to those regimes. We have identified and discussed the possible differences between the two regions (Tatra mountains and Alps) based on the observations presented in the literature. Such an exercise has helped us to identify the parameters that differ in both regions. Although Neimark-Sacker bifurcation occurs with respect to all the parameters, not all of them can differ in the two places, as some of these are species-specific parameters[78].

The effect of variation of two parameters on the system are studied by making videos[78]. The bifurcation videos shows interesting features. Regions like source and sink are created which seem to repel and attract points. Bubbling phenomena, crises, oscillation death, Neimark-Sacker bifurcation are all seen when two parameters are varied.

In Chapter 7, we discussed an extension to the tritrophic larch budmoth system, by considering the effect of a fourth species, which is another parasitoid. This was motivated from experiments performed in the Alpine region, where spraying of bacillus strains on the larches resulted in the postponement of budmoth outbreaks. Our four dimensional model is able to reproduce this observed fact, and we find that depending on the relative strengths of the parasitoids the outbreak time could vary[90].

The four dimensional model was proposed to check how the addition of another parameter would alter the original system. This four dimensional system is more general and more realistic as it exhibits phenomenon such as oscillation death, partial amplitude death and bursting. Partial amplitude death corresponds to the phenomenon of one of the species becoming extinct locally. This is something that is observed everywhere in nature.
This model also shows co-existence of attractors, implying that different initial conditions could cause the same system to land up in different dynamical regimes, in different basins. Since after 1981, the outbreaks have ceased, there is a possibility that the Alpine region has settled down in a different basin of attraction or has slipped into a longer time period, or the parameter values have undergone an extreme change stopping the cycles completely.

This thesis discusses the entire gamut of features of this q-deformed, tritrophic ecological model. Our model can account for all the possibilities that can actually happen in nature, making it a versatile and realistic one, which can be used to make realistic predictions, once its parameters are calibrated using quantitative numbers from observations.

BIBLIOGRAPHY

[1] R.P. Crease and C.C. Mann, “The Second Creation: makers of the revolution in twentieth-century physics", Rutgers University Press (1996).

[2] E. N. Lorenz, “Deterministic nonperiodic flow", *J. Atmos. Sci.*, **20**, 130-141 (1963).

[3] M.L. Rosenzweig, et. al, “Paradox of enrichment: destabilization of exploitation ecosystems in ecological time", *Science*, **171**, 385-387 (1971).

[4] C. Tsallis, “Possible generalization of Boltzmann-Gibbs statistics", *J. Stat. Phys.*, **52**, 479-487 (1988).

[5] F. H. Jackson, “A Generalisation of the Functions $\Gamma(n)$ and x^n", *Proc. Roy. Soc. London*, **74**, 64-72 (1904).

[6] C. Tsallis, R. S. Mendes, and A.R. Plastiono, “The role of constraints within the generalized non extensive statistics", *Physica A*, **261**, 534-554 (1998).

[7] E.M.F. Curado and C. Tsallis, “Generalized statistical mechanics: connection with thermodynamics", *J. Phys. A: Math. Gen.*, **24**, L69-L72 (1991).

[8] M. Gell-mann and C. Tsallis, *“Nonextensive Entropy-Interdisciplinary Applications”*, Edited by Murray Gell-Mann and C Tsallis, pp. 440. Oxford University Press, ISBN-10: 0195159764. ISBN-13: 9780195159769, (2004).

[9] F. Schlögl and C. Beck, *“Thermodynamics of chaotic systems”*, Cambridge University Press (CUP) (1993).

[10] E. Heine, “*Handbuch der Kuqelfunktionen*’, **1**, Reimer, Berlin(1878), reprinted by Physica-Verlag, Wurzburg (1961).

[11] C. Tsallis, “Nonextensive statistics: theoretical, experimental and computational evidences and connections", *Brazilian Journal of Physics*, **29**, 1-35 (1999).

[12] A. Pluchino, A. Rapisarada and C. Tsallis, “Nonergodicity and central-limit behavior for long-range Hamiltonians", *EPL*, **80**, 26002 (2007).

[13] G. Kaniadakis, A. Lavagno, and P. Quarati, “Generalized statistics and solar neutrinos", *Phys. Lett. B*, **369**, 308-312 (1996).

[14] Y. Fukuda, et. al, “Evidence for oscillation of atmospheric neutrinos", *Phys. Rev. Lett.*, **81**,1562-1567 (1998).

[15] D. Clayton, “Maxwellian relative energies and the solar neutrinos", *Nature*, **249**, 131-134 (1977).

[16] M. Coraddu, G. Kaniadakis, A. Lavagno, M. Lissia, G. Mezzorani and P. Quarati, “Thermal Distributions in Stellar Plasmas, Nuclear Reactions and Solar Neutrinos ", *Braz. J. Phys*, **29**, 153- (1999).

[17] C. Beck, E.G.D. Cohen, S. Rizzo, “Atmospheric turbulence and superstatistics", *Euro Phys. News*, **36**, 189,Äì191 (2005).

[18] A.R. Plastino, “S_q entropy and self gravitating systems", *Euro Phys. News*, **36**, 208-210 (2005).

[19] A. Rapisarda and A. Pluchino, “Non extensive thermodynamics and glassy behavior", *Euro Phys. News*, **36**, 202-206 (2005).

[20] F. A. Tamarit and C. Anteneodo, “Relaxation and aging in a long-range interacting system", *Euro Phys. News*, **36**, 194-197 (2005).

[21] A. Upadhyaya, J.P. Rieu, J.A. Glazier and Y. Sawada, “Anomalous diffusion and non-Gaussian velocity distribution of Hydra cells in cellular aggregates", *Physica:A*, **293**, 549-558 (2001).

[22] G.L. Barnes, “Origins of the Japanese Islands: The New “Big Picture"", *Japan Review*, **15**, 3-50 (2003).

[23] S. Abe, U. Tirnakli and P.A. Varotsos, “Complexity of seismicity and nonextensive statistics", *Euro Phys. News*, **36**, 206,Äì208 (2005).

[24] G.M. Viswanathan, et. al, “Optimizing the success of random searches", *Nature*, **401**, 911-914 (1999).

[25] A.M. Edwards, et. al, “Revisiting Lèvy flight search patterns of wandering albatrosses, bumblebees and deer.", *Nature*, **449**, 1044-1048 (2007).

[26] P.C.A. da Silva, T.V. Rosembach, A.A. Santos, M.S. Rocha and M.L. Martins, “Normal and Tumoral Melanocytes exhibit q-Gaussian Random Search Patterns.", *PLOS One*, **9**, e104253, 1-13 (2014).

[27] F.L. Schuster and M. Levandowsky, “Chemosensory responses of Acanthamoeba castellanii: visual analysis of random movement and responses to chemical signals", *J. Euk. Microbiol.*, **43**, 150-158 (1996).

[28] J. Cartwright, “Roll over, Boltzmann Does Tsallis entropy really add up? ", *Physics World*, **27**, 31-35 (2014).

[29] P.R.B. Diniz, L.O. Murtha-Junior, D.G. Brum, D.B. de Araujo and A.C. Santos, “Brain tissue segmentation using q-entropy in multiple sclerosis magnetic resonance images.", *Braz. J. Med. Biol. Res.*, **43**, 77-84 (2010).

[30] J. Mohanalin, P.K. Kalra, and N. Kumar, “Tsallis entropy based contrast enhancement of microcalcifications", in proceedings of *International Conference on Signal Acquisition and Processing, 2009. ICSAP 2009.*, 3-7 (2009).

[31] P. Douglas, S. Bergamini, and F. Renzoni, “Tunable Tsallis distributions in dissipative optical lattices", *Phys. Rev. Lett.*, **96**, 110601 (2006).

[32] E. Lutz, “Anomalous diffusion and Tsallis statistics in an optical lattice", *Phys. Rev. A*, **67**, 051402(R) (2003).

[33] R. Jaganathan, and S. Sinha, “A q-deformed non linear map.", *Phys. Lett. A*, **338**, 277-287 (2005).

[34] S. Banerjee and S. Parthasarathy, “ A q-deformed logistic map and its implication.", *J. Phys. A: Math. Theor.*, **44**, 045104(1-9) (2011).

[35] V. Patidar, and K.K. Sud, “A comparative study on the co-existing attractors in the Gaussian map and its q-deformed version." *Communications in Nonlinear Science and Numerical Simulation*, **14**, 827-838 (2009).

[36] V. Patidar, G. Purohit, and K.K. Sud, “Dynamical Behavior of q-deformed Henon map.", *IJBC*, **21**, 1349-1356 (2011).

[37] S.V. Iyengar and J. Balakrishnan, “Studies of some $q-$deformed nonlinear maps", *submitted* (2016)

[38] G. Duffing, *“Erzwungene Schwingungen bei Veränderlicher Eigenfrequenz.”*, F. Vieweg u. Sohn, Braunschweig, (1918).

[39] C. Grebogi, E. Ott, and J.A. Yorke, “Chaotic attractors in crisis.", *Phys. Rev. Lett.*, **48**, 1507–1510 (1982).

[40] E. Sander, and J.A. Yorke, “Connecting period-doubling cascades to chaos", *IJBC*, **22**, (2012) 1250022.

[41] A. Chao, “Nonlinear Dynamics in Accelerator Physics.", *Chin. J. Phys.*, **30**, 1013.

[42] T. Sen, J.A. Ellison, and S.K. Kauffmann, “Collective behaviour of an ensemble of forced duffing oscillators near the 1: 1 resonance", *Physica D*, **81**, 44–78 (1995).

[43] E. Forest and K. Hirata, “*Contemporary Guide to Beam Dynamics*", KPC Report, 92-12, August (1992).

[44] S.R. Mane and T. Weng, “Using the Minimal Normal Form Method With Discrete Maps", *Technical report submitted to Brookhaven National Laboratory (BNL)*, (1992).

[45] Ikeda, K., “Multiple-valued stationary state and its instability of the transmitted light by a ring cavity system.", *Optics communications*, **30**, 257-261 (1979).

[46] S. M. Hammel, C. K. R. T. Jones and J. V. Moloney, “Global dynamical behavior of the optical field in a ring cavity", *J. Opt. Soc. Am. B*, **2**, 552-564 (1985).

[47] E. Mosekilde, “*Topics in nonlinear dynamics: Applications to physics, biology and economic systems*, published by World Scientific (1997).

[48] S.V. Iyengar and J. Balakrishnan, “Numerical exploration of $q-$deformed Tinkerbell map", *submitted* (2016).

[49] S. Yuan, T. Jiang, and Z. Jing, “Bifurcation and Chaos in the Tinkerbell Map", *IJBC*, **21**, (2011) 3137–3156.

[50] J. Guckenheimer, and P. Holmes, *“Nonlinear oscillations, dynamical systems, and bifurcations of vector fields”*, **42**, Springer Verlag (1983).

[51] M. Han and P. Yu, *“Normal forms, Melnikov functions and bifurcations of limit cycles”*, **181**, Springer Verlag (2012).

[52] G. Hanchinamani and L. Kulkarni, “A Novel Approach for Image Encryption based on Parametric Mixing Chaotic System", *IJCA*, **96**, (2014) 30-37.

[53] G.C. Layek, *“An Introduction to Dynamical Systems and Chaos”*, published by Springer (2015).

[54] M. McGuinness, Y. Hong, D. Galletly, and P. Larsen, “Arnold tongues in human cardiorespiratory systems", *Chaos*, **14**, 1–6 (2004).

[55] L. Glass, “Cardiac arrhythmia’s and circle maps- A classical problem", *Chaos*, **1**, 13–19 (1991)

[56] L. Glass, M.R. Guevara, J. Belair, and A. Shrier, “Global bifurcations of a periodically forced biological oscillator.", *Phys. Rev. A*, **29**, 1348-1357 (1983).

[57] P. Turchin, *“Complex population dynamics , a theoretical/empirical synthesis”*, **35**, Princeton University Press (2003).

[58] W.E. Ricker, “Stock and recruitment", *Journal of the Fisheries Board of Canada*, **11**, 559-623 (1954).

[59] J. M. Mahaffy, Lecture notes on “More applications of Nonlinear Dynamical Systems", in the course **Math 636 - Mathematical Modeling**, in the SanDiego State University (2011).

[60] A.J. Lotka, *“Elements of physical biology”*, Dover Publications (1956).

[61] V. Volterra, “Variazioni e fluttuazioni del numero d’individui in specie animali conviventi", published by C. Ferrari (1927).

[62] A.J. Nicholson and V.A. Bailey, “The Balance of Animal Populations.Part I.", *J. Zool.*, **105**, 551-508 (1935).

[63] J. R. Beddington, “Mutual interference between parasites or predators and its effect on searching efficiency", *J. Anim. Ecol.*, **44**, 331-340 (1975).

[64] W. Baltensweiler and A. Fischlin, “The larch budmoth in the Alps", in *Dynamics of forest insect populations*, 331-351, Springer publications (1988).

[65] R. A. Werner, “Biology and behavior of a larch bud moth, *Zeiraphera sp.,* in Alaska", Research note PNW-356, forest service, United States Department of Agriculture, (1980).

[66] A.A. Berryman, “What causes population cycles of forest Lepidoptera?", *Trends. Ecol. Evol.*, **11**, 28-32, (1996).

[67] J. Esper, U. Büntgen, D.C. Frank, D. Nievergelt and A. Liebhold, “1200 years of regular outbreaks in alpine insects", *Proc. R. Soc. Lond. [Biol.]* , **274**, 671-679, (2007).

[68] O. Konter, J. Esper, A. Liebhold, T. Kyncl, L. Schneider, E. Düthorn and U. Büntgen U., “Tree-ring evidence for the historical absence of cyclic larch budmoth outbreaks in the Tatra Mountains ", *Trends. Ecol. Evol.*, **29**, 809-814 (2015).

[69] D.M. Johnson, O.N. Bjørnstad and A.M. Liebhold, “Landscape geometry and travelling waves in the larch budmoth", *Ecol. Lett.*, **7**, 967-974 (2004).

[70] L.V. Nodorezov and D.L. Sadykova, “Dynamics of larch bud moth populations: Application of Moran-Ricker models with time lag", *Ecol. Modell.*, **297**, 26-32 (2015).

[71] W. Baltensweiler, “Why the larch bud-moth cycle collapsed in the subalpine larch-cembran pine forests in the year 1990 for the first time since 1850", *Oecologia* ,**94**, 62-66 (1993).

[72] V. Delucchi, “Parasitoids and hyperparasitoids of Zeiraphera Diniana and their role in population control in outbreak areas", *Entomophaga*, **27**, 77-92 (1982).

[73] C. S. Holling, “Some characteristics of simple types of predation and parasitism 1", *Can. Entomol.*, **91**, 385-398 (1959).

[74] P. Turchin et al., “Population Cycles of the Larch Budmoth in Switzerland", in *Population cycles: The case of trophic interactions*, ed. A. Berryman, pp.130-141, Oxford University Press (2002).

[75] P. Turchin, et al., “Dynamical effects of plant quality and parasitism on population cycles of larch budmoth", *Ecology*, **84**, 1207-1214 (2003).

[76] R-J. Jang Sophia and D.M. Johnson, “Dynamics of discretetime larch budmoth population models", *J. Biol. Dynam.*, **3**, 209-223 (2009).

[77] S.V. Iyengar, and J. Balakrishnan, “q-deformations and the dynamics of the larch bud-moth population cycles" in *Nature’s Longest Threads , New Frontiers in the Mathematics and Physics of Information in Biology.* Eds by Balakrishnan, J. & Sreekantan, B V. Published by World Scientific Publishing Co. Pte. Ltd., 2014. ISBN# 9789814612470, **1**, 65-80 (2014).

[78] S.V. Iyengar, J. Balakrishnan, and J. Kurths, “Impact of Climate change on Larch Budmoth cyclic outbreaks", *Sci. Rep.*, **6**, 27845 (2016).

[79] K.E. Carpenter, et. al, “One-third of reef-building corals face elevated extinction risk from climate change and local impacts", *Science*, **321**, 560-563 (2008).

[80] G.R. Walther, et. al, “Ecological responses to recent climate change", *Nature*, **416**, 389-395 (2002).

[81] M. Strum, C. Racine and K. Tape, “Climate change: increasing shrub abundance in the Arctic", *Nature*, **411**, 546-547 (2001).

[82] U. Pratap and T. Ya, “The Human Pollinators of Fruit Crops in Maoxian County, Sichuan, China: A Case Study of the Failure of Pollination Services and Farmers’ Adaptation Strategies", *Mountain Research and Development*, **32**, 176-186 (2012).

[83] D. Goulson, “Decline of bees forces China’s apple farmers to pollinate by hand", *China Dialogue*, **2**, (2012).

[84] S.G. Potts, et. al, “Global pollinator declines: trends, impacts and drivers", *Trends in ecology & evolution*, **25**, 345-353 (2010).

[85] D.M. Johnson, et al., “Climatic warming disrupts recurrent Alpine insect outbreaks", *Proc. Natl. Acad. Sci. USA*, **107**, 20576-20581 (2010).

[86] W. Baltensweiler, G. Benz, P. Bovey and V. Delucchi, “Dynamics of larch bud moth populations", *Annual review of entomology*, **22**, 79-100 (1977).

[87] P.C. Reid, et al., “Global impacts of the 1980 regime shift", *Glob. Chang. Biol.*, **22**, 682-703 (2016).

[88] E. Brocard, et al., “Upper air temperature trends above Switzerland 1959-2011", *J. Geophys. Res.- Atmos.*, **118**, 4303-4317 (2013).

[89] J. Maynard-Smith, *Models in ecology*, published by CUP Archive, (1978).

[90] S.V. Iyengar, J. Balakrishnan, and J. Kurths, “Co-existence of periodic bursts and death of cycles in a population dynamics system", *submitted* (2016).

[91] G. Battipaglia, et. al., “Long-term effects of climate and land-use change on larch budmoth outbreaks in the French Alps", *Clim. Res.*, **62**, 1-14 (2014).

[92] P.A. Abrams, “When does greater mortality increase population size? The long history and diverse mechanisms underlying the hydra effect", *Ecology Letters*, **12**, 462-474 (2009).

[93] C.N.K. Anderson et.al., “Why fishing magnifies fluctuations in fish abundance", *Nature*, **452**, 835-839 (2008).

[94] E. Liz. and A. Ruiz-Herrera, “The hydra effect, bubbles, and chaos in a simple discrete population model with constant effort harvesting", *J. Math. Biol.*, **65**, (2012) 997-1016.

[95] B. Dennis, R.A. Desharnais, J. M. Cushing, R.F. Costantino, “Transitions in population dynamics: equilibria to periodic cycles to aperiodic cycles", *J. Anim. Ecol.*, , 704-729 (1997).

[96] L. Stone, “Period-doubling reversals and chaos in simple ecological models", *Nature*, **365**, 617-620 (1993).

[97] N. Marwan, M. Carmen Romano, M. Thiel and J. Kurths, “Recurrence plots for analysis of complex systems", *Phys. Rep.*, **438**, 237-329 (2007).

[98] A. Koseka, E. Volkov, and J. Kurths, “Oscillation quenching mechanisms: Amplitude vs. Oscillation death.", *Phys. Rep.*, **531**, 173-199 (2013).

APPENDIX A

ROUTH-HURWITZ CRITERION

From dynamical systems theory and linearisation about a fixed point, it is clear that eigenvalue of the characteristic equation obtained from the Jacobian, which is obtained from the linearized system, determines the stability of the fixed point. A positive real part of the eigenvalue implies an instability in the system, while a negative real part indicates a stability. Hence there is an easy way to identify the system's stability or instability by knowing how many negative and positive real parts of the roots of the characteristic polynomial exists.
The way to compute the same is known as the Routh-Hurwitz criterion.

A.1 Theory

Consider a characteristic equation given by

$$\Sigma_0^n a_n \lambda^n = 0 \tag{A.1}$$

where λ is the eigenvalue of the Jacobian matrix. The coefficients of the terms in the Jacobian matrix are then arranged in a following way,

a_n	a_{n-2}	a_{n-4}	a_{n-6}	. .
a_{n-1}	a_{n-3}	a_{n-5}	a_{n-7}	. .
$a_{n-2} - \frac{a_n}{a_{n-1}} a_{n-3}$	$a_{n-4} - \frac{a_n}{a_{n-1}} a_{n-5}$	$a_{n-6} - \frac{a_n}{a_{n-1}} a_{n-7}$		
$a_{n-3} - \frac{a_{n-1}}{b_1} b_2$	$a_{n-5} - \frac{a_{n-1}}{b_1} b_3$			
$b_2 - \frac{b1}{c1} c_2$				

The above table is called the Routh array. The entries in the first array play a vital role in determining the stability of the system. If all the entries are positive, then the system is stable, however, if there is a sign change it is an indicator of instability.
Thus, from Routh array, we can always calculate the region in space where the system is unstable, by changing the parameter values in the system we consider.

APPENDIX B

RECURRENCE PLOTS

Recurrence plots are a novel way to visualize a higher dimensional data. As the name suggests the plot displays the recurrences extracted from the time series. A recurrence is said to have occurred when the system visits the vicinity of the point in phase space again after some time[97]. Consider a time series of a quantity x, that is available to us for analysis. x_i represents the value of x at time i, where $i = 1,2,3...N$ RP for this system is defined as

$$R_{i,j} = 1 \; if \; x_i = x_j \tag{B.1}$$

$$= 0 \; if \; x_i \neq x_j \tag{B.2}$$

The above definition for RP assigns a value of 1, whenever the $x_i = x_j$, that is when the system visits the exact point in the phase space again, else a value of zero is assigned. This is then plotted with the black color being assigned to 1 and white color being assigned to 0. Thus, this plot will contain black regions when there is a recurrence, else it will be blank. However, for practical purposes, we consider recurrence to have occurred when the system visits the original state with a threshold. This threshold is the most important factor in the RP. If the threshold is large, then RP will record a lot of recurrences, which might not be meaningful, with a lower threshold recurrence are lost. The other factors that affect the analysis using recurrence plot are the embedding dimension and the time lag. By choosing a proper embedding dimension spurious recurrences are removed. Introducing a proper time lag reduces redundant information in the system.

From the basic definition as above, it is easily evident that the generated image will have one main diagonal which represents $i = j$ states. All other points in the plot occur whenever x_i equals x_j. That is the state is said to have recurred.
Modern definitions of an RP (recurrence plot) from [97], as follows

$$R_{i,j}(\epsilon) = \Theta(\epsilon - ||\vec{x_i} - \vec{x_j}||). \; i,j = 1,.....N \tag{B.3}$$

ϵ is the threshold, which decides on the closeness between states or the neighborhood of a state. $\Theta()$ is the Heaviside function. Using the concept of delay and embedding dimension once can unfold more details from a time series. The delay is computed using the mutual information in the time series. An appropriate embedding dimension can be found by using the false nearest neighbor method. Even a multidimensional system can be visualized using RP method.

B.1 Structures in RP

1. Single isolated points represent rare events that persist for a small time. They could also signify a presence of a strong fluctuation in the system.
2.A diagonal line parallel to the main diagonal occurs when two states run parallel to each other. The length of this diagonal is also related to K_2 Renyi entropy and also to the maximum Lyapunov exponent of the system.
3. Vertical and horizontal lines represent the laminar states in the system, i.e., system doesn't change or changes very slowly. This is also a representation of intermittent behavior.
‘

B.2 Typical patterns

A stationary system shows a homogeneity while a system containing drift shows typical fading to the upper left and lower right corners. Disruptions in the form of the white bands show transitory behavior, diagonal lines show an underlying periodic behavior.

B.3 More RPs

A cross recurrence plot or the CRP is defined for two different time series of different nature.Let x and y be two time series. A recurrence point is defined as

$$R_{i,j}(\epsilon) = \Theta(\epsilon - ||\overrightarrow{x_i} - \overrightarrow{y_{j+\tau}}||).\ i,j = 1,.....N \tag{B.4}$$

That is, this record events when the first system visits a certain point and at the same time the second system also visits the same point in the phase space.
A joint recurrence plot or the JRP is defined as follows

$$R_{i,j}(\epsilon) = \Theta(\epsilon - ||\overrightarrow{x_i} - \overrightarrow{x_{j+\tau}}||).\Theta(\epsilon - ||\overrightarrow{y_i} - \overrightarrow{y_{j+\tau}}||).\ i,j = 1,.....N \tag{B.5}$$

This records events when recurrence occurs in both the systems simultaneously. JRPs can also be used for phase synchronization.

B.4 Dynamical invariants recovered from an RP

The following dynamical invariants are obtained from a recurrence plot.

B.4.1 Recurrence Rate

This is the ratio of total number of ones (recurrence points) in an RP by total number of points.

$$RR(\epsilon) = \frac{1}{N^2}\Sigma_{i,j=1}^{N} R_{i,j}(\epsilon) \tag{B.6}$$

More the recurrence higher is the recurrence rate. Hence a slowly varying signal will have more recurrence rate than a fast one.

B.4.2 Determinism

Determinism or DET, as represented in literature is defined as the ratio of total number of points that form a diagonal or minimum length say l_{min} to the total number of recurrence points.

$$DET = \frac{\Sigma_{l=lmin}^{N} lP(l)}{\Sigma_{l=1}^{N} lP(l)} \tag{B.7}$$

here l is the length of the diagonal. Periodic systems show diagonal structures in RP and hence have higher values of determinism.
Hence DET can be seen as an indicator of predictability, lesser DET implies a more stochastic nature in the dynamics of the system. $P(l)$ is the histogram of l.

B.4.3 Average diagonal length

$$L = \frac{\Sigma_{l=lmin}^{N} lP(l)}{\Sigma_{l=lmin}^{N} P(l)} \tag{B.8}$$

The above is measure of prediction time. That is the time for which two trajectories are closer to each other.

B.4.4 DIV

Divergence or DIV is the inverse of the maximum diagonal. L denotes the time for which two trajectories are closer in the phase space. Shorter DIV implies that trajectories separate faster, hence DIV is higher.

$$L_{max} = max(l_i)_{i=1}^{N} \quad DIV = \frac{1}{L_{max}} \tag{B.9}$$

L_{max} is a very good estimator of Reyni entropy K_2.

B.4.5 Entropy

Shannon entropy is used as a measure of entropy.

$$p(l) = P(l)/N_l \tag{B.10}$$

$$ENTR = -\Sigma_{l=l_{min}}^{N} p(l) \ln\ p(l) \tag{B.11}$$

For uncorrelated events the complexity is low and hence the value of ENTR is also low.

B.4.6 TREND

This is a stochastic measure of stationary in the data. This is the slope of Recurrence rate as a function of displacement from the diagonal. All the above mentioned quantities are properties that are measured with respect to the diagonal line. The same quantities can be computed for any line parallel to the diagonal.This is also known in the literature as τ -Determinism τ-RR, τ-DIV etc.

B.4.7 Recurrence time of first and second type

Let x_i be a time series. ϵ is a radius around x_i. Recurrence by definition implies that for some other instant of time t the system visits the neighborhood of the original state in the phase space. Let A be a set of all points in that threshold. Recurrence time of type 1 is defined as time differences between two states occurring chronologically. If there are ten states insides the ball of radius ϵ, recurrence time of type 1 will have 9 entries.
For computing Recurrence time of type II, one removes the sojourn points. The resulting set is set B. Now time differences between the various states chronologically are calculated. This is a definition of recurrence time of the second type.
Recurrence time of type I is useful in detecting nonstationarity in the data. The mean of these two types of time also gives some information about the information dimension of the system.

B.4.8 Laminarity, V_{max},Trapping time (TT)

LAM is analogous to DET, the only difference that this being computed about a vertical line rather than a diagonal. LAM is a strong indicator of laminar states in intermittent regimes. Similarly V_{max} is analogous to L_{max} and TT or the trapping time is analogous to average diagonal length. This is also an indicator of how long the system remains constant - and is trapped in a particular state.

APPENDIX C

METHOD TO GENERATE HISTOGRAM

The 1200 years of alpine larch bud moth outbreak data is available. Using this [67] have generated a histogram. The relative frequency mentioned in [67], is calculated the following way.

Let N be the total number of outbreak events, which is 123, in the case of the Alpine region. Let n_i be the total number of events associated with a cycle with time period i. This n_1 is the number of events which have a one year cycle and so on. Then we define f_i which is $\frac{n_i}{N}$, has the relative frequency.

Using this definition, we are able to reproduce the results of [67].

To make a similar histogram for our model for comparison with Alpine data ([67]), we adopt almost a similar procedure. We fix all other parameters at the following value. q_y =1.13, q_z =1.34, c =12,m =13,α =0.5, and vary h and s from 0 to 1, vary λ from 1 to 13. All in steps of 0.1. For each combination of the parameters, time series are generated. FFT is performed to move from the time domain to frequency domain. Power is then calculated by taking the square of the absolute value of intensity at the each frequency. The power spectrum is scanned to find the maxima, and corresponding frequency is noted down. The inverse of this frequency is the time period corresponding the maximum power this noted down.

Hence, for each value of parameters the time period is noted down and finally, a histogram is plotted using the time period data.

Sometimes there are no cycles, in that case, that combination of the parameters is discarded, as it is certainly known that there have been cycles in the Alpine region in the last 1200 years. If there is no dominant peak or just flat power spectrum, then this is also discarded for the same reason as before.

The collected data is then segregated into different period bins. A value of $X-0.5$ to $X+0.5$ is assigned to X^{th} bin, that is to say, a cycle of time period 7.5 years to 8.5 years will be assigned to

8-year cycle.
The total number of entries in each bin is calculated and divided by the total number of events, excluding the flat spectra response and no cycle response. Incidentally excluding them doesn't change the shape of the spectrum, it only alters the magnitude slightly.
The relative frequencies are then plotted against each year.
The same is done for other models which have been used to make the comparative studies.

APPENDIX D

METHOD TO GENERATE THE BIFURCATION VIDEO

The bifurcation diagram, is a pictorial representation of end states (the state in which the system settles) of a system for a given value of the parameter. As the parameter change, the number of states may change, which, is reflected in the bifurcation diagram. Here we present a novel way to study the co-dimension 2 bifurcations, which occur due to change in two parameters. The entire structure in the bifurcation diagram changes, providing a new insight into the system.

There are 8 parameters in the system. To study the effect of two parameters at the same time, a bifurcation video is made using the following procedure. Since from the alpine data, it is clear that LBM and the larch needle lengths have a 8 to 9-year cycle, the parameters are fixed so as to get the same 8-9 year cycle.The values of the parameters chosen are c=12 and m=13. $\alpha = 0.5$, q_y=1.13, q_z=1.34, λ=8,$h = 0.5$ and $s = 0.5$.. These values give 9-year cycle.

To generate the bifurcation video, we fix all but 2 parameters, say X and Y, to the above-mentioned values. Now with respect to X we generate the bifurcation diagram, once when it is done, we change Y and again bifurcation diagram with respect to X is plotted. A video is made using the frames generated by Matlab.

This method helps us to visualize the effect of two parameters on the system.

APPENDIX E

PUBLICATIONS BASED ON THE THESIS

1. Iyengar., S. V., Balakrishnan, J., “q-deformations and the dynamics of the larch budmoth population cycles" in *Nature’s Longest Threads , New Frontiers in the Mathematics and Physics of Information in Biology.* Eds by Balakrishnan, J. & Sreekantan, B V. Published by World Scientific Publishing Co. Pte. Ltd., 2014. ISBN# 9789814612470, **1**, 65-80 (2014).

2. Iyengar, S.V., Balakrishnan, J. and Kurths, J., “Impact of Climate change on Larch Budmoth cyclic outbreaks", *Sci. Rep.* (Nature Publishing Group), **6**, 27845 (2016).

3. Iyengar., S. V., Balakrishnan, J., and Kurths, J., “Co-existence of periodic bursts and death of cycles in a population dynamics system", *submitted* (2016).

4. Iyengar., S. V., Balakrishnan, J., “Numerical exploration of $q-$deformed Tinkerbell map ",*submitted* (2016).

5. Iyengar., S. V., Balakrishnan, J., “Studies of some $q-$deformed nonlinear maps", *submitted* (2016).

APPENDIX F

CONFERENCES ATTENDED

1. Participated in a National workshop on “Physics at small scales" on 18th and 19th March 2011 at School of Physics, University of Hyderabad. Presented a poster on " A study of accuracy of Algorithms for Planetary longitudes in India Astronomy".

2. Attended the workshop on "Workshop on Networks: Structure and Function" held at IISc, Bangalore from 4 November to 6 November (2011).

3. Attended the "ICTP-ICTS Winter School on Quantitative Systems Biology" held at ICTS, inside IISc, Bangalore from Monday 09 Dec, 2013 - Friday 20 Dec, 2013.

4. Attended the workshop on " Indo-US Workshop on Time Series Analysis" Organized jointly by IISER, Pune, and SAMSI, USA held at Indian Institute of Science Education and Research (IISER), Pune, from May 25 to May 30, 2015.

APPENDIX G

CHECK FOR PLAGIARISM

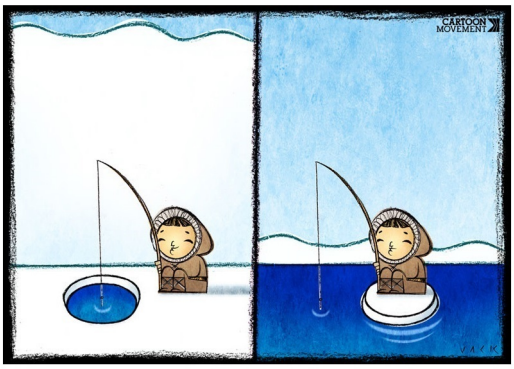

Save the world for the future generations.
They too deserve a nice place to play and enjoy.
Had our forefathers been selfish we wont be
surviving today.

Dedicated to my family